ISSN 2686-7575 (Online)

ТОНКИЕ ХИМИЧЕСКИЕ ТЕХНОЛОГИИ

Fine Chemical Technologies

- Theoretical Bases of Chemical Technology
- Chemistry and Technology of Organic Substances
- Chemistry and Technology of Medicinal Compounds and Biologically Active Substances
- Synthesis and Processing of Polymers and Polymeric Composites
- Chemistry and Technology of Inorganic Materials
- Analytical Methods in Chemistry and Chemical Technology
- Mathematical Methods and Information Systems in Chemical Technology

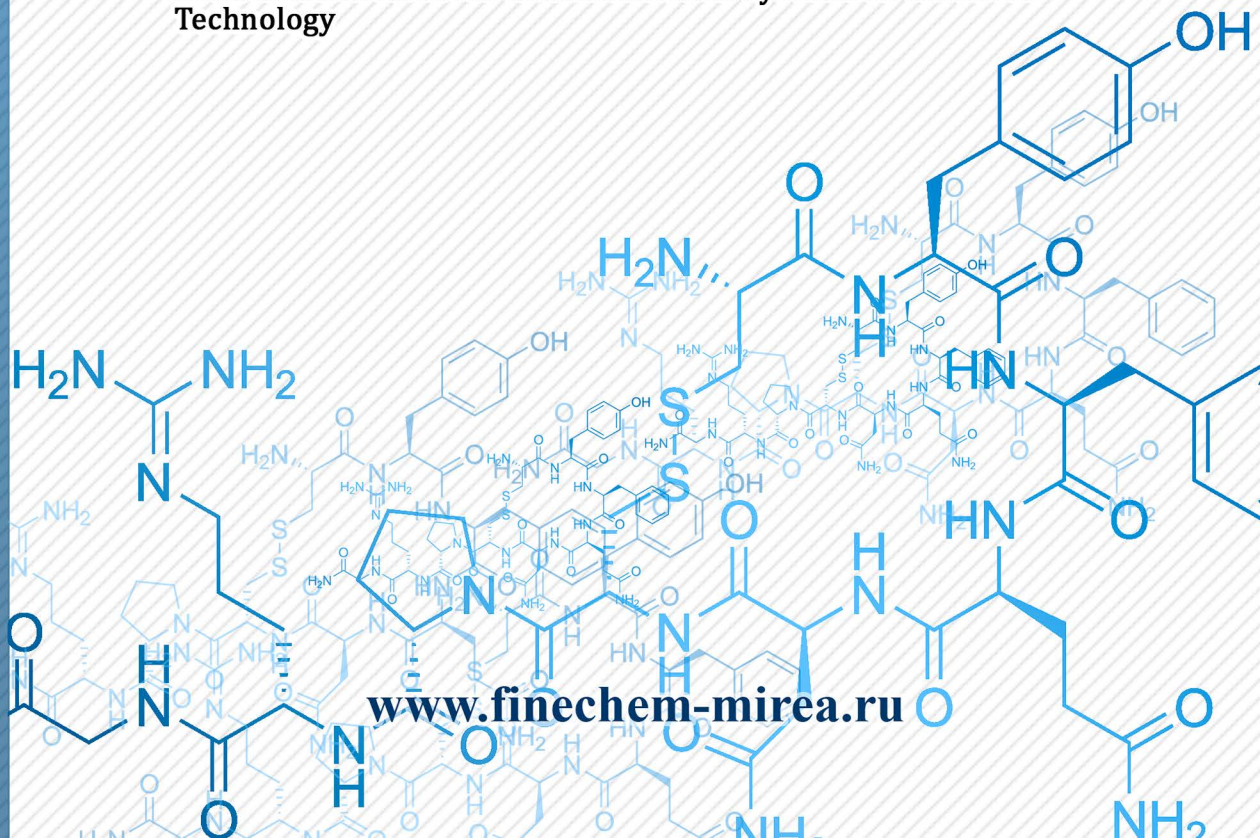

16(5)
2021

www.finechem-mirea.ru

ISSN 2686-7575 (Online)

ТОНКИЕ ХИМИЧЕСКИЕ ТЕХНОЛОГИИ

Fine Chemical Technologies

- Theoretical Bases of Chemical Technology
- Chemistry and Technology of Organic Substances
- Chemistry and Technology of Medicinal Compounds and Biologically Active Substances
- Synthesis and Processing of Polymers and Polymeric Composites
- Chemistry and Technology of Inorganic Materials
- Analytical Methods in Chemistry and Chemical Technology
- Mathematical Methods and Information Systems in Chemical Technology

Tonkie Khimicheskie Tekhnologii =
Fine Chemical Technologies
Vol. 16, No. 5, 2021

Тонкие химические технологии =
Fine Chemical Technologies
Том 16, № 5, 2021

https://doi.org/10.32362/2410-6593-2021-16-5
www.finechem-mirea.ru

https://doi.org/10.32362/2410-6593 www.finechem-mirea.ru

**Tonkie Khimicheskie Tekhnologii =
Fine Chemical Technologies
2021, vol. 16, no. 5**

The peer-reviewed scientific and technical journal Fine Chemical Technologies highlights the modern achievements of fundamental and applied research in the field of fine chemical technologies, including theoretical bases of chemical technology, chemistry and technology of medicinal compounds and biologically active substances, organic substances and inorganic materials, synthesis and processing of polymers and polymeric composites, analytical and mathematical methods and information systems in chemistry and chemical technology.

Founder and Publisher

Federal State Budget
Educational Institution of Higher Education
"MIREA – Russian Technological University"
78, Vernadskogo pr., Moscow, 119454, Russian Federation.
Publication frequency: bimonthly.
The journal was founded in 2006. The name was Vestnik MITHT until 2015 (ISSN 1819-1487).

The journal is included into the List of peer-reviewed science press of the State Commission for Academic Degrees and Titles of the Russian Federation.
The journal is indexed:
SCOPUS, DOAJ, Chemical Abstracts, Science Index, RSCI, Ulrich's International Periodicals Directory

86, Vernadskogo pr., Moscow, 119571, Russian Federation.
Phone: +7(495) 246-05-55 (#2-88)
E-mail: *seredina@mirea.ru*

Registration Certificate ПИ № ФС 77–74580, issued on December 14, 2018 by the Federal Service for Supervision of Communications, Information Technology, and Mass Media of Russia

The subscription index of *Pressa Rossii*: **36924**

**Тонкие химические технологии =
Fine Chemical Technologies
2021, том 16, № 5**

Научно-технический рецензируемый журнал «Тонкие химические технологии» освещает современные достижения фундаментальных и прикладных исследований в области тонких химических технологий, включая теоретические основы химической технологии, химию и технологию лекарственных препаратов и биологически активных соединений, органических веществ и неорганических материалов, синтез и переработку полимеров и композитов на их основе, аналитические и математические методы и информационные системы в химии и химической технологии.

Учредитель и издатель

федеральное государственное бюджетное
образовательное учреждение высшего образования
«МИРЭА – Российский технологический университет»
119454, РФ, Москва, пр-кт Вернадского, д. 78.
Периодичность: один раз в два месяца.
Журнал основан в 2006 году. До 2015 года издавался под названием «Вестник МИТХТ» (ISSN 1819-1487).

Журнал входит в Перечень ведущих рецензируемых научных журналов ВАК РФ.
Индексируется:
SCOPUS, DOAJ, Chemical Abstracts, РИНЦ (Science Index), RSCI, Ulrich's International Periodicals Directory

119571, Москва, пр. Вернадского, 86, оф. Л-119.
Тел.: +7(495) 246-05-55 (#2-88)
E-mail: *seredina@mirea.ru*

Свидетельство о регистрации СМИ: ПИ № ФС 77-74580 от 14.12.2018 г. выдано Федеральной службой по надзору в сфере связи, информационных технологий и массовых коммуникаций (Роскомнадзор)

Индекс по Объединенному каталогу «Пресса России»: **36924**

ТОНКИЕ ХИМИЧЕСКИЕ ТЕХНОЛОГИИ
Fine Chemical Technologies
16(5)
2021

CONTENTS

СОДЕРЖАНИЕ

THEORETICAL BASES OF CHEMICAL TECHNOLOGY

ТЕОРЕТИЧЕСКИЕ ОСНОВЫ ХИМИЧЕСКОЙ ТЕХНОЛОГИИ

ISSN 2686-7575 (Online)

https://doi.org/10.32362/2410-6593-2021-16-5-379-389

UDC 66.011

RESEARCH ARTICLE

Algorithm and software for the optimal technological design of a system of simple distillation columns

Nadir N. Ziyatdinov[@], Ilia I. Emelyanov, Alina A. Ryzhova, Petr S. Chernakov

Kazan National Research Technological University, Kazan, 420111 Russia
[@]Corresponding author, e-mail: nnziat@yandex.ru

Abstract

Objectives. *The formalized problem of the optimal design of distillation column systems belongs to the class of mixed integer nonlinear program problems. Discrete search variables are the number of trays in the rectifying and stripping sections of columns, whereas the continuous ones are the operating modes of columns. This study aimed to develop an algorithm and a software package for the optimal technological design of a system of simple distillation columns based on the criterion of total reduced capital and energy costs using rigorous mathematical distillation models.*

Methods. *The solution to this problem is based on the branch and bound method. A computer model of the distillation column system was developed in the environment of the Aspen Hysys software package. The Inside–Out module was used as the distillation model. The developed algorithm is implemented in the software environment of the Matlab mathematical package. To solve the conditional optimization problem, a sequential quadratic programming method-based model was used. The interaction between software add-ins in Matlab and Aspen Hysys is implemented using a Component Object Model interface.*

Results. *Approaches to obtain the lower and upper bounds of the optimality criterion and the branching method for the implementation of the branch and bound method have been developed. In addition, an algorithm for the optimal design of a distillation column of a given topology based on the branch and bound method has been developed. Furthermore, using Matlab, a software package that implements the developed algorithm and is integrated with the universal modeling software AspenHysys has been created.*

Conclusions. *An algorithm and a software package have been developed and implemented that allows automating the design process of distillation column systems and integration with advanced mathematical programming packages, respectively. The performance of the algorithm and software package has been evaluated using the optimal design of the debutanization column as an example.*

Keywords: *distillation, branch and bound method, optimization, design, Matlab, AspenHysys*

For citation: Ziyatdinov N.N., Emelyanov I.I., Ryzhova A.A., Chernakov P.S. Algorithm and software for optimal technological design of a system of simple distillation columns. *Tonk. Khim. Tekhnol. = Fine Chem. Technol.* 2021;16(5):379–389 (Russ., Eng.). https://doi.org/10.32362/2410-6593-2021-16-5-379-389

НАУЧНАЯ СТАТЬЯ

Алгоритм и программный комплекс оптимального технологического проектирования простых ректификационных колонн

Н.Н. Зиятдинов[@], И.И. Емельянов, А.А. Рыжова, П.С. Чернаков

Казанский национальный исследовательский технологический университет, Казань, 420111 Россия
[@]Автор для переписки, e-mail: nnziat@yandex.ru

Аннотация

Цели. *Формализованная задача оптимального проектирования систем ректификационных колонн относится к классу задач дискретно-непрерывного нелинейного программирования. Дискретными поисковыми переменными являются число тарелок в укрепляющей и исчерпывающей частях колонн, а непрерывными – режимы работы колонн. Цель работы – разработать алгоритм и программный комплекс оптимального технологического проектирования системы простых тарельчатых ректификационных колонн по критерию суммарных приведенных капитальных и энергетических затрат на основе строгих математических моделей ректификации.*

Методы. *Решение поставленной задачи базируется на методе ветвей и границ. Компьютерная модель системы ректификационных колонн построена в среде программного комплекса Aspen Hysys. В качестве модели ректификации использован модуль Inside-Out. Разработанный алгоритм реализован в программной среде математического пакета Matlab. Для решения задачи условной оптимизации использован модуль, основанный на методе последовательного квадратичного программирования. Взаимодействие программной надстройки, построенной в Matlab, с Aspen Hysys реализовано с помощью COM-интерфейса.*

Результаты. *Разработаны подходы к получению нижних и верхних границ критерия оптимальности и способ ветвления при реализации метода ветвей и границ. Разработан алгоритм оптимального проектирования ректификационной колонны заданной топологии на основе метода ветвей и границ. В математическом пакете Matlab создан программный комплекс, реализующий предложенный алгоритм и интегрированный с универсальной моделирующей программной AspenHysys.*

Выводы. *Разработан алгоритм и реализован программный комплекс, позволяющий автоматизировать процесс проектирования систем ректификационных колонн и интеграцию с передовыми пакетами математического программирования. Работоспособность алгоритма и программного комплекса апробирована на примере оптимального проектирования колонны дебутанизации.*

Ключевые слова: *ректификация, метод ветвей и границ, оптимизация, проектирование, Matlab, AspenHysys*

Для цитирования: Зиятдинов Н.Н., Емельянов И.И., Рыжова А.А., Чернаков П.С. Алгоритм и программный комплекс оптимального технологического проектирования простых ректификационных колонн. *Тонкие химические технологии.* 2021;16(5):379–389. https://doi.org/10.32362/2410-6593-2021-16-5-379-389

INTRODUCTION

One of the main processes in the chemical, petrochemical, and oil and gas processing industry is distillation. This process is characterized by high energy and metal consumption [1–5]. Therefore, at the design stage of distillation columns and systems, it is necessary to make decisions aimed at minimizing these costs while meeting design requirements [6–12]. Currently, simplified methods [1, 5], thermodynamic methods [4, 13], and methods based on rigorous mathematical models [9, 10, 14–16] are used to solve such design problems. The essence of a simplified approach, as implemented in the methods of Fenske–Underwood–Gilliland and Lvov is to determine the minimum reflux number by which the optimal number of column and food trays is calculated to yield a given quality of output product. Simplified methods have low accuracy. Thermodynamic methods focus on minimizing energy costs and do not fully take into account capital costs. As a result, the task of developing effective methods for designing distillation column systems (DCS) that are optimal according to technical and economic criteria is important. The latter, in turn, requires the use of rigorous mathematical models and optimization methods. In this case, given the quality of products obtained, the optimal design task is to find a compromise between capital and operating costs, a sum that determines the optimality criterion [16]. An effective tool for computer modeling and optimization in chemical technology is the use of chemical process simulator (CPS) built on strict mathematical models of distillation processes, which are based on the laws of conservation of energy, mass, and momentum, the so-called mass, equilibrium, summation, and heat (MESH) models. These models are contained in the libraries of all leading CPS, such as Aspen Plus [17], AspenHysys [18], Unisim [19], and ChemCad [20, 21], allowing the investigation, design, and management of technological processes at all stages of their life cycle [22]. The CPS also contain effective nonlinear programming methods, including sequential quadratic programming and modified Lagrange function methods. However, these optimization methods can only solve problems of continuous nonlinear programming with discrete values of constructive and operational technological parameters. Because the problem of optimal DCS design is solved in the space of both continuous and discrete search variables, the development of DCS design methods remains relevant.

MATHEMATICAL SUBSTANTIATION OF THE PROBLEM OF OPTIMAL DESIGN OF DCS

The optimal design problem formulated above belongs to the class of mixed integer nonlinear program (MINLP) problems [6, 16], where the discrete search variables are the number of trays in the rectifying and stripping sections of the projected columns, whereas the continuous ones are the parameters that determine the operating modes of the columns. Let us present this problem in a formalized form:

$$f = \min_{x^j, u^j, m_s^j} \sum_{j=1}^{N} f^j\left(x^j, u^j, m_s^j\right), \tag{1}$$

$$\varphi_k^j(x^j, u^j, m_s^j) = 0,\ s = 1, 2,\ j = 1,\ldots,N,\ 1 \le m_s^j \le m_s^{j,\max},$$
$$k = 1,\ldots,\ m_s^{j,\max}, \tag{2}$$

$$\psi^j(x^j, u^j) \le 0,\ j = 1,\ldots, N, \tag{3}$$

$$F^{j_g} - D^g = 0,\ F^{r_g} - W^g = 0,\ j_g, r_g = 1,..,N, \tag{4}$$

$$\varphi_k^j(x^j, u^j, m_s^j) = \begin{Bmatrix} \varphi_{s_0}^j(x^j, u_0^j), s = 1 \\ \varphi_{s_1}^j(x^j, F^j), s = 2 \\ \varphi_{s_k}^j(x^j), 1 \le k \le m_s^j \\ \varphi_{m_s^j+1}^j(x^j, u_{m_s^j+1}^j), s = 2 \end{Bmatrix}, \tag{5}$$

where $f^j(x^j,u^j,m_s^j)$ in Equation (1) is a cost function that includes the total given capital and operating costs of the *j*th column; Equation (2) is a mathematical model of the *j*th column; x^j, u^j represent state and control variables of the *j*th distillation column; N represents the number of columns in the system; *j* represents the ordinal number of the distillation column; *s* represents the index of the column section (*s* = 1–rectifying section; *s* = 2–stripping section); m_s^j represents the number of trays in each section of the *j*th distillation column with values ranging from 1 to $m_s^{j,\max}$; $m_s^{j,\max}$–the maximum number of trays; in Equation (5), $\varphi_{1_0}^j(x^j,u_0^j)$, $\varphi_{s_k}^j(x^j)$, $\varphi_{2_1}^j(x^j,F^j)$ and $\varphi_{m_2^j+1}^j(x^j,u_{m_2^j+1}^j)$ are mathematical models of the dephlegmator, *k*th trays, food trays, and boiler of the *j*th column, respectively; the inequalities in Equation (3) are design constraints; Equation (4) is a ratio describing the DCS structure, which means that when $F^{j_g}-D^g=0$ the feed flow of the j_gth column is the distillate of the *g*th column; when $F^{r_g}-W^g=0$, the feed flow of the r_gth column is the bottom product of the *g*th column; j_g, r_g = 1,..., N, j, g = 1,..., N–the numbers of the columns. Furthermore, for the simplicity of the algorithm under consideration, Equations (4) and (5) will be omitted.

Various methods exist for solving MINLP problems, among which one of the most effective is the method of branches and boundaries [16]. However, this method is not fully formalized because its application to a specific problem necessitates the development of a branching procedure on a tree graph, as well as the formalization of tasks of finding the upper and lower estimates of the optimality criterion. This fully applies to the design problem under consideration, where the main difficulty lies in developing an approach to calculate the lower estimate of the optimality criterion. To do this, it is necessary that all search variables, including the number of trays, can take continuous values. Then, the problem of finding the lower estimate of the criterion will be reduced to a nonlinear programming problem. Solving the minimization problem with continuous search variables will give a better solution than with discrete variables, i.e., a lower bound. The latter is infeasible since the discrete search variable in the number of plates in columns cannot be fractional. In [16], we proposed a technique that allows us to switch from discrete to continuous variables based on the problem under consideration.

To obtain a lower estimate for each column plate, we proposed introducing an additional fictitious structural parameter into the equation of the relationship between the equilibrium and working concentrations of the *i*th component of the *k*th tray α_{sk}^j:

$$y_{is}^{jk}=y_{is}^{j,k+1}+\alpha_{sk}^j E_{is}^j(y_{is}^{*jk}-y_{is}^{j,k+1}). \quad (6)$$

This parameter accepts a value of 0 or 1. If $\alpha_{sk}^j=0$, the tray is missing; otherwise, if α_{sk}^j = 1, the tray is present.

Taking into account the introduced modification, Equations (1)–(3) will take the form of Equations (7)–(9):

$$f=\min_{x^j,u^j,\alpha_s^j}\sum_{j=1}^{N}f^j(x^j,u^j,\alpha_s^j), \quad (7)$$

$$\varphi^j(x^j,u^j,\alpha_s^j)=0, \quad (8)$$

$$\psi^j(x^j,u^j)\le 0, j=1,\ldots,N, \quad (9)$$

$$\alpha_s^j=[0,\ 1],$$

where α_s^j represents a vector whose components are α_{sk}^j, $k=1,\ldots,\ m_s^{j,\max}$.

Thus, the task of the optimal design of DCS is reduced to determining the optimal values of structural parameters and control variables. The continuity of the values of structural parameters α_{sk}^j allows us to calculate the lower estimates of the optimality criterion.

To solve the problem Equation (7) by the method of branches and boundaries, sets of M_s^{jl} plates are introduced in the rectifying and stripping sections of the *j*th column (*s* = 1, 2), where the structural parameter α_{sk}^j accepts a value of 0 or 1. The number of plates is determined in the previous steps of the branch and boundary method. Let us consider the formulation of the problem at the *l*th step:

$$f^l=\min_{x^j,u^j,\alpha_{sk}^j}\sum_{j=1}^{N}f^j(x^j,u^j,\alpha_s^j),\ \ k\notin M_s^{jl}, \quad (10)$$

$$\varphi^j(x^j,u^j,\alpha_s^j)=0,$$

$$\psi^j(x^j,u^j)\le 0,\ j=1,\ldots,N,\ s=1,\ 2,$$

where the set $\alpha_{sk}^{j} = [0, 1]$ at $k \in M_s^{jl}$, found in the previous iterations, is constant; at the same time, α_{sk}^{j} at $k \notin M_s^{jl}$ are binary search variables.

To obtain the lower estimate Equation (10), we solve the following problem:

$$\mu^l = \min_{x^j, u^j, \alpha_{sk}^j} \sum_{j=1}^{N} f^j\left(x^j, u^j, \alpha_s^j\right), \; k \notin M_s^{jl} \;, \qquad (11)$$

$$\varphi^j(x^j, u^j, \alpha_{sk}^j) = 0, \; j = 1,..., N,$$

$$\psi^j(x^j, u^j) \le 0, \; j = 1,..., N,$$

$$0 \le \alpha_{sk}^j \le 1, \text{ for all } k \notin M_s^{jl}.$$

The value of the upper estimate of the optimality criterion is determined by the values of parameters α_{sk}^{*j} obtained from the solution of the problem in Equation (11) at the value $\overline{\alpha}_{sk}^{j}$ obtained in the previous iterations. To do this, we solve Equation (12) under the conditions that, for $k = 1,...p_s^j$, $\overline{\alpha}_{sk}^{j} = 1$, where $p_s^j = \left[\sum_{k \notin M_s^{jl}} \alpha_{sk}^{*j}\right] + \sum_{k \in M_s^{jl}} \overline{\alpha}_{sk}^{j}$ is the set of the nearest integer sum of the structural parameters, and for the remaining k $\overline{\alpha}_{sk}^{j} = 0$, the following problem is solved:

$$\eta^l = \min_{x^j, u^j} \sum_{j=1}^{N} f^j(x^j, u^j, \overline{\alpha}_{sk}^j), \qquad (12)$$

$$\varphi^j(x^j, u^j, \overline{\alpha}_{sk}^j) = 0, \; j = 1,..., N, \; k = 1,..., m_s^{j,\max},$$

$$\psi^j(x^j, u^j) \le 0, \; j = 1,..., N.$$

The branching rule is as follows. The number of trays of each section (s = 1, 2) of each column (j = 1,…,N) is divided into two subsets. In the first subset, parameters for α_{sk}^{j} for which k lies in the interval $\left(\left[\frac{m_s^{jl}}{2}\right]+1, \; m_s^{jl}\right)$ vary, and the parameters for α_{sk}^{j} for which k belongs to the interval $\left(1, \left[\frac{m_s^{jl}}{2}\right]\right)$ are equal to 1, where m_s^{jl} represents the number of trays for which $k \notin M_s^{jl}$. In the second subset, the values of parameters α_{sk}^{j} for which k lies in the interval $\left(1, \left[\frac{m_s^{jl}}{2}\right]\right)$ vary, and α_{sk}^{j} is 0 for those for which k varies in the interval $\left(\left[\frac{m_s^{jl}}{2}\right]+1, \; m_s^{jl}\right)$.

At each iteration, the two problem Equations (11) and (12) are solved to determine the lower and upper estimates of the optimality criterion. The obtained values of the objective function are compared. If, in the lth step, the difference between the upper and lower estimates is less than the specified accuracy ε, the solution found is considered optimal. Otherwise, for further branching, the vertex with the lowest lower score is selected from all hanging vertices.

Aspen Hysys was chosen to solve the problem of the optimal design of DCS with a given topology, as it can be integrated with advanced mathematical programming packages and can model complex petrochemical processes, including DCSs; it contains libraries of many rigorous models of technological equipment with advanced calculation algorithms and a built-in optimization module; and it has a friendly interface that provides a simple and concise representation of a technological scheme. However, because of the software closeness of the optimization module and a limited set of tuning parameters of optimization methods in the Aspen Hysys, it cannot create a program of the proposed algorithm.

SOFTWARE PACKAGE AND ALGORITHM FOR DESIGNING OPTIMAL DCS

To automate the process of designing an optimal system of distillation columns, the software implementation of the algorithm is performed in the Matlab mathematical package. It has a built-in programming language, advanced optimization methods, and is a convenient and relatively simple package for managing the calculation process in the Aspen Hysys. It also enables the development of an interface linking these software tools using Component Object Model/ActiveX technology. In the Aspen Hysys environment, a preliminary assembly of the projected DCS is performed, and its calculation is based on the values of search variables generated in the algorithm implemented in Matlab.

Figure 1 shows the structure of the developed software package for designing an optimal system of distillation columns.

We describe an expanded algorithm for implementing the developed software package.

Step 0. Inputting initial data: the initial number of trays and specifications that are used as search variables; boundaries of changes in the values of specifications and structural parameters of plates; initial approximations of

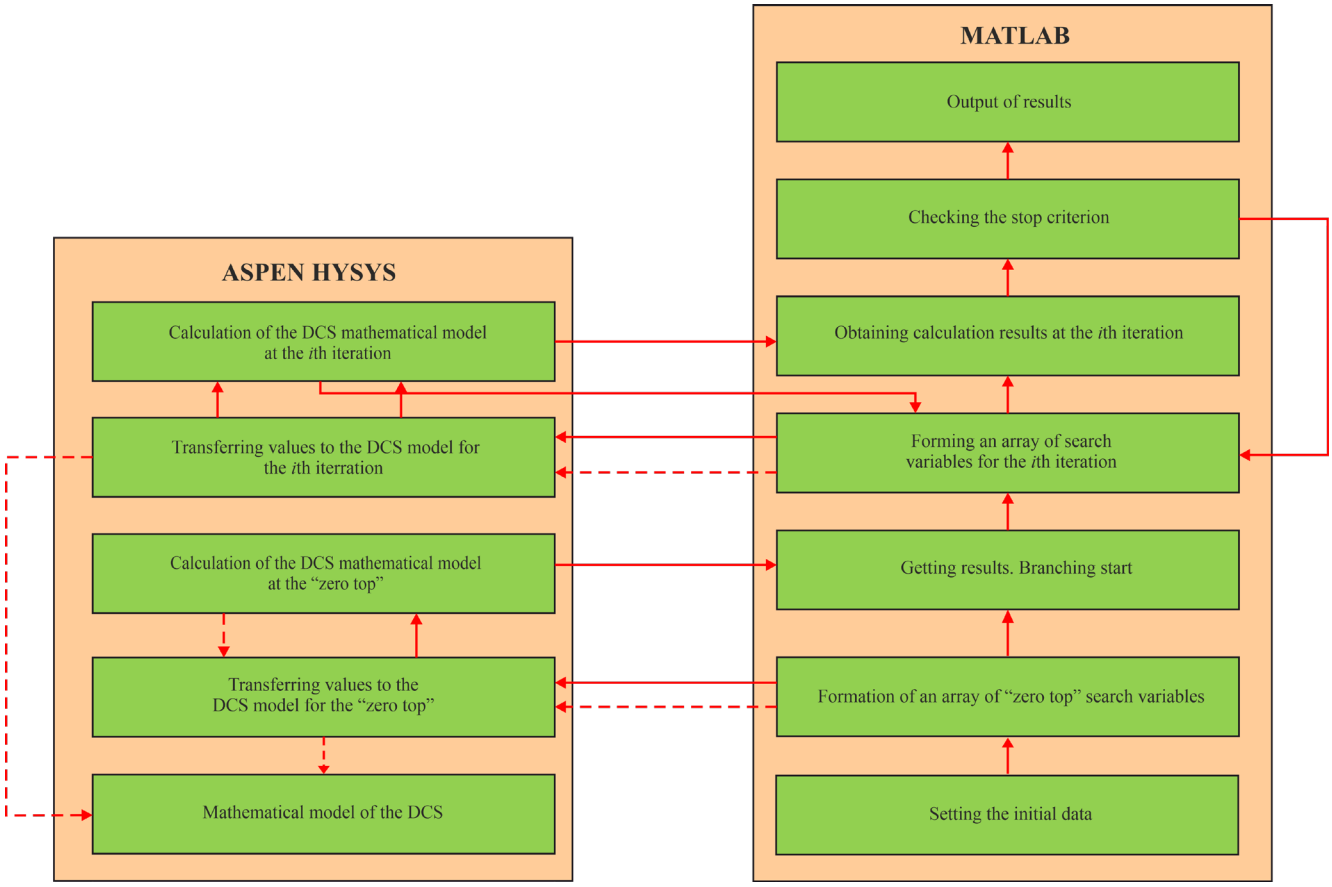

Fig. 1. The structure of the software package.

the values of specifications and structural parameters of trays; cost coefficients; the mathematical model's calculation accuracy of the distillation column and optimization method; refrigerant and steam temperatures.

Step 1. Formation of an array of search variables: the lower and upper estimates of the criterion at the zero vertex, obtained by solving Equations (11) and (12).

Step 2. Splitting of a promising vertex by choosing the smallest upper bound $\overline{\eta} = \min\{\overline{\eta}, \eta_l^d\}$, $l = 1, 2$, where d represents the iteration index, and l represents the index of the descendant of the vertex of the branch tree at the iteration d, by solving Equation (11) and (12).

Step 3. Exclusion of unpromising vertices $\mu_l^t > \overline{\eta}$, $l = 1, 2$, $t = 1, d$.

Step 4. Searching for a promising vertex $\{l^*, t^*\}$ among the remaining ones $\mu_{l^*}^{t^*} = \min_{\mu_l^t \in M} \mu_l^t$.

Step 5. Checking the end of the solution. If the end condition is met,

$$\eta_{l^*}^{t^*} = \overline{\eta} \text{ and } \left|\mu_{l^*}^{t^*} - \eta_{l^*}^{t^*}\right| / \mu_{l^*}^{t^*} \le \varepsilon,$$

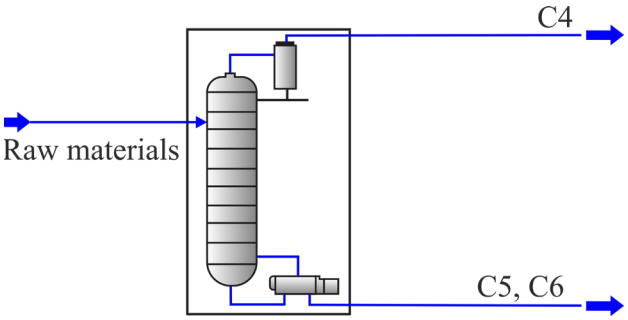

Fig. 2. Diagram of the debutanizing column.

where ε represents the accuracy of the solution, the completion of the algorithm, and the output of the results. Otherwise, go to step 2.

The effectiveness of the developed algorithm and software package was tested on the example of designing an optimal distillation column of debutanization (Fig. 2). To solve the problem in the Aspen Hysys environment, a MESH model of the distillation column was selected, including the Inside-Out method, which is an effective method in terms of time and accuracy of the obtained solution.

Problem statement: with the given parameters of the feedstock (Table 1), it is required to find such values of search variables (the number of plates in

Table 1. Raw material flow parameters

Parameter	Value
Pressure, bar	5
Temperature, °C	80
Mass flow, kg/h	10000
Mass fraction of *n*-butane	0.35
Mass fraction of *n*-pentane	0.30
Mass fraction of *n*-hexane	0.35

stripping and rectifying sections of the column, the value of the reflux ratio, and the temperature in the cube of the column) that the criterion given the total capital and operating costs has a minimal value and to restrict the quality of the partial products: the content of *n*-butane in the distillate is greater than 0.99 mass fraction but less than 0.01 in the cube of the column. The pressure at the top of the column was assumed to be equal to 4 bar, taking into account the possibility of condensation of the upper products by submerged water. The efficiency of the plates for the distillation column was assumed to be equal to 1, the initial approximation of the fictitious structural parameter is 0.7, the specified accuracy ε of the solution is equal to 0.05, and the initial approximation of the number of trays in the column is 30.

The progress of solving the problem is shown in Table 2 and Fig. 3. The optimum corresponds to the vertex 41. Tables 3 and 4 show the data of the material balance of the column and parameters and technical and economic indicators of the column, respectively.

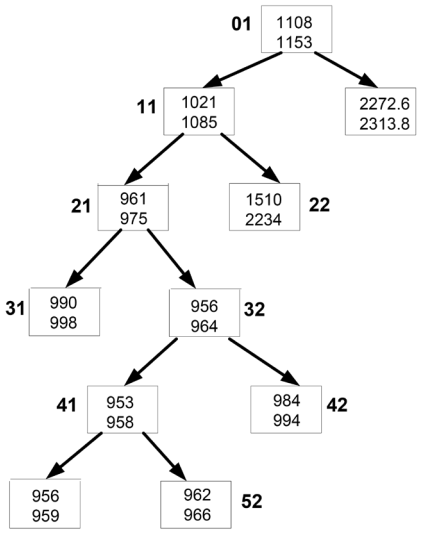

Fig. 3. Tree graph of the solution of the problem (at the vertices of the graph, the lower and upper estimates of the optimality criterion are given).

Table 2. Progress in solving the problem

Vertex No.	Lower estimate, c.u./h	Upper estimate				Accuracy
		Number of trays		Reflux ratio	Criterion c.u./h	
		Rectifying section	Stripping section			
01	1107.9	8	7	2.31	1153.3	0.039
11	1021.1	11	7	2.12	1085.0	0.054
12	2272.6	4	7	5.02	2313.7	0.017
21	960.9	10	10	1.81	974.7	0.014
22	1509.6	11	4	4.74	2233.8	0.320
31	990.3	12	10	1.82	997.7	0.007
32	956.0	9	11	1.83	963.6	0.0078
41	952.6	9	13	1.81	957.9	0.005
42	983.9	9	9	1.93	993.9	0.010
51	955.8	9	12	1.82	958.9	0.003
52	962.3	8	13	1.86	966.3	0.004

Table 3. Parameters of fed and obtained products

Raw materials flow parameters	Flow No.		
	Raw materials	C4	C5, C6
Pressure, bar	5	4	4.5
Temperature, °C	80	42.6	102
Mass flow rate, kg/h	10000	3444	6556
Composition	Mass fract.		
Butane	0.35	0.99	0.01
Pentane	0.30	0.01	0.45
Hexane	0.35	0	0.53

Table 4. Parameters and technical and economic indicators of the column

Indicators	Rectifying section	Stripping section
Number of trays in section	9	13
Reflux ratio	1.8	–
Cube temperature, °C	42.6	102
Section diameter, m	1.1	0.9
Section height, m	5.4	7.8
Interdisciplinary distance, m	0.6	0.6
Heat duty, kcal/h	−516280	658352
Capital costs, c.u./h	112.4	
Operating costs, c.u./h	845.6	
Optimality criterion, c.u./h	958	

CONCLUSIONS

An algorithm for the optimal design of a distillation column of a given topology, based on the method of branches and boundaries, is presented. A software package based on the Matlab mathematical programming package has also been implemented, which allows automating the design process and integration with Aspen Hysys. The effectiveness of the developed algorithm and software package was tested on the example of a distillation column of debutanization.

Acknowledgments

This work was supported by the Ministry of Science and Higher Education of the Russian Federation, grant No. 075-00315-20-01 "Energy-saving processes for the separation of liquid mixtures for the isolation of industrial solvents."

Authors' contribution

N.N. Ziyatdinov – formulation of research goals and objectives, development of a method and algorithm, general management of the research process.

I.I. Emelyanov – development of a software package, experimental research, processing of the obtained experimental data.

A.A. Ryzhova – processing of the obtained experimental data, preparation of materials for publication.

P.S. Chernakov – preparation of materials for publication.

The authors declare no potential or actual conflicts of interest.

REFERENCES

1. Komissarov Yu.A., Dam Kuang Shang. *Khimicheskaya tekhnologiya: Mnogokomponentnaya rektifikatsiya* (*Chemical Technology: Multicomponent Rectification*). Moscow: Yurait; 2019. 255 p. (in Russ.). ISBN 978-5-534-05626-6

2. Klauzner P.S., Rudakov D.G., Anokhina E.A., Timoshenko A.V. Energy saving in the extractive distillation of isobutyl alcohol–isobutyl acetate with n-butyl propionate. *Tonk. Khim. Tekhnol. = Fine Chem. Technol.* 2020;15(4):14–29 (in Russ.). https://doi.org/10.32362/2410-6593-2020-15-4-14-29

3. Serafimov L.A., Frolkova A.K., Bushina D.I. Extractive distillation of binary azeotropic mixtures. *Theor. Found. Chem. Eng.* 2008;42(5):507–516. https://doi.org/10.1134/S0040579508050059

[Original Russian Text: Serafimov L.A., Frolkova A.K, Bushina D.I. Extractive distillation of binary azeotropic mixtures. *Teoreticheskie Osnovy Khimicheskoi Tekhnologii.* 2008;42(5):521–530 (in Russ.).]

4. Tsirlin A.M., Sukin I.A., Balunov A.I. Estimates of energy consumption and selection of optimal distillation sequence for multicomponent distillation. *Theor. Found. Chem. Eng.* 2016;50(3):250–259. https://doi.org/10.1134/S0040579516030131

[Original Russian Text: Tsirlin A.M., Sukin I.A., Balunov A.I. Estimates of energy consumption and selection of optimal distillation sequence for multicomponent distillation. *Teoreticheskie Osnovy Khimicheskoi Tekhnologii.* 2016;50(3):258–267 (in Russ.). https://doi.org/10.7868/S0040357116030131]

5. Komisarov Yu.A, Gordeev L.S., Vent D.P. *Khimicheskaya tekhnologiya: Nauchnye osnovy protsessov rektifikatsii* (*Chemical technology: Scientific foundations of rectification processes*). In 2 v. V. 2. Moscow: Yurait; 2019. 416 p. (in Russ.). ISBN 978-5-534-10977-1

6. Ostrovskii G.M., Ziyatdinov N.N., Lapteva T.V., Ryjov D.A. Selection of optimal feed trays in a closed-loop system of distillation columns. Theor. Found. Chem. Eng. 2008;42(4):386–397. https://doi.org/10.1134/S0040579508040064

[Original Russian Text: Ostrovskii G.M., Ziyatdinov N.N., Lapteva T.V., Ryjov D.A. Selection of optimal feed trays in a closed-loop system of distillation columns. *Teoreticheskie Osnovy Khimicheskoi Tekhnologii.* 2008;42(4):401–412 (in Russ.).]

7. Kister H.Z. Distillation design. McGraw-Hill Professional; 1992. 710 p.

8. Timoshenko A.V., Morgunov A.V., Anokhina E.A. Flowsheet synthesis for the extractive distillation of azeotropic mixtures in systems consisting of columns with partially coupled heat and material flows. *Theor. Found. Chem. Eng.* 2007;41(6):845–850. https://doi.org/10.1134/S0040579507060097

[Original Russian Text: Timoshenko A.V., Morgunov A.V., Anokhina E.A. Flowsheet synthesis for the extractive distillation of azeotropic. *Teoreticheskie Osnovy Khimicheskoi Tekhnologii*. 2007;41(6):649–655 (in Russ.).]

СПИСОК ЛИТЕРАТУРЫ

1. Комиссаров Ю.А., Дам Куанг Шанг. *Химическая технология: Многокомпонентная ректификация*: учебное пособие для вузов. М.: Юрайт; 2019. 255 с. ISBN 978-5-534-05626-6

2. Клаузнер П.С., Рудаков Д.Г., Анохина Е.А., Тимошенко А.В. Энергосбережение в экстрактивной ректификации смеси изобутиловый спирт-изобутилацетат с бутилпропионатом. *Тонкие химические технологии.* 2020,15(4):14–29. https://doi.org/10.32362/2410-6593-2020-15-4-14-29

3. Серафимов Л.А., Фролкова А.К., Бушина Д.И. Ректификация азеотропных бинарных смесей с экстрактивным агентом. *Теор. основы хим. технологии.* 2008;42(5):521–530.

4. Цирлин А.М., Балунов А.И., Сукин И.А. Оценки затрат энергии и выбор оптимальной последовательности разделения многокомпонентных смесей. *Теор. основы хим. технологии.* 2016;50(3):258–268. https://doi.org/10.7868/S0040357116030131

5. Комисаров Ю.А, Гордеев Л.С., Вент Д.П. *Химическая технология: Научные основы процессов ректификации*: учебное пособие для вузов. В 2 ч. Ч. 2. М.: Юрайт; 2019. 416 с. ISBN 978-5-534-10977-1

6. Островский Г.М., Зиятдинов Н.Н., Лаптева Т.В., Рыжов Д.А. Выбор оптимальных тарелок питания в замкнутой системе ректификационных колонн. *Теор. основы хим. технологии.* 2008,42(4):401–412.

7. Kister H.Z. Distillation design. McGraw-Hill Professional; 1992. 710 p.

8. Тимошенко А.В., Моргунов А.В., Анохина Е.А. Синтез схем экстрактивной ректификации азеотропных смесей в комплексах колонн с частично связанными тепловыми потоками. *Теор. основы хим. технологии.* 2007,41(6):649–654.

9. Caballero J.A., Grossman I.E. Design of distillation sequences: from conventional to fully thermally coupled distillation systems. *Comp. Chem. Eng.* 2004,28(11):2307–2329. https://doi.org/10.1016/j.compchemeng.2004.04.010

10. Grossman I.E., Aquirre P.A., Barttfeld M. Alternative representations and formulations for the economic optimization of multicomponent distillation columns. *Comp. Chem. Eng.* 2003;27(3):363–383. https://doi.org/10.1016/S0098-1354(02)00213-2

11. Клаузнер П.С., Рудаков Д.Г., Анохина Е.А., Тимошенко А.В. Оптимальные режимы бокового отбора в системах экстрактивной ректификации с тепловым насосом при разделении смеси аллиловый спирт–аллилацетат с бутилпропионатом. *Тонкие химические технологии.* 2021;16(3):213–224. https://doi.org/10.32362/2410-6593-2021-16-3-213-224

12. Лаптев А.Г., Карпеев С.В., Лаптева Е.А. Моделирование и модернизация тарельчатых колонн при проведении реакционно-массообменных процессов. *Теор. основы хим. технологии.* 201;52(1):3–12. https://doi.org/10.7868/S0040357118010013

9. Caballero J.A., Grossman I.E. Design of distillation sequences: from conventional to fully thermally coupled distillation systems. *Comp. Chem. Eng.* 2004,28(11):2307–2329. https://doi.org/10.1016/j.compchemeng.2004.04.010

10. Grossman I.E., Aquirre P.A., Barttfeld M. Alternative representations and formulations for the economic optimization of multicomponent distillation columns. *Comp. Chem. Eng.* 2003;27(3):363–383. https://doi.org/10.1016/S0098-1354(02)00213-2

11. Klauzner P.S., Rudakov D.G., Anokhina E.A., Timoshenko A.V. Optimal modes of side-section flow in heat-pump-assisted extractive distillation systems for separating allyl alcohol–allyl acetate mixtures with butyl propionate. *Tonk. Khim. Tekhnol. = Fine Chem. Technol.* 2021;16(3):213–224 (in Russ.). https://doi.org/10.32362/2410-6593-2021-16-3-213-224

12. Laptev A.G., Karpeev S.V., Lapteva E.A. Modeling and Modernization of Tray Towers for Reactive Distillation Processes. *Theor. Found. Chem. Eng.* 2018,52(1):1–10. https://doi.org/10.1134/S0040579518010098

[Original Russian Text: Laptev A.G., Karpeev S.V., Lapteva E.A. Modeling and Modernization of Tray Towers for Reactive Distillation Processes. *Teoreticheskie Osnovy Khimicheskoi Tekhnologii.* 2018;52(1):3–12 (in Russ.). https://doi.org/10.1134/S0040579518010098]

13. Tsirlin A.M. Separation of ideal mixtures in multistage systems: An algorithm for selecting a separation sequence. *Theor. Found. Chem. Eng.* 2012.46(2):128–134. https://doi.org/10.1134/S0040579512010150

[Original Russian Text: Tsirlin A.M. Separation of ideal mixtures in multistage systems: An algorithm for selecting a separation sequence. *Teoreticheskie Osnovy Khimicheskoi Tekhnologii.* 2012;46(2):162–168 (in Russ.).]

14. Lang Y-D, Biegler L.T. Distributed Stream method for Tray Optimization. *AIChE J.* 2002;48(3):582–595. https://doi.org/10.1002/aic.690480315

15. Huss R.S., Westerberg A.W. Collocation Methods for Distillation Design. 1. Model Description and Testing. *Ind. Egn. Chem. Res.* 1996;35(5):1603–1610. https://doi.org/10.1021/ie9503499

16. Ostrovskii G.M., Ziyatdinov N.N., Lapteva T.V., Bogula N.K. Optimal design of a distillation column system of a given topology. Theor. Found. Chem. Eng. 2011;45(1):89–98. https://doi.org/10.1134/S004057951006103X

[Original Russian Text: Ostrovskii G.M., Ziyatdinov N.N., Lapteva T.V., Bogula N.K. Optimal design of a distillation column system of a given topology. *Teoreticheskie Osnovy Khimicheskoi Tekhnologii.* 2011;45(1):42–43 (in Russ.).]

17. Kholodnov V.A., Viktorov V.K., Krasnoborod'ko D.A., Khaidarov V.K., Kulishenko R.Yu., Fonar' V.V. *Modelirovanie i optimizatsiya khimiko-tekhnologicheskikh sistem s pomoshch'yu interaktivnoi informatsionno-modeliruyushchei programmy Aspen Plus*: Uchebnoe posobie (*Modeling and optimization of chemical engineering systems using the interactive information and modeling program Aspen Plus*). St. Peterburg: SPBGTI (TU); 2013. 214 p. (in Russ.).

18. Lisitsyn N.V., Viktorov V.K., Kuzichkin N.V. *Khimiko-tekhnologicheskie sistemy: Optimizatsiya i resursosberezhenie* (*Chemical-technological systems: Optimization and resource conservation*). St. Peterburg: Mendeleev; 2007. 312 p. (in Russ.). ISBN 5-94922-024-2

19. Ziyatdinov N.N., Lapteva T.V., Emel'yanov I.I., Loginova I.V. *Komp'yuternoe modelirovanie i optimizatsiya khimiko-tekhnologicheskikh protsessov i sistem s ispol'zovaniem universal'noi modeliruyushchei programmy Unisim*: Uchebnoe posobie (*Computer modeling and optimization of chemical-technological processes and systems using the universal modeling program Unisim*). Kazan: RAR Publishing House; 2019. p. 106. (in Russ.).

13. Цирлин А.М. Алгоритм выбора последовательности разделения идеальных смесей в многостадийных системах. *Теор. основы хим. технологии.* 2012,46(2):162–168.

14. Lang Y-D, Biegler L.T. Distributed Stream method for Tray Optimization. *AIChE J.* 2002;48(3):582–595. https://doi.org/10.1002/aic.690480315

15. Huss R.S., Westerberg A.W. Collocation Methods for Distillation Design. 1. Model Description and Testing. *Ind. Egn. Chem. Res.* 1996;35(5):1603–1610. https://doi.org/10.1021/ie9503499

16. Островский Г.М., Зиятдинов Н.Н., Лаптева Т.В., Богула Н.Ю. Оптимальное проектирование системы ректификационных колонн с заданной топологией. *Теор. основы хим. технологии.* 2011;45(1):88–97.

17. Холоднов В.А., Викторов В.К., Краснобородько Д.А., Хайдаров В.К., Кулишенко Р.Ю., Фонарь В.В. *Моделирование и оптимизация химико-технологических систем с помощью интерактивной информационно-моделирующей программы Aspen Plus*: учебное пособие. СПб.: СПбГТИ (ТУ); 2013. 214 с.

18. Лисицын Н.В., Викторов В.К., Кузичкин Н.В. *Химико-технологические системы: Оптимизация и ресурсосбережение*. СПб.: Менделеев; 2007. 312 с. ISBN 5-94922-024-2

19. Зиятдинов Н.Н., Лаптева Т.В., Емельянов И.И., Логинова И.В. *Компьютерное моделирование и оптимизация химико-технологических процессов и систем с использованием универсальной моделирующей программы Unisim*: учебное пособие. Казань: Изд-во РАР; 2019. 106 с.

20. Гартман Т.Н., Советин Ф.С. Применение пакетов программ ChemCad для моделирования процессов многокомпонентной ректификации в тарельчатых колоннах при получении синтетического жидкого топлива. *Химическая техника*. 2010;(2):36–38.

21. Зиятдинов Н.Н., Лаптева Т. В., Рыжов Д. А. *Математическое моделирование химико-технологических систем с использованием программы ChemCad*: учебно-методическое пособие. Казань: Издательство Казан. гос. технол. ун-та; 2008. 160 с. ISBN 978-5-7882-0583-0

22. Кузнецов А.С., Корнюшко В.Ф. Интеллектуальная система управления химико-технологическими процессами структурирования многокомпонентных эластомерных композитов на основе продукционной модели. *Тонкие химические технологии.* 2017;12(5):88–96. https://doi.org/10.32362/2410-6593-2017-12-5-88-96

20. Gartman T.N., Sovetin F.S. Application of ChemCad software packages to simulate multicomponent rectification processes in tray columns for synthetic liquid fuel production. *Khimicheskaya tekhnika*. 2010;(2):36–38 (in Russ.).

21. Ziyatdinov N.N., Lapteva T. V., Ryzhov D. A. *Matematicheskoe modelirovanie khimiko-tekhnologicheskikh sistem s ispol'zovaniem programmy ChemCad*: Uchebno-metodicheskoe posobie (*Mathematical modeling of chemical technological systems using the ChemCad program*). Kazan: KGTU; 2008. 160 p. ISBN 978-5-7882-0583-0

22. Kuznetsov A.S., Kornushko V.F. Intelligent control system of chemical-technological processes of structuring of multicomponent elastomer composites based on the production model. *Tonk. Khim. Tekhnol. = Fine Chem. Technol.* 2017;12(5):88–96 (in Russ.). https://doi.org/10.32362/2410-6593-2017-12-5-88-96

About the authors:

Nadir N. Ziyatdinov, Dr. Sci. (Eng.), Professor, Head of the Department of Process System Engineering, Kazan National Research Technological University (68, Karl Marx ul., Kazan, 420015, Republic of Tatarstan, Russia). E-mail: nnziat@yandex.ru. https://orcid.org/0000-0002-2314-8935

Ilia I. Emelianov, Cand. Sci. (Eng.), Associate Professor, Department of Process System Engineering, Kazan National Research Technological University (68, Karl Marx ul., Kazan, 420015, Republic of Tatarstan, Russia). E-mail: ilyaemelyan@gmail.com. https://orcid.org/0000-0003-0257-0739

Alina A. Ryzhova, Postgraduate Student, Department of Process System Engineering, Kazan National Research Technological University (68, Karl Marx ul., Kazan, 420015, Republic of Tatarstan, Russia). E-mail: alinagainullina0@yandex.ru. https://orcid.org/0000-0001-5918-8296

Petr S. Chernakov, Student, Department of Process System Engineering, Kazan National Research Technological University (68, Karl Marx ul., Kazan, 420015, Republic of Tatarstan, Russia). E-mail: systech2@yandex.ru

Об авторах:

Зиятдинов Надир Низамович, д.т.н., профессор, зав. кафедрой системотехники, ФГБОУ ВО «Казанский национальный исследовательский технологический университет» (420015, Россия, Республика Татарстан, Казань, ул. К. Маркса, д. 68). E-mail: nnziat@yandex.ru. https://orcid.org/0000-0002-2314-8935

Емельянов Илья Игоревич, к.т.н., доцент, доцент кафедры системотехники, ФГБОУ ВО «Казанский национальный исследовательский технологический университет» (420015, Россия, Республика Татарстан, Казань, ул. К. Маркса, д. 68). E-mail: ilyaemelyan@gmail.com. https://orcid.org/0000-0003-0257-0739

Рыжова Алина Альбертовна, аспирант, кафедра системотехники, ФГБОУ ВО «Казанский национальный исследовательский технологический университет», (420015, Россия, Республика Татарстан, Казань, ул. К. Маркса, д. 68). E-mail: alinagainullina0@yandex.ru. https://orcid.org/0000-0001-5918-8296

Чернаков Петр Станиславович, студент, кафедра системотехники, ФГБОУ ВО «Казанский национальный исследовательский технологический университет» (420015, Россия, Республика Татарстан, Казань, ул. К. Маркса, д. 68). E-mail: systech2@yandex.ru

The article was submitted: August 26, 2021; approved after reviewing: September 20, 2021; accepted for publication: October 25, 2021.

Translated from Russian into English by N. Isaeva
Edited for English language and spelling by Enago, an editing brand of Crimson Interactive Inc.

CHEMISTRY AND TECHNOLOGY OF ORGANIC SUBSTANCES

ХИМИЯ И ТЕХНОЛОГИЯ ОРГАНИЧЕСКИХ ВЕЩЕСТВ

ISSN 2686-7575 (Online)

https://doi.org/10.32362/2410-6593-2021-16-5-390-398

UDC 665.6

RESEARCH ARTICLE

Hydrodynamic activation of heavy oil residues

Vera B. Terenteva[2], Boris V. Peshnev[1], Alexander I. Nikolaev[1,@]

[1]MIREA – Russian Technological University (M.V. Lomonosov Institute of Fine Chemical Technologies), Moscow, 119571 Russia
[2]The 25th State Research Institute of Himmotology, Ministry of Defence of Russian Federation, Moscow, 121467 Russia
[@]Corresponding author, e-mail: nikolaev_a@mirea.ru

Abstract

Objectives. *Recently, there has been a tendency to increase the volume of high-viscosity heavy oils in the total volume of oil produced. The processing of these oils requires new technological approaches. This task is closely related to the need to increase the depth of oil refining. Among the approaches proposed to solve these problems, mechanochemical activation, which is based on the cavitation effect produced by ultrasonic or hydrodynamic methods, has been suggested. This study evaluated the effects of cavitation in increasing the depth of oil refining.*

Methods. *Straight-run and "secondary" oil products were used as raw materials: vacuum gas oil, catalytic cracking gas oil, and fuel oil. Activation was carried out in a high-pressure disintegrator. The principle of operation was to compress the oil product and then pass it through a diffuser. When the oil was passed through the diffuser, there was a sharp pressure release to atmospheric pressure, which caused cavitation in the hydrodynamic flow. The pressure gradient on the diffuser and the number of processing cycles ranged from 20 to 50 MPa and 1 to 10, respectively. The density, refractive index, and the fractional composition of petroleum products were determined using standard and generally accepted methods.*

Results. *This paper reports the influence of mechanochemical activation of petroleum products on their physical and chemical characteristics. An increase in the pressure gradient and the number of processing cycles leads to a decrease in the boiling point of the petroleum products and their density and an increase in the yield of fractions that boil off below 400°C. The yield of the fractions with boiling points of 400–480°C and the remainder were reduced. The density and refractive index of fractions with boiling points up to 480°C decreased, and the density of the residue increased. The effects of cavitation (an increase in the yield of fractions with boiling points up to 400°C and a decrease in the density of the petroleum products) increased with increasing pressure gradient and the number of processing cycles.*

Conclusions. *The changes in the density, boiling point, and the yield of fractions increased with increasing the pressure from 20 to 50 MPa and the number of hydrodynamic cavitation cycles from 1 to 5. Increasing the number of processing cycles to more than five had little additional effect. The effects of cavitation increased with increasing initial density of the oil product. The average molecular weight of these fractions was estimated from the densities and boiling points of individual fractions of the petroleum products. The calculation confirmed the assumption regarding the course of cracking reactions of petroleum products under the influence of cavitation and indicates the course of the compaction processes.*

Keywords: *cavitation, oil, yield, light fractions, oil fractions*

For citation: Terenteva V.B., Peshnev B.V., Nikolaev A.I. Hydrodynamic activation of heavy oil residues. *Tonk. Khim. Tekhnol. = Fine Chem. Technol.* 2021;16(5):390–398 (Russ., Eng.). https://doi.org/10.32362/2410-6593-2021-16-5-390-398

НАУЧНАЯ СТАТЬЯ

Гидродинамическая активация тяжелых нефтяных остатков

В.Б. Терентьева[2], Б.В. Пешнев[1], А.И. Николаев[1,@]

[1]МИРЭА – Российский технологический университет (Институт тонких химических технологий им. М.В. Ломоносова), Москва, 119571, Россия
[2]25 ГосНИИ химмотологии Минобороны России, Москва, 121467 Россия
[@]Автор для переписки, e-mail: nikolaev_a@mirea.ru

Аннотация

Цели. *В последние годы прослеживается тенденция увеличения в общем объеме добываемой нефти высоковязких, тяжелых нефтей, переработка которых требует новых технологических подходов. Эта задача тесно связана с необходимостью повышения глубины переработки нефти. Среди подходов, предлагаемых для решения отмеченных задач, встречается метод механохимической активации, который основан на использовании эффекта кавитации, создаваемого ультразвуковым или гидродинамическим способами. Цель работы заключалась в исследовании возможности использования эффекта кавитации для повышения глубины переработки нефти.*

Методы. *В качестве сырья использовались прямогонные и «вторичные» нефтепродукты: вакуумный газойль, газойль каталитического крекинга, мазуты. Активация проводилась в дезинтеграторе высокого давления, принцип действия которого заключался в сжатии нефтепродукта с последующим его пропусканием через диффузор. При этом происходил резкий «сброс» давления до атмосферного, и в гидродинамическом потоке возникало явление кавитации. Градиент давлений на диффузоре варьировался от 20 до 50 МПа, а количество циклов обработки от 1 до 10. Определение плотности, коэффициента рефракции и фракционного состава нефтепродуктов осуществлялось с использованием стандартных и общепринятых методов.*

Результаты. *В работе представлены результаты влияния механохимической активации нефтепродуктов на изменение их физико-химических характеристик. Показано, что повышение градиента давлений и числа циклов обработки приводит к снижению температур начала кипения нефтепродуктов, их плотности и увеличению выхода фракций, выкипающих до 400 °С. Выход фракции с температурами кипения 400–480 °С и остатка при этом снижается. Отмечено снижение плотности и показателя преломления фракций с температурами кипения до 480 °С и повышение плотности остатка. Установлено, что эффект от явления кавитации (увеличение выхода фракций с температурами кипения до 400 °С, снижение плотности нефтепродукта) возрастал при увеличении градиента давлений и количества циклов обработки.*

Выводы. *Показано, что увеличение давления от 20 до 50 МПа и количества циклов гидродинамической кавитации способствует большему изменению плотности, температуры начала кипения и выхода фракций. Установлено, что повышение числа циклов обработки свыше 5 нецелесообразно. Отмечено, что с увеличением исходной плотности нефтепродукта эффективность воздействия возрастает. По плотностям и температурам кипения отдельных фракций нефтепродуктов оценена средняя молекулярная масса этих фракций. Расчет подтвердил предположение о протекании реакций крекинга нефтепродуктов под воздействием кавитации и свидетельствует о протекании процессов уплотнения.*

Ключевые слова: *кавитация, нефть, выход, светлые фракции, масляные фракции*

Для цитирования: Терентьева В.Б., Пешнев Б.В., Николаев А.И. Гидродинамическая активация тяжелых нефтяных остатков. *Тонкие химические технологии.* 2021;16(5):390–398. https://doi.org/10.32362/2410-6593-2021-16-5-390-398

INTRODUCTION

Efficient processing of heavy oil residues is an urgent problem of the petrochemical industry. The depletion of reserves of traditional light and medium oils, which were a source of raw materials for the production of motor fuels and the petrochemical industry, has highlighted the need to increase the depth of oil refining. Heavy high-viscosity oils are being increasingly involved in the fuel and energy balance, but their processing requires new technological approaches. The resources of heavy and bituminous oils significantly exceed the reserves of light oils and are estimated to be 750 billion tons. Canada (386 billion tons) and Venezuela (335 billion tons) have the largest reserves of heavy oils. The reserves of heavy oils in Russia (the fields of the Volga–Ural, Timan–Pechora, and West Siberian oil-and-gas provinces) are estimated at 30–75 billion tons. Heavy, high-viscosity oils are characterized by a high content of polyaromatic hydrocarbons and asphaltene–resinous substances. In these indicators, they are close to heavy oil residues. This potentially allows a uniform approach to their processing [1–3].

The coking process is the most common method for processing heavy oil residues and accounts for up to 40% of residues. The following processes have been used in the order of the processing volumes: visbreaking (~34%), hydrotreating (~18%), hydrocracking (~4%), and deasphalting (~3.5%) [4]. The same processes are also considered methods of processing heavy oils, and research has been carried out in many scientific centers [4–7].

Simultaneously with the traditional methods of processing heavy oils and oil products, an active search for new technological approaches to their processing is underway [4, 8–10]. Mechanochemical activation is often considered a new unconventional method of treating heavy oil feedstock. This suggests the generation of cavitation in an oil flow. Cavitation is a physical process of nucleation (bubble formation) in a liquid media followed by bubble collapse [11–15]. Researchers have noted local increases in temperature of up to 10000 K caused by collapsing cavitation bubbles [16, 17]. As a result, cracking reactions become possible, which affects the fractional composition of oil and petrochemicals. On the other hand, information on the changes in the physicochemical characteristics of oil is contradictory. Some researchers noted a decrease in the density and viscosity of the resulting oil products, while others suggested an increase in the content of heavy oil fractions. A possible reason for these contradictions is the difference in characteristics and processing conditions [11–15]. This study examined the influence of mechanochemical activation on the physicochemical characteristics of petroleum products.

Table 1. Physicochemical characteristics of the samples

Indicator	Sample			
	CCG	M1	M2	VG
Density, g/cm^3	1.1002	0.9684	0.9478	0.8998
Yield of fractions boiling in the temperature range, wt %				
From the initial boiling point (T_{IBP}) to 350°C	5.2	5.0	13.2	8.4
350–400°C	25.8	9.0	15.8	34.5
400–480°C	69.0	28.0	47.0	40.9
Above 480°C		58.0	24.0	16.2

Note: CCG – catalytic cracking gas oil, VG – vacuum gas oil.

MATERIALS AND METHODS

Straight-run and "secondary" petroleum products were used as raw materials: vacuum gas oil (VG), catalytic cracking gas oil (CCG), and masut (fuel oil, M1, and M2). Table 1 lists their characteristics.

The activation of petroleum product samples was carried out in a high-pressure disintegrator described elsewhere [18]. The principle of action is that an oil sample is compressed to a pressure of 20–50 MPa and passed through a diffuser. When passing through the diffuser, there is a sharp decrease in pressure to atmospheric pressure, and cavitation occurs in hydrodynamic flow. The passage of a minimum amount of a sample (0.5 L) through the diffuser from the high-pressure zone to the atmospheric zone is considered a single cycle. The number of cycles of such treatment of the raw material ranged from 1 to 10. The temperature at which the samples were activated was chosen because gas bubbles in the liquid volume are the nuclei of cavitation, according to previous reports [19, 20]. Accordingly, the cavitation intensity increases with increasing number of nuclei in the volume of oil products. Because an increase in temperature leads to the degassing of samples, activation was carried out at a minimum temperature that ensures the pumpability of the oil product through the apparatus. Thus, for the VG, HCC, and M1 and M2 samples, pumpability was achieved at 30°C, 50°C, and 70°C, respectively.

The sample density was determined using the pycnometric method. The initial boiling point, the yield of fractions of the vacuum distillation of petroleum products, and the refractive index were examined by refractometry.

For fuel oil and VG oil samples, the yield of fractions boiling out over the temperature ranges, T_{IBP}–350°C, 350–400°C, 400–480°C, and >480°C, was determined. For CCG oil, the yield was determined for fractions boiling up to 350°C and higher. The fractions were combined (350°C and higher) for CCG oil because an increase in temperature above 350°C (calculated for atmospheric pressure) during the analysis led to hydrocarbon decomposition.

RESULTS AND DISCUSSION

For all samples investigated, the boiling-onset temperatures and density decreased after treatment. For example, the boiling point of sample M2 was 280°C. After five treatment cycles at a pressure gradient of 50 MPa, the boiling-onset temperature decreased to 250°C. More severe the activation conditions (higher pressure gradient, more exposure cycles) resulted in a lower density of the product obtained (Fig. 1). Simultaneously, the characteristics of the samples did not change after five processing cycles.

The significant change in density was attributed to a change in the yield of the fractions (Fig. 2). As a result of activation, the yield of fractions boiling up to 400°C increased, whereas the yield of the heavy oil fraction and residue decreased. The increase in the total yield of light and medium oil fractions depended on the treatment pressure gradient. Hence, the total yield of these fractions in the VG sample was 43 wt %. After five treatment cycles at 20 and 50 MPa, the yield was 46.5 and 52.6 wt %, respectively, showing an increase with increasing pressure.

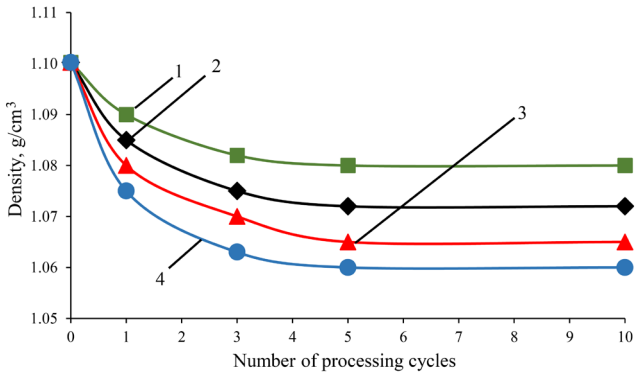

Fig. 1. Influence of the activation conditions on the CCG sample density. Pressure gradient, MPa: (1) 20; (2) 30; (3) 40; (4) 50.

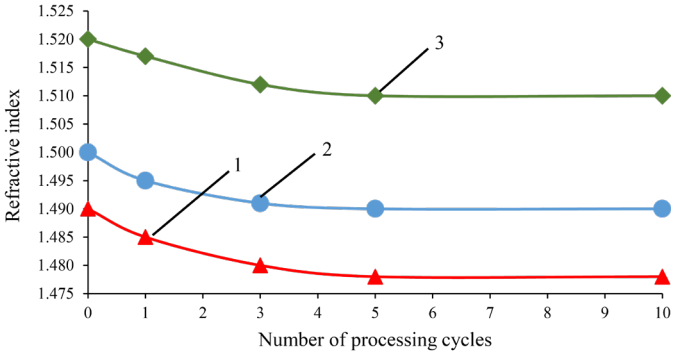

Fig. 3. Influence of the number of activation cycles on the refractive index of the M2 sample fractions. Pressure gradient was 40 MPa. The boiling temperature of the fractions, °C: (1) T_{IBP}–350; (2) 350–400; (3) 400–480.

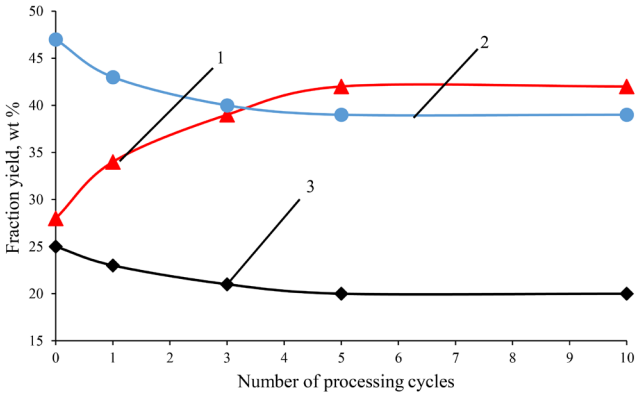

Fig. 2. Influence of the number of activation cycles on the M2 sample fractional composition. Pressure gradient 50 MPa. Fractions: (1) T_{IBP}–400°C; (2) 400–480°C; (3) residue.

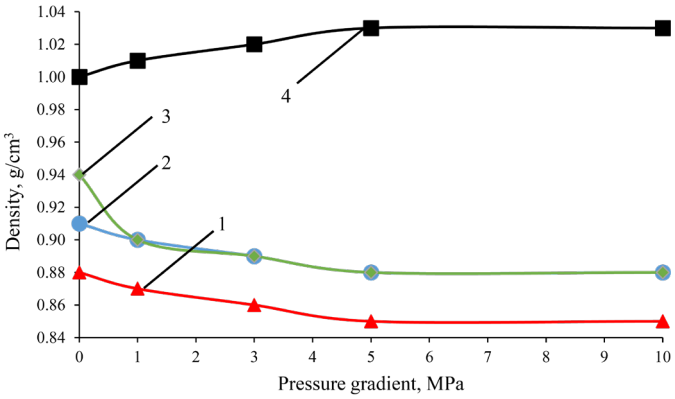

Fig. 4. IInfluence of the pressure gradient on the M1 sample fractions density; five cycles of activation. The boiling temperature of the fractions, °C: (1) T_{IBP}–350; (2) 350–400; (3) 400–480; (4) residue.

After sample activation, both the fractional composition and the physicochemical characteristics of the individual fractions changed (density and refractive index). For all samples studied, an increase in the pressure gradient and the number of processing cycles led to a decrease in the refractive index and the density of fractions boiling up to 480°C. Simultaneously, the density of the fraction with a boiling point above 480°C increased (Figs. 3 and 4).

The changes in the density and refractive index for all oil products under consideration were identical. Increasing the number of activation cycles of samples to more than five had little additional effect on the sample characteristics.

The relationship between the original sample density and the changes that occurred as a result of its processing was noted: the higher its density, the more significant the changes. For example, the yield of fractions with a boiling point of up to 400°C for the VG sample (initial density 0.8998 g/cm³) was 42.9 wt %. After five-time treatment at 50 MPa, it increased to 52.6 wt %, i.e., it increased by 9.7%. For the M1 sample (density 0.9684 g/cm³), the yield of this fraction under the same processing conditions increased by 14.8%, and for the GCC sample (density 1.1002 g/cm³), by 24.5 wt %.

The authors of [21] have revealed the formation of unsaturated hydrocarbons when treating alkanes, a decrease in the samples boiling points studied by us, and a change in the physicochemical characteristics of their individual fractions. We can explain this by an increase in temperature as a result of the gas

Table 2. Influence of the activation conditions on the average molecular weight of the fraction boiling in the T_{IBP}–350°C temperature range

Mechanochemical activation conditions		Average molecular weights of samlpes			
Number of processing cycles	Processing pressure, MPa	VG	M1	M2	CCG
Original sample		219	239	236	200
1	20	218	238	235	197
	50	213	230	229	192
5	20	215	232	230	194
	50	210	225	224	189

bubbles collapse upon cavitation. We assumed that a local increase in temperature resulted in the formation of alkenes and hydrocarbons with a lower molecular weight as a result of cracking reactions. These hydrocarbons are characterized by lower densities and refractive indexes.

Table 2 shows the influence of the activation conditions on the average molecular weight of the fraction boiling out in the T_{IBP}–350°C temperature range for the samples studied.

The average molecular weight was estimated using the formula recommended for narrow oil fractions [19]:

$$M = (160 - 5K) - 0.075T_{av.} + 0.000156KT_{av.}^2 ,$$

where $T_{av.}$ is the fraction average boiling point, and K is the characteristic factor calculated based on the fraction density and average boiling point [22].

This formula was chosen because the difference between the calculated and experimental values (determined by the cryoscopic method in a Cryon-1 installation, benzene solvent) did not exceed 10%. For example, for the fraction with boiling points of 400–480°C (sample M1, 5 treatment cycles at a pressure of 50 MPa), the experimental and calculated average molecular weights were 350 and 388 units, respectively.

For all the samples studied, the average molecular weight of the fraction boiling at T_{IBP}–350°C decreased. The molecular weight of fractions with boiling points of 350–400°C remained relatively unchanged. In the case of fractions with high boiling points, the molecular weight increased. For fractions with boiling points above 480°C (residue), the result was consistent with an increase in density.

CONCLUSIONS

The results indicated the effectiveness of a mechanochemical treatment to increase the depth of oil refining (to increase the yield of light and oil fractions). This method has the potential for processing high-viscosity, highly resinous oils. These results also showed that along with cracking reactions, compaction processes also occur, which confirms the data on the occurrence of hydrocarbon cracking reactions under the influence of cavitation reported elsewhere.

Authors' contribution

V.B. Terenteva – conducting the experimental research, determining physicochemical parameters of objects studied and products obtained;

B.V. Peshnev – setting objectives, planning the experimental studies, processing the data obtained, preparation of the data obtained for publication;

A.I. Nikolaev – setting objectives, planning and conducting the experimental research, processing the data obtained, preparation of the data obtained for publication.

The authors declare no conflicts of interest.

REFERENCES

1. Halikova D.A, Petrov S.M., Bashkirtseva N.Y. Review of promising technologies of heavy high-viscisity oils and natural bitumen refinery. *Vestnik Kazanskogo Tehnologicheskogo Universiteta = Bulletin of the Kazan Technological University*. 2013;16(3):217–221 (in Russ.).

2. Muslimov R.H., Romanov G.V., Kayukova G.P., *et al*. *Kompleksnoe osvoenie tyazhelykh neftei i prirodnykh bitumov permskoi sistemy Respubliki Tatarstan* (*Integrated development of heavy oil and natural bitumen of the Perm system of the Tatarstan Republic*). Kazan': FEN; 2012. 396 p. (in Russ.).

3. Muslimov R.Kh., Romanov G.V., Kayukova G.P., Yusupova T.N., Petrov S.M. Oil production prospects. *Vserossiiskii ekonomicheskii zhurnal EKO = ECO Journal.* 2012;(1):35–40 (in Russ.).

4. Galiullin E.A., Fakhrutdinov R.Z. New technologies for processing heavy oils and natural bitumen. *Vestnik technologicheskogo universiteta = Bulletin of the Technological University*. 2016;19(4):47–51 (in Russ.).

5. Shakirzyanova G.I., Sladovskaya O.Yu., Sladovskii A.G., Zimnyakova A.S., Nigmetzyanov N.S. Delayed coking as effective technology of oil refinery deepening. *Vestnik technologicheskogo universiteta = Bulletin of the Technological University.* 2017;20(14):75–78 (in Russ.).

6. Solodova N.L., Terenteva N.A. Current state and development trends of catalytic petroleum cracking. *Vestnik Kazanskogo Tehnologicheskogo Universiteta = Bulletin of the Kazan Technological University.* 2012;15(1):141–147 (in Russ.).

7. Hadzhiev N.S. Nanoheterogeneous catalysis—a new sector of nanotechnology in chemistry and petrochemistry (Review). *Neftekhimiya = Petroleum Chemistry.* 2011;51(1):3–16 (in Russ.).

8. Galimov R.A., Krotov V.V., Mardanshin R.N., Harlampidi H.E., Kutuev A.A. Oil differentiation in a magnetic field. *Vestnik technologicheskogo universiteta = Bulletin of the Technological University.* 2010;(3):467–471 (in Russ.).

9. Mozgovoy I.V., Gryaznov V.A., Mironova E.V., Mozgovoy E.I. Perspective of ultrasound application at pyrolysis. *Omskii nauchnyi vestnik = Omsk Scientific Bulletin.* 2010;3(93):300–303 (in Russ.).

10. Promtov M.A. Prospects of the cavitation technologies application for intensification of chemical technological processes. *Vestnik TGTU = Transactions of the TSTU*. 2008;14(4):861–869 (in Russ.).

11. Promtov M.A. Change in fractional composition of oil in hydro-pulse cavitation cavitation processing. *Vestnik TGTU = Transactions of the TSTU*. 2017;23(3):412–419 (in Russ.). https://doi.org/10.17277/vestnik.2017.03.pp.412-419

12. Besov A.S., Koltunov K.U., Brulev S.O., Kirilenko V.N., Kuzmenkov S.I., Palchikov E.I. Destruction of hydrocarbons in the cavitation area in the electric field upon activation with aqueous solutions of electrolytes. *Pis'ma v ZhTF = Technical Physics Letters*. 2003;29(5):71–77 (in Russ.).

13. Kravchenko O.V. Hydrocarbon compounds physicochemical transformations using new cavitation devices. *Aviatsionno-kosmitcheskaya technika i technologia = Aerospace Engeneering and Technology*. 2007;1(37):65–69 (in Russ.).

14. Bakhtin B.I., Desyatov A.V., Korba O.I., Kubyshkin A.P., Skorokhodov A.S. Low-temperature cracking of hydrocarbons in cavitation ultrasonic fields. Mir nefteproduktov. *Vestnik neftyanykh kompanii = World of Petroleum Products.* 2009;(6):14–19 (in Russ.).

СПИСОК ЛИТЕРАТУРЫ

1. Халикова Д.А., Петров С.М., Башкирцева Н.Ю. Обзор перспективных технологий переработки тяжелых высоковязких нефтей и природных битумов. *Вестник Казанского технологического университета.* 2013;16(3):217–221.

2. Муслимов Р.Х., Романов Г.В., Каюкова Г.П. и др. *Комплексное освоение тяжелых нефтей и природных битумов пермской системы Республики Татарстан.* Казань: ФЭН; 2012. 396 с. ISBN 978-5-9690-0175-8

3. Муслимов Р.Х., Романов Г.В., Каюкова Г.П., Юсупова Т.Н., Петров С.М. Перспективы тяжелых нефтей. *Всероссийский экономический журнал ЭКО*. 2012;(1):35–40.

4. Галиуллин Э.А., Фахрутдинов Р.З. Новые технологии переработки тяжелых нефтей и природных битумов. *Вестник технологического университета*. 2016;19(4):47–51.

5. Шакирзянова Г.И., Сладовская О.Ю., Сладовский А.Г., Зимнякова А.С., Нигметзянов Н.С. Замедленное коксование как эффективная технология углубления переработки нефти. *Вестник технологического университета.* 2017;20(14):75–78.

6. Солодова Н.Л., Терентьева Н.А. Современное состояние и тенденции развития каталитического крекинга нефтяного сырья. *Вестник Казанского технологического университета.* 2012;15(1):141–147.

7. Хаджиев С.Н. Наногетерогенный катализ – новый сектор нанотехнологий в химии и нефтехимии (Обзор). *Нефтехимия*. 2011;51(1):3–16.

8. Галимов Р.А., Кротов В.В., Марданшин Р.Н., Харлампиди Х.Э., Кутуев А.А. Дифференциация нефти в магнитном поле. *Вестник технологического университета.* 2010;(3):467–471.

9. Мозговой И.В., Грязнов В.А., Миронова Е.В., Мозговой Е.И. Перспективы использования ультразвука в пиролизе. *Омский научный вестник*. 2010;3(93):300–303.

10. Промтов М.А. Перспективы применения кавитационных технологий для интенсификации химико-технологических процессов. *Вестник ТГТУ*. 2008;14(4):861–869.

11. Промтов М.А. Изменение фракционного состава нефти при гидроимпульсной кавитационной обработке. *Вестник ТГТУ.* 2017;23(3):412–419. https://doi.org/10.17277/vestnik.2017.03.pp.412-419

12. Бесов А.С., Колтунов К.Ю., Брулев С.О., Кириленко В.Н., Кузьменков С.И., Пальчиков Е.И. Деструкция углеводородов в кавитационной области в присутствии электрического поля при активации водными растворами электролитов. *Письма в ЖТФ*. 2003;29(5):71–77.

13. Кравченко О.В. Физико-химические преобразования углеводородных соединений с использованием новых кавитационных устройств. *Авиационно-космическая техника и технология*. 2007;1(37):65–69.

14. Бахтин Б.И., Десятов А.В., Корба О.И., Кубышкин А.П., Скороходов А.С. Низкотемпературный крекинг углеводородов в кавитационных ультразвуковых полях. Мир нефтепродуктов. *Вестник нефтяных компаний.* 2009;(6):14–19.

15. Иванов С.В., Антонюк Н.С., Луцковская В.А., Кравченко В.В., Воробьев С.И., Торховский В.Н. О возможности увеличения глубины отбора вакуумных дистиллатов при перегонке нефти за счет предварительной механоактивации. *Вестник МИТХТ* (*Тонкие химические технологии*). 2012;7(2):48–50.

15. Ivanov S.V., Antonyuk P.S., Lutskovskaya V.A., Kravchenko V.V., Vorobyov S.I., Torkhovsky V.N. About the possibility of increasing the amount of vacuum gasoil from oil distillation by preliminary mechanical activation of oil. *Tonkie khimicheskie tekhnologii = Fine Chemical Technologies.* 2012;7(2):48–50 (in Russ.).

16. Bhangu S.K., Ashokkumar M. Theory of sonochemistry. *Top. Curr. Chem. (Z)*. 2016;374(4):56. https://doi.org/10.1007/s41061-016-0054-y

17. Avvaru B., Venkateswaran N., Uppara P., Iyengar S.B., Katti S.S. Current knowledge and potential applications of cavitation technologies for the petroleum industry. *Ultrasonics Sonochemistry.* 2018;42:493–507. https://doi.org/10.1016/j.ultsonch.2017.12.010

18. Vorobyev S.I., Torhovsky V.N., Tutorsky I.A., Kazmaly I.K. Mechanodestruction of raw oil hydrocarbons by high-pressure disintegrator. *Tonkie khimicheskie tekhnologii = Fine Chemical Technologies.* 2008;3(3):78–85 (in Russ.).

19. Sirotyuk M.G. *Akusticheskaya kavitatsiya* (*Acoustic cavitation*). Moscow: Nauka; 2008. 271 p. (in Russ.). ISBN 978-5-02-036656-5

20. Smorodov E.A., Galiakhmetov R.N., Il'gamov M.A. *Fizika i khimiya kavitatsii: monografiya* (*Physics and chemistry of cavitation: monograph*). Moscow: Nauka; 2008. 225 p. (in Russ.). ISBN 978-5-02-036626-8

21. Rudin M.G., Somov V.E., Fomin A.S. *Karmannyi spravochnik neftepererabotchika* (*Oil refinery pocket guide*). Moscow: TsNIITEneftekhim; 2004. 336 p. (in Russ.).

22. Glagoleva O.F., Kapustin V.M. *Tekhnologiya pererabotki nefti* (*Oil refining technology*). In 2 v. V. 1. Moscow: Khimiya. KolosS; 2007. 400 p. (in Russ.).

16. Bhangu S.K., Ashokkumar M. Theory of sonochemistry. *Top. Curr. Chem. (Z)*. 2016;374(4):56. https://doi.org/10.1007/s41061-016-0054-y

17. Avvaru B., Venkateswaran N., Uppara P., Iyengar S.B., Katti S.S. Current knowledge and potential applications of cavitation technologies for the petroleum industry. *Ultrasonics Sonochemistry.* 2018;42:493–507. https://doi.org/10.1016/j.ultsonch.2017.12.010

18. Воробьев С.И., Торховский В.Н., Туторский И.А., Казмалы И.К. Механодеструкция углеводородов нефти с помощью дезинтегратора высокого давления. *Вестник МИТХТ* (*Тонкие химические технологии*). 2008;3(3):78–85.

19. Сиротюк М.Г. *Акустическая кавитация*. М.: Наука; 2008. 271 с. ISBN 978-5-02-036656-5

20. Смородов Е.А., Галиахметов Р.Н., Ильгамов М.А. *Физика и химия кавитации: монография*. М: Наука; 2008. 225 с. ISBN 978-5-02-036626-8

21. Рудин М.Г., Сомов В.Е., Фомин А.С. *Карманный справочник нефтепереработчика*. М.: ЦНИИТЭнефтехим; 2004. 336 с.

22. Глаголева О.Ф., Капустин В.М. *Технология переработки нефти*. В 2-х частях. Часть первая. М.: Химия. КолосС; 2007. 400 с.

About the authors:

Vera B. Terenteva, Engineer, The 25-th State Research Institute of Himmotology, Ministry of Defence of the Russian Federation (10, Molodogvardeyskaya ul., Moscow, 121467, Russia). E-mail: terenteva-vb@mail.ru. https://orcid.org/0000-0003-4624-1507

Boris V. Peshnev, Dr. Sci. (Tech.), Professor, A.N. Bashkirov Department of Petrochemical Synthesis and Artificial Liquid Fuel Technology, M.V. Lomonosov Institute of Fine Chemical Technologies, MIREA – Russian Technological University (86, Vernadskogo pr., Moscow, 119571, Russia). E-mail: peshnevbv@mail.ru. https://orcid.org/0000-0002-0507-2754

Alexander I. Nikolaev, Dr. Sci. (Tech.), Professor, A.N. Bashkirov Department of Petrochemical Synthesis and Artificial Liquid Fuel Technology, M.V. Lomonosov Institute of Fine Chemical Technologies, MIREA – Russian Technological University (86, Vernadskogo pr., Moscow, 119571, Russia). E-mail: nikolaev_a@mirea.ru. https://orcid.org/0000-0001-8594-2985

Об авторах:

Терентьева Вера Борисовна, инженер, 25 Государственный научно-исследовательский институт химмотологии Минобороны России (121467, Россия, Москва, ул. Молодогвардейская, д. 10). E-mail: terenteva-vb@mail.ru. https://orcid.org/0000-0003-4624-1507

Пешнев Борис Владимирович, д.т.н., профессор кафедры технологии нефтехимического синтеза и искусственного жидкого топлива им. А.Н. Башкирова Института тонких химических технологий им. М.В. Ломоносова ФГБОУ ВО «МИРЭА – Российский технологический университет» (119571, Россия, Москва, пр-т Вернадского, д. 86). E-mail: peshnev@mirea.ru. https://orcid.org/0000-0002-0507-2754

Николаев Александр Игоревич, д.т.н., профессор кафедры технологии нефтехимического синтеза и искусственного жидкого топлива им. А.Н. Башкирова Института тонких химических технологий им. М.В. Ломоносова ФГБОУ ВО «МИРЭА – Российский технологический университет» (119571, Россия, Москва, пр-т Вернадского, д. 86). E-mail: nikolaev_a@mirea.ru. https://orcid.org/0000-0001-8594-2985

The article was submitted: October 23, 2020; approved after reviewing: December 11, 2020; accepted for publication: October 04, 2021.

Translated from Russian into English by M. Povorin
Edited for English language and spelling by Enago, an editing brand of Crimson Interactive Inc.

CHEMISTRY AND TECHNOLOGY OF MEDICINAL COMPOUNDS AND BIOLOGICALLY ACTIVE SUBSTANCES

ХИМИЯ И ТЕХНОЛОГИЯ ЛЕКАРСТВЕННЫХ ПРЕПАРАТОВ И БИОЛОГИЧЕСКИ АКТИВНЫХ СОЕДИНЕНИЙ

ISSN 2686-7575 (Online)

https://doi.org/10.32362/2410-6593-2021-16-5-399-413

UDC 541.64+678.55+632.952

RESEARCH ARTICLE

Synthesis and properties of vinyl benzyl alcohol copolymers with styrene

Maxim V. Gusarov[1,@], Alexander V. Krylov[1], Elena A. Deshevaya[2], Vladimir A. Tverskoy[1]

[1]MIREA – Russian Technological University (M.V. Lomonosov Institute of Fine Chemical Technologies), Moscow, 119571 Russia
[2]State Scientific Center of the Russian Federation, Institute of Biomedical Problems, Russian Academy of Sciences, Moscow, 123007 Russia
[@]Corresponding author, e-mail: gusarovmv@mail.ru

Abstract

Objectives. *Synthesis and study of the properties of copolymers of vinyl benzyl alcohol (VBA) with styrene with antimicrobial properties.*
Methods. *The study employed infrared (IR) and nuclear magnetic resonance (NMR) spectroscopy, thin-layer chromatography, viscometry, and elemental analysis. The sessile drop method and the pencil method were respectively utilized to determine the contact angles and hardness of the films. The process of testing the film coatings' resistance to the effects of molds consisted of contaminating the film coatings applied to the glass with mold spores of the All-Russian Collection of Microorganisms in a solution of mineral salts without sugar (Czapek–Dox medium).*
Results. *Homopolymers of vinyl benzyl acetate and its copolymers with styrene were synthesized in this study. Homo- and copolymers of VBA were obtained by saponification. IR and proton NMR (^{1}H NMR) spectroscopy determined the composition of the copolymers. Employing IR spectroscopy, the degree of saponification was monitored by the appearance of the hydroxyl group absorption band and the disappearance of the ester group absorption band. According to the IR spectroscopy data, only an insignificant (~3%) amount of ester groups remains in the saponified copolymers. The influence of the copolymers' composition on their solubility in various solvents is demonstrated. IR spectroscopy of the copolymers revealed hydrogen-bond formation between the unreacted ester groups and hydroxyl groups formed due to the saponification. The viscometry of the solutions of mixtures of saponified and unsaponified copolymers, solutions of mixtures of saponified copolymer with polyvinyl acetate, and viscometry of saponified*

copolymers in various solvents all support this conclusion. These bonds' concentration depends on the copolymer's composition and can be controlled by the nature of the solvent from which these copolymers' films are formed. Saponified copolymer solutions form smooth, transparent film coatings with excellent adhesion to metals and silicate glass surfaces. The contact angle of these films, like the hardness, decreases as the VBA units' concentration in the copolymers increases and depends on the solvent polarity used to form the films. It has been demonstrated that increasing the VBA units concentration suppresses the microorganisms' growth.
Conclusions. *Film coatings made of copolymers of styrene with VBA have been shown to have high biocidal activity against molds; can be used to protect structural materials and products from the effects of microorganisms.*

Keywords: *biocidal properties, vinyl benzyl acetate, hydrogen bonds, saponification, film coatings, polyvinyl benzyl alcohol, copolymerization, styrene*

For citation: Gusarov M.V., Krylov A.V., Deshevaya E.A., Tverskoy V.A. Synthesis and properties of vinyl benzyl alcohol copolymers with styrene. *Tonk. Khim. Tekhnol. = Fine Chem. Technol.* 2021;16(5):399–413 (Russ., Eng.). https://doi.org/10.32362/2410-6593-2021-16-5-399-413

НАУЧНАЯ СТАТЬЯ

Синтез и свойства сополимеров винилбензилового спирта со стиролом

М.В. Гусаров[1,@], А.В. Крылов[1], Е.А. Дешевая[2], В.А. Тверской[1]

[1]МИРЭА – Российский технологический университет (Институт тонких химических технологий им. М.В. Ломоносова), Москва, 119571 Россия
[2]Государственный научный центр Российской Федерации, Институт медико-биологических проблем Российской академии наук, Москва, 123007 Россия
[@]Автор для переписки, e-mail: gusarovmv@mail.ru

Аннотация

Цели. *Синтез и изучение свойств сополимеров винилбензилового спирта (ВБС) со стиролом, обладающих антимикробными свойствами.*
Методы. *В работе использованы такие методы как ИК- и ЯМР-спектроскопия, тонкослойная хроматография, вискозиметрия и элементный анализ. Краевые углы смачивания и твердость пленок определяли методом сидячей капли и «методом карандаша», соответственно. Метод испытаний стойкости пленочных покрытий к воздействию плесневых грибов заключался в заражении пленочных покрытий, нанесенных на стекла, спорами плесневых грибов Всероссийской коллекции микроорганизмов в растворе минеральных солей без сахара (среда Чапека-Докса).*
Результаты. *В работе синтезированы гомополимеры винилбензилацетата и его сополимеры со стиролом. Их омылением получены гомо- и сополимеры ВБС. Состав сополимеров определен ИК- и ^{1}Н ЯМР-спектроскопией. Степень омыления контролировали ИК-спектроскопией по появлению полосы поглощения гидроксильной группы и исчезновению полосы*

поглощения сложноэфирной группы. По данным ИК-спектроскопии в омыленных сополимерах остается лишь незначительное (~3%) количество сложноэфирных групп. Показано влияние состава сополимеров на их растворимость в растворителях различной природы. ИК-спектроскопией сополимеров показано образование водородных связей между непрореагировавшими сложноэфирными группами и образовавшимися в результате омыления гидроксильными группами. Этот вывод подтвержден вискозиметрией растворов смесей омыленного и неомыленного сополимеров, растворов смесей омыленного сополимера с поливинилацетатом и вискозиметрией омыленных сополимеров в растворителях различной природы. Концентрация этих связей зависит от состава сополимера и может регулироваться природой растворителя, из которого формируются пленки этих сополимеров. Из растворов омыленных сополимеров формируются гладкие прозрачные пленочные покрытия с высокой адгезией к поверхностям металлов и силикатного стекла. Краевой угол смачивания этих пленок, как и твердость, уменьшается с увеличением концентрации в сополимерах звеньев ВБС и зависит от полярности растворителя, из раствора в котором сформированы пленки. Показано, что увеличение концентрации звеньев ВБС приводит к подавлению роста микроорганизмов.

Выводы. *Показано, что пленочные покрытия из сополимеров стирола с ВБС обладают высокой биоцидной активностью по отношению к плесневым грибам и могут быть использованы для защиты конструкционных материалов и изделий из них от воздействия микроорганизмов.*

Ключевые слова: *биоцидные свойства, винилбензилацетат, водородные связи, омыление, пленочные покрытия, поливинилбензиловый спирт, сополимеризация, стирол*

Для цитирования: Гусаров М.В., Крылов А.В., Дешевая Е.А., Тверской В.А. Синтез и свойства сополимеров винилбензилового спирта со стиролом. *Тонкие химические технологии*. 2021;16(5):399–413. https://doi.org/10.32362/2410-6593-2021-16-5-399-413

INTRODUCTION

The synthesis and investigation of the properties of polymers containing functional groups of diverse nature with antimicrobial properties have piqued the interest of researchers in recent years, as summarized in reviews and monographs [1–9]. Unlike low molecular weight compounds, polymer biocides allow the formation of protective films that are resistant to microorganism colonization, and they do not "sweat out" the biocide. The biocidal properties of such polymers should, of course, depend on the concentration of the functional groups that provide these properties. In most cases, these polymers are obtained by chemically modifying precursor polymers containing functional groups that can be converted through chemical reactions into biocidal ones or introducing groups with biocidal properties into the structure of a macromolecule [10].

Phenols, other aromatic alcohols, and their derivatives are known to have a broad spectrum of biocidal action [11]. Carbon-chain polymers containing phenolic groups can only be obtained through chemical modification, which is associated with the inhibition of polymerization of monomers containing groups of aromatic phenols and a benzyl alcohol group with properties similar to them. Thus, in [12–16], polymers containing units of vinyl benzyl alcohol (VBA) were obtained by chemical modification of polymers containing units of vinyl benzyl chloride (VBC). The modification included the acylation of the polymers' benzyl chloride groups with potassium acetate, followed by their saponification with the VBC units formation. However, according to [14–16], intermolecular simple ether bonds are formed in polymers with a high content of chloromethyl groups, resulting from saponification, and benzyl alcohol groups, resulting from the interaction of residual chloromethyl groups with benzyl alcohol groups. It was proposed in [17] that obtaining copolymers of VBA by copolymerization of vinyl benzyl acetate (VBAc) followed by saponification of these copolymers will lead to excluding the formation of these intermolecular bonds.

This study employed this method to synthesize polyvinyl benzyl alcohols and copolymers of VBA with styrene and study their properties.

EXPERIMENTAL

Materials

VBC (*Sigma-Aldrich*, USA), which is a mixture of *m*-(60%) and *p*-isomers (40%) stabilized with 4-*tert*-butylpyrocatechin (*Sigma-Aldrich*), is used for VBA synthesis without additional purification.

Styrene, *pur.* (*Angara-Reaktiv*, Russia), was washed from hydroquinone using a 30% aqueous solution of caustic potassium, washed with water from excess alkali to a neutral reaction of washing waters, dried over calcined calcium chloride, and distilled under vacuum, selecting a fraction at 46°C and a pressure of 30 mm Hg.

Potassium acetate, *puriss.* (*Reachim*, Russia), was drained by azeotropic distillation of water with benzene.

Dimethyl sulfoxide (DMSO), *puriss*. (*Chimmed*, Russia), was dried by holding over calcined calcium chloride for several days, then held over calcium hydride for 6 h at 80°C, followed by distillation over a fresh portion of calcium hydride at 130°C and a residual pressure of 25 mm Hg.

Before use, azobisisobutyronitrile (AIBN) was recrystallized from methyl alcohol.

The remaining reagents and solvents were used without additional purification because they were purely reactive.

Methods of analysis

Using ^{1}H NMR and IR spectroscopy, the composition of VBAc copolymers with styrene and the degree of their saponification were calculated. The ^{1}H NMR spectra of the VBAc copolymer solutions in C_6D_6 and VBA copolymers in DMSO-d_6 were recorded on a DPX-300 spectrometer (*Bruker,* Germany). Quantitative processing of ^{1}H NMR spectra was carried out in the MestReNova program[1]. IR spectroscopic studies were performed on an Equinox 55 spectrometer (*Bruker*) in KBr tablets and polymer films formed on germanium plates.

Viscometric measurements were conducted in a Ubbelohde viscometer at 30°C.

Films were formed from polymer solutions on silicate glass substrates to determine the film coatings' hardness, the wetting edge angles, and the resistance of these films to the effects of mold fungi.

The wetting edge angles at the sample-water-air interface were determined by the sedentary drop method.

The films' hardness was determined by the pencil method [18] according to GOST P 54586-2011 (ISO 15184:1998)[2].

The film coatings' resistance to the effects of mold fungi was evaluated using mold fungi of the All-Russian Collection of Microorganisms of the following species according to GOST 9.049-91[3] (method 1): *Aspergillus niger van Tieghem*, VKM F-1119; *Aspergillus terreus Thom*, VKM F-1025; *Aspergillus oryzae (Ahlburg) Cohn*, VKM F-55; *Chaetomium globosum Kunze*, VKM F-109; *Paecilomyces varioti Bainier*, VKM F-378; *Penicillium funiculosum Thom*, VKM F-1115; *Penicillium chrysogenum Thom*, VKM F-245; *Penicillium cyclopium Westling*, VKM F-265; *Trichoderma viride Pers. ex S. F. Gray*, VKM F-1117.

In the absence of mineral and organic contaminants, this method establishes the materials' fungus resistance and their components. An association of fungal spores with a concentration of $9 \cdot 10^6$ in 1 mL ($1 \cdot 10^6$ in 1 mL of each type of spore) was used for infection.

The films were tested using the following method, which establishes the mushroom resistance of the materials in the absence of mineral and organic contaminants under optimal conditions for the mold fungi development, but without an additional power source.

The test method consisted in infecting the film coatings applied to the glass with mold fungi spores in a solution of mineral salts without sugar (Chapek–Doks medium). As a result, fungi could only grow in the nutrients contained in the material.

Infection of samples in sterile Petri dishes was carried out by evenly applying a prepared suspension of fungal spores to the surface of the dishes. The open Petri dishes with samples were kept for 28 days, after which the content and composition of microorganisms were taken into account on experimental samples according to the six-point scale (GOST 9.049-91) given in Table 1.

Synthesis methods

The acylation of VBC was done using a method similar to that described in [12, 19]. DMSO (85 mL), VBC (34 mL, 0.24 mol), and potassium acetate

[1] Mestrelab Research S.L. https://mestrelab.com/

[2] GOST P 54586-2011 (ISO 15184:1998). Paints and varnishes. Determination of film hardness by pencil test. Moscow: Standartinform; 2012.

[3] GOST 9.049-91 (Method 1). Unified system of corrosion and ageing protection. Polymer materials and their components. Methods of laboratory tests for mould resistance. Moscow: Izd. Standartov; 1992.

Table 1. Scale of fungi growth in scores

Score	Score characteristic
0	Mold growth is not visible when viewed under a microscope
1	When viewed under a microscope, germinated spores and slightly developed mycelium in the form of unbranched hyphae are visible
2	When viewed under a microscope, mycelium is visible in the form of branching hyphae, sporulation is possible
3	When viewed with the naked eye, fungal growth is barely visible, but clearly visible under a microscope
4	When viewed with the naked eye, the growth of fungi is clearly visible, covering less than 25% of the tested surface
5	When viewed with the naked eye, the growth of fungi is clearly visible, covering more than 25% of the tested surface

(27 g, 0.28 mol) were sequentially loaded into a flask and stirred for 48 h at 40°C. The filtered acetate and potassium chloride solution was then poured into 300 mL of water, and VBAc was extracted with ethyl acetate. The extract was rinsed with a 3% sodium bicarbonate aqueous solution and dried over sodium sulfate. After removal at a reduced pressure of ethyl acetate, an oily brown product was obtained. The precipitate of 4-*tert*-butylpyrocatechin released from the product was removed from the filter after it was diluted with hexane. The resulting VBAc was separated from the unreacted VBC on a chromatographic column (silica gel, hexane–ethyl acetate 5:1 mixture). Hexane and ethyl acetate were removed on a rotary evaporator. The VBAc had a 65% yield. Elemental analysis, thin-layer chromatography, and IR spectroscopy all confirmed the absence of VBC in the product. In the IR spectrum, there are no bands of valence vibrations of the C–Cl bond at ν = 683 cm^{-1} and fan deformation vibrations of the CH_2Cl group δ = 1266 cm^{-1}. In turn, the appearance in the IR spectrum of the product of valence vibrations of the ester group ν = 1745 cm^{-1} confirms the presence of acetate groups in the reaction products.

VBAc polymerization and its copolymerization with styrene were carried out at 70°C in benzene in nitrogen-purged ampoules with a total concentration of monomers of 1.75 mol/L. AIBN (3.00 mol % relative to the total concentration of monomers) was employed as the initiator. Polymers from the solution were precipitated with isopropyl alcohol at the end of copolymerization and re-precipitated from the solution in benzene with isopropyl alcohol. The resulting white polymers were vacuum dried to a constant mass at 50°C.

Saponification of the obtained VBAc copolymers with styrene and polyvinyl benzyl acetate (PVBAc) was carried out with sodium hydroxide in a mixture of 1,4-dioxane with water (2/1 by volume) at 80°C for 20 h while stirring the solution with a magnetic stirrer. At the end of the process, the polymers were precipitated from the solution with a weak hydrochloric acid solution, repeatedly washed with this solution, vacuum dried at room temperature to a constant mass.

RESULTS AND DISCUSSION

The copolymerization constants of styrene and VBAc were calculated using the Feineman–Ross method for the compositions of copolymers determined by ^{1}H NMR spectroscopy at low (up to 10%) conversion of monomers.

In the ^{1}H NMR spectrum, the signals of proton-containing PVBAc groups (Fig. 1) represent broadened signals that is characteristic for polymers. The signals of the methylene (CH_2) and methine (CH) groups of the macromolecule's main chain are manifested in the region δ = 1.58–2.04 ppm. The signals of acetate groups (CH_3) δ = 1.87 ppm fall

into the same region, which makes it possible to determine the ratio of phenyl and phenyl acetate units in the copolymer using the ^{1}H NMR method. The signals of –CH_2– groups of benzyl acetate fragments are significantly shifted to the low-field region and manifest themselves at δ = 5.1 ppm. Additionally, the ratio of units in the copolymer was checked analyzing the material balance using the signals of the aromatic ring protons in the region δ = 6.71–7.57 ppm.

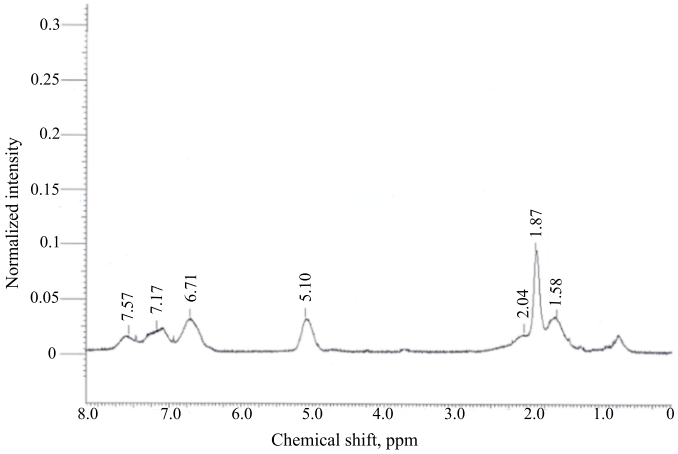

Fig. 1. ^{1}H NMR spectrum of PVBAc in C_6D_6.

The values of copolymerization constants found were r_1 = 0.9 and r_2 = 1.0, and they were close to the values of these constants previously determined using the Kelen–Tudosh method [17]: r_1 = 0.78 and r_2 = 1.33. In this study, polymerization was conducted in toluene at 60°C.

The close reactivity of these monomers under the copolymerization conditions adopted in this study made it possible to synthesize copolymers whose macromolecules differ little in composition regardless of the degree of monomer conversion. These copolymers dissolve in the same solvents as polystyrene: in benzene, toluene, 1,4-dioxane, tetrahydrofuran, chloroform, acetone, and *N,N*-dimethylformamide (DMFA), and do not dissolve in lower alcohols and water. Unlike polystyrene, copolymers containing from 28 to 84 mol % of VBAc units are dissolved in DMSO.

IR spectroscopy of PVBAc and VBAc copolymers with styrene of various compositions confirmed the data obtained using ^{1}H NMR spectroscopy.

The analysis of the IR spectra of these polymers showed that the position of the valence vibration band of the carbonyl group ν(C=O) in the VBAc units varied depending on the content of these units in the copolymer. Thus, in the IR spectra of PVBAc and a copolymer containing 84 mol % of VBAc units, there was one band at 1737 cm^{-1} (Fig. 2a and 2b). With a decrease in the content of VBAc units in the copolymer to 52 mol %, this band split into two bands with maxima at 1746 and 1728 cm^{-1} (Fig. 2c).

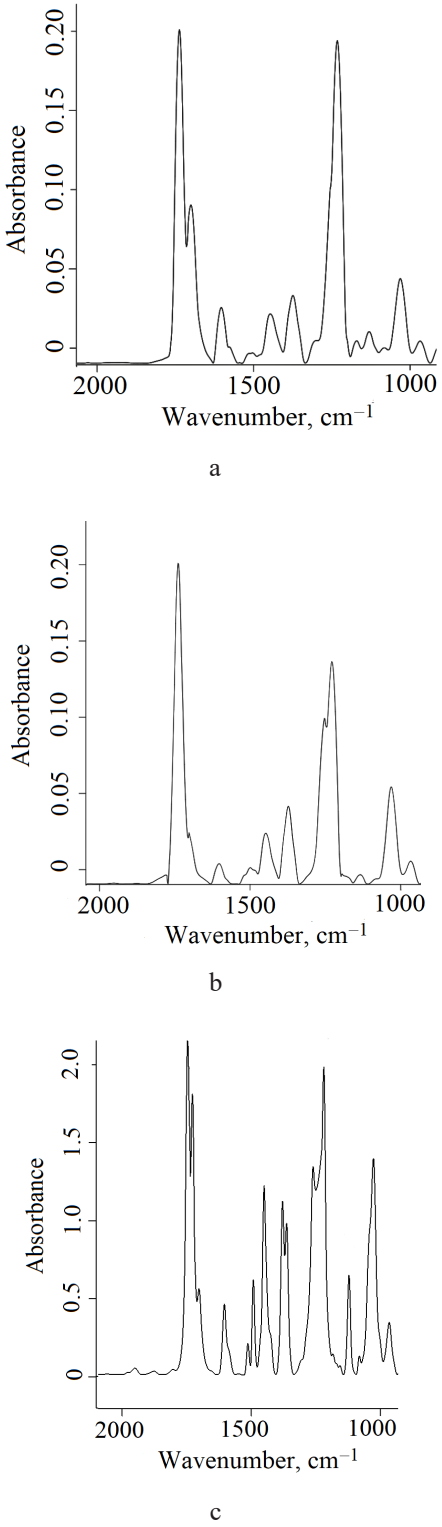

Fig. 2. IR spectrum of (a) PVBAc, (b) styrene copolymers with VBAc containing 84 mol % and (c) 52 mol % of VBAc units.

The position of the valence vibration band of the ether group also changed. In PVBAc and a copolymer containing 84 mol % of VBAc units, this band had a maximum at 1031 cm^{-1} (Figs. 2a and 2b). In the IR spectrum of a copolymer containing 52 mol % of VBA units, this maximum shifted to 1027 cm^{-1} (Fig. 2c).

It is possible that this shift and splitting of the vibration band of the carbonyl group are associated with a change in the macromolecule conformation caused by a change in the balance of hydrophobic (styrene) and hydrophilic (VBAc) units in it.

As described in Experimental, the saponification of ester groups in the synthesized VBAc copolymers with styrene and PVBAc was conducted with sodium hydroxide in a solution of an 1,4-dioxane/water mixture at 80°C for 20 h with a significant excess of alkali in relation to the number of acetate groups. Table 2 shows the ratios of the concentrations of copolymers and alkali solution and the yields of the saponified copolymers obtained.

The solubility of saponified copolymers in various solvents depends on their composition (Table 3). They do not dissolve in water and dissolve in such highly polar organic solvents as DMFA and DMSO. Saponified copolymers containing less than 60 mol % of styrene units do not dissolve in benzene and toluene. All unsaponified copolymers do not dissolve in lower alcohols. On the contrary, copolymers with a high content of VBA units (more than 62 mol %) acquire solubility in them after saponification.

In ^{1}H NMR spectra in DMSO-d_6 (Fig. 3) obtained by saponification of copolymers, positions of the CH_2 and CH groups' signals in the main chain of the macromolecule changed little compared to unsaponified samples and were manifested in the region δ = 1.42–2.04 ppm. The chemical shifts of protons of the phenyl groups were observed in the region δ = 6.54–7.56 ppm. The most significant change was observed for the signal –CH_2– group benzyl acetate fragment, the chemical shift of which moved from δ = 5.10 to 4.40 ppm due to the lower polarity of the hydroxyl group in comparison with the acetate group.

IR spectra of saponified copolymers confirmed the data of ^{1}H NMR spectroscopy. In the IR spectra of saponified copolymers (Fig. 4), compared with the considered spectra of unsaponified copolymers (Fig. 2), there were a wide valence vibration band (3442–3355 cm^{-1}) and an in-plane deformation vibration band (1374–1368 cm^{-1}) of the benzyl alcohol hydroxyl group. In the spectrum, a band of 1122 cm^{-1} corresponding to valence vibrations of the C–O bond in alcohols appeared, whereas the bands of 1746–1728 cm^{-1} related to vibrations of the carbonyl group practically disappeared. This allows concluding that there is a high degree of saponification in all the copolymers obtained and a low concentration of residual acetate groups in them.

The appearance of a band with a maximum of ~1700–1691 cm^{-1} in the spectra of saponified copolymers suggests the presence of intermolecular and intramolecular hydrogen bonds between the carbonyl group of unsaponified chain units with the hydroxyl group of VBA units. Moskala [20] observed such a low-frequency shift of the carbonyl group band in the IR spectra of a mixture of polyvinylphenol (PVP) with polyvinyl acetate (PVA). The valence vibration band of the PVA carbonyl group had a maximum of 1739 cm^{-1}. When mixing PVA with PVP, a shift of this band to 1714 cm^{-1} was observed. The intensity of this band increased with an increase in the content of PVP. This band refers to the valence vibrations of the carbonyl group bound via a hydrogen bond with the hydroxyl group of phenol.

Table 2. Conditions for the saponification of PVBAc and VBAc copolymers with styrene and the yields of saponified copolymers

Copolymers' composition, mol % of units		Number of VBAc units, mmol of units	NaOH quantity, mmol	[NaOH]/[VBAc], mmol/mmol of units	H_2O volume, mL	1,4-Dioxane volume, mL	Yield, %
Styrene	VBAc						
82	18	1.5	15.1	10.1	9.3	18.6	81
60	40	3.0	30.0	10.0	60.0	120.0	52
48	52	2.4	24.3	10.1	5.5	11.0	79
38	62	4.2	20.9	4.9	8.3	16.6	80
16	84	5.2	25.8	5.0	8.3	16.6	99
0	100	1.1	5.6	5.1	1.7	3.4	49

Table 3. Solubility of styrene copolymers with VBAc and with VBA in solvents of various nature ("+" is soluble, "–" is insoluble)

Copolymer form	Copolymer composition, mol % of units			Solvents											
	Styrene	VBAc	VBA	1,4-Dioxane	Benzene	Toluene	Chloroform	Tetrahydrofuran	Isopropanol	Acetone	Ethanol	Methanol	DMFA	DMSO	Water
–	100	0	0	+	+	+	+	+	–	+	–	–	+	–	–
Acetate	82	18	–	+	+	+	+	+	–	+	–	–	+	–	–
Saponified		2	16	+	+	+	+	+	–	+	–	–	+	+	–
Acetate	60	40	–	+	+	+	+	+	–	+	–	–	+	+	–
Saponified		2	38	–	–	–	–	–	–	–	–	–	+	+	–
Acetate	48	52	–	+	+	+	+	+	–	+	–	–	+	+	–
Saponified		7	45	+	–	–	+	+	–	+	–	–	+	+	–
Acetate	38	62	–	+	+	+	+	+	–	+	–	–	+	+	–
Saponified		3	59	+	–	–	+	+	+	+	+	+	+	+	–
Acetate	16	84	–	+	+	+	+	+	–	+	–	–	+	+	–
Saponified		3	81	+	–	–	–	+	+	+	+	+	+	+	–
Acetate	0	100	–	+	+	–	+	+	–	+	–	–	+	–	–
Saponified		3	97	+	–	–	–	+	–	–	+	+	+	+	–
Dielectric constant				2.2	2.3	2.4	4.7	7.6	18.3	20.9	24.3	32.6	36.7	45.0	81.0

Comparison of the IR spectra of saponified copolymers showed that with increasing the saponified units' content in the copolymer, the maximum friequency of the valence vibration band of the –OH group in the region ν = 3500–3100 cm^{-1} shifted to lower frequencies (Fig. 5), indicating the formation of more strong hydrogen bonds involving hydroxyl groups. The reduction in the width of this band in its half-height indicates an increase in the exchange rate between free and associated hydroxyl groups.

In the IR spectra of saponified copolymers with a low (16 mol %) content of VBA units, there is a band of 3583 cm^{-1} (Fig. 6) related to vibrations in free nonhydrogen-bonded –OH groups, whereas is no this band in the spectra of copolymers with a high (81 mol %) content of these units (Fig. 4b).

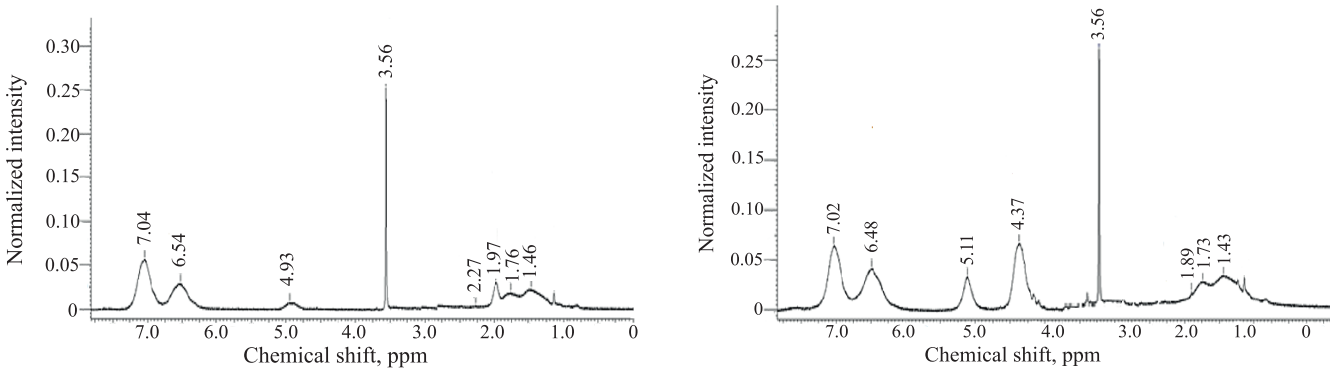

a b

Fig. 3. ^{1}H NMR spectra of dissolved in DMSO-d_6 (a) styrene copolymers (82 mol %) containing VBAc (2 mol %) and VBA (16 mol %) units and (b) VBAc copolymers (3 mol %) containing VBA (97 mol %) units.

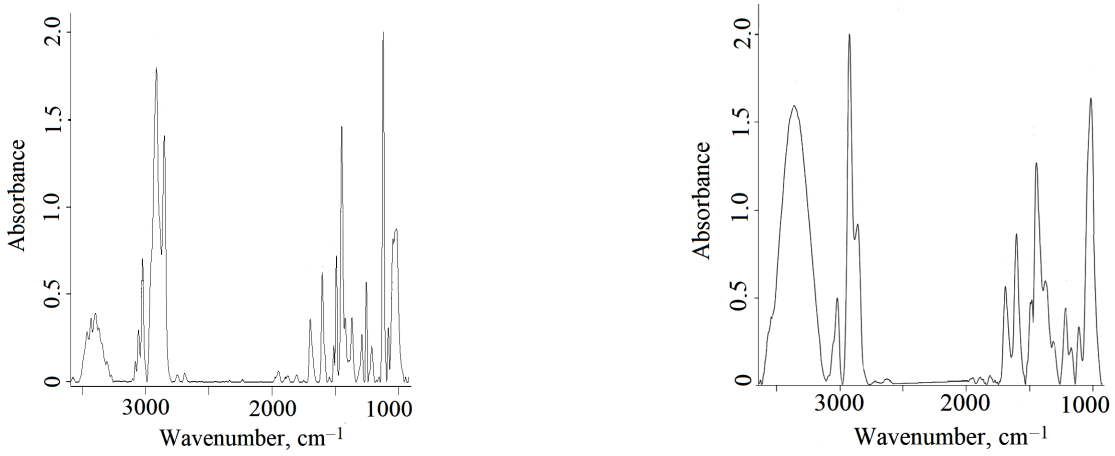

a b

Fig. 4. IR spectra of (a) styrene copolymers (48 mol %) containing VBAc (7 mol %) and VBA (45 mol %) units and (b) styrene copolymers (16 mol %) containing VBAc (3 mol %) and VBA (81 mol %) units.

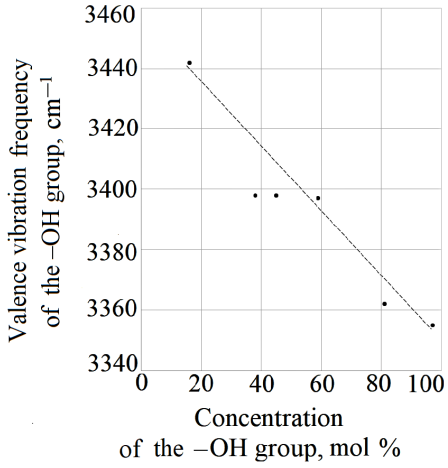

Fig. 5. Dependence of the maximum of the 3442–3355 cm^{-1} band in the IR spectra of saponified VBAc copolymers with styrene on the content of VBA units in them.

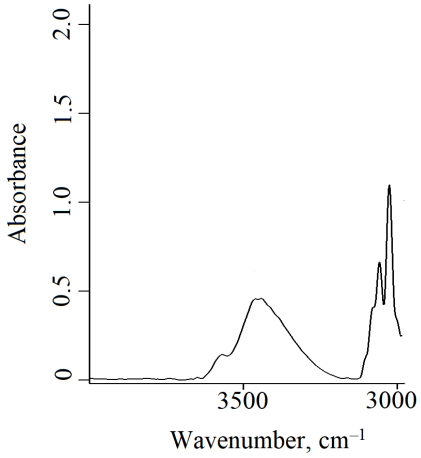

Fig. 6. IR spectrum of the styrene copolymers (82 mol %) containing VBAc (2 mol %) and VBA (16 mol %) units.

The formation of hydrogen bonds between the hydroxyl and carbonyl groups in these copolymers was confirmed using IR spectroscopy of a mixture of saponified (60%) and unsaponified (40%) copolymers with a low (16 mol %) content of styrene units (Fig. 7). In comparison with the IR spectrum of the saponified copolymer, the maximum of the valence vibration band was strongly shifted to the low-frequency region in the spectrum of the mixture: from 3442 cm^{-1} in the spectrum of the saponified copolymer to 3387 cm^{-1} in the spectrum of the polymer mixture.

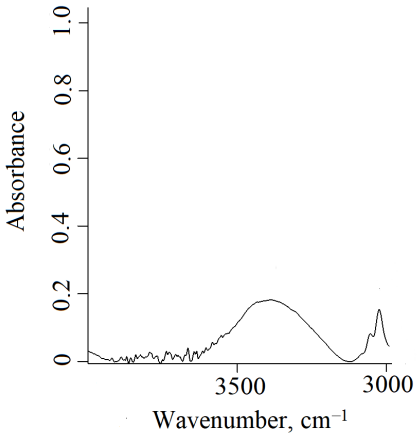

Fig. 7. IR spectrum of the mixture of saponified (60%) and unsaponified (40%) VBAc copolymers containing 16 mol % of styrene units.

A similar low-frequency shift of this band was observed in the IR spectrum of a saponified copolymer and PVA mixture (Fig. 8). These conclusions are consistent with the results of the study [20] on inter and intramolecular interactions in a mixture of PVP–PVA.

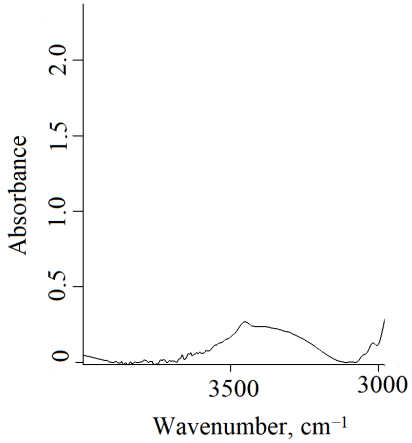

Fig. 8. IR spectrum of the mixture of saponified VBAc copolymers containing 16 mol % of styrene (40%) with PVA (60%) units.

The conclusion about the formation of intermolecular hydrogen bonds was confirmed using the viscometry of the copolymer mixtures' solutions before and after saponification and by the dependence of the reduced viscosity on the concentration of copolymer solutions with a high content of VBA units.

Figure 9 shows the dependence of the reduced viscosity of the solutions of saponified and unsaponified copolymer mixtures (containing 16 mol % of styrene units) on the composition of these mixtures and a similar dependence for mixtures of the same saponified copolymer with PVA. The deviation of these graphs upwards from additivity indicates clearly the formation of intermolecular bonds in the solutions of these polymer mixtures.

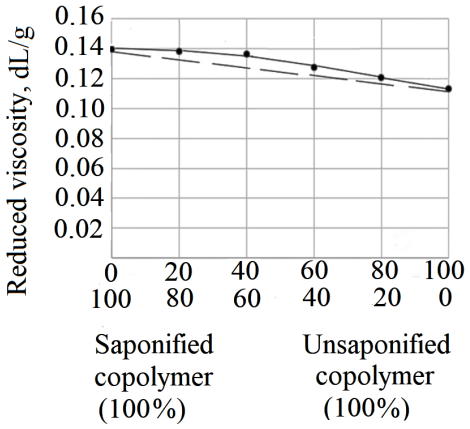

a

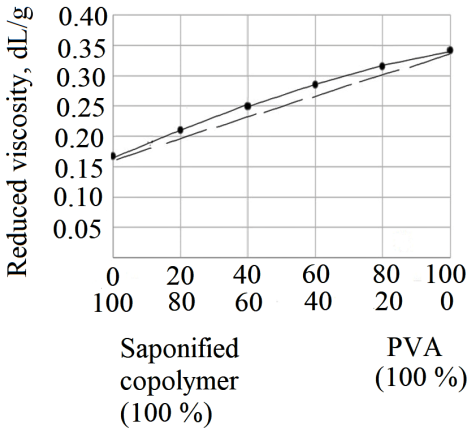

b

Fig. 9. Dependence of the reduced viscosity of the solutions on the composition of (a) saponified and unsaponified copolymer mixtures containing 16 mol % of styrene units, and (b) saponified copolymer mixtures containing 16 mol % of styrene units with PVA. The solvent is 1,4-dioxane, 30°C. The concentration of the polymer mixture, g/dL: (a) 1 and (b) 2.

The viscometry of saponified copolymer solutions in various solvents also indicated the formation of intermolecular hydrogen bonds in them (Fig. 10). The dependencies of the reduced viscosity on the concentration of the solutions of polystyrene and copolymers with a high content of styrene units in benzene are linear (Fig. 10a). In a nonpolar solvent, such as benzene, macromolecules of copolymers have a conformation in which the VBA units are located inside the tangle of the macromolecule. These dependencies are also linear for the solutions of polystyrene and copolymer with a high (48 mol %) content of styrene units in 1,4-dioxane (Fig. 10b). However, for the solutions of copolymers with a low (16 mol %) content of styrene units and a copolymer that does not contain styrene units, these dependencies are nonlinear. There is an increase in the reduced viscosity associated with the formation of intermolecular hydrogen bonds. These dependencies for the solutions of copolymers with a high content of VBA units in isopropanol have similar forms (Fig. 10c).

As the result, hydrogen bonds between both hydroxyl and hydroxyl and carbonyl groups are realized in the VBA copolymers. The concentration of these bonds depends on the composition of the copolymer and can be regulated by the solvent from which the films of these copolymers are formed.

Solutions of VBA and styrene copolymers form smooth rigid transparent colorless film coatings with high adhesion to metal and silicate glass surfaces.

Table 4 shows that the films' wetting contact angles characterizing the hydrophobicity of their surface decrease with increasing the concentration of VBA units in the polymers. The wettability of the films depends on the solvent from which the films were formed. The contact angles of the films with a high content of VBA hydrophilic units and a low (16 mol %) content of styrene units were higher when forming films from a solution in 1,4-dioxane (dielectric constant is 2.2) than when forming from solutions in a more polar solvent—isopropyl alcohol (dielectric constant is 18.3). Such a change in the contact angle is due to the dependence of the macromolecule conformation on the solvent, which leads to a change in the concentration of VBA hydrophilic groups on the surface of the macromolecule tangle, i.e., their concentration is higher when the formation of films from a solution in isopropyl alcohol.

Such a change in the conformation of macromolecules is reflected in the hardness of the formed films too. Table 4 shows that the film formed from a solution in isopropanol had a lower hardness than the film formed from a solution in 1,4-dioxane. As expected, for films formed from the same solvent (1,4-dioxane), the polystyrene film has the highest hardness. The hardness decreases wth an increase in the VBA units' concentration in the polymer.

Table 5 shows the results of microbiological tests of the saponified VBAc copolymers with styrene. Polystyrene had low fungicidal activity (fungi growth is 3 points). The introduction of even a small concentration

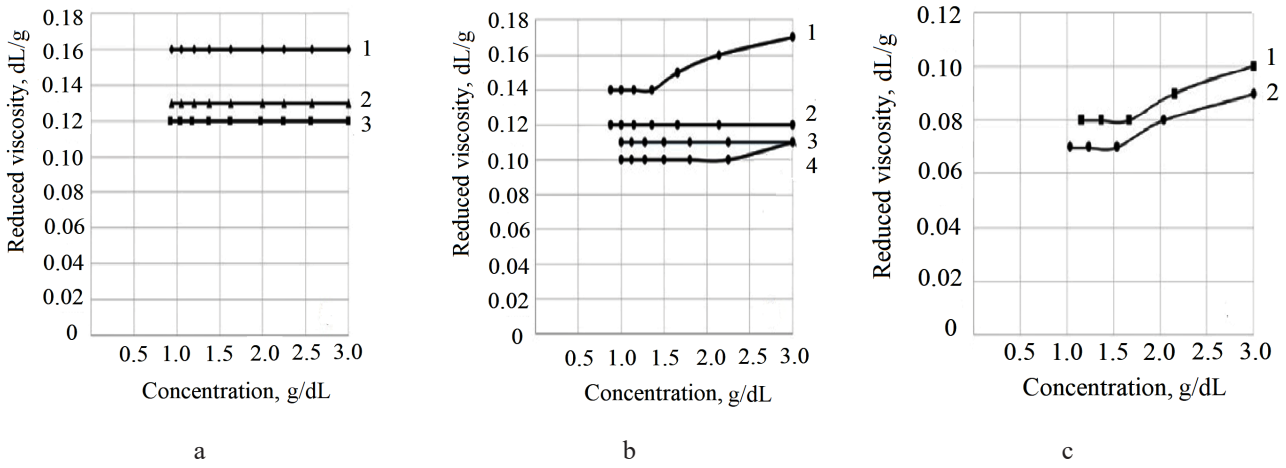

Fig. 10. Dependence of the reduced viscosity on the concentration of solutions of styrene copolymer with VBA at 30°C in (a) benzene, (b) 1,4-dioxane, and (c) isopropanol.
(a): 1–polystyrene; 2–styrene copolymer (48 mol %) with VBAc (7 mol %) and VBA (45 mol %) units; 3–styrene copolymer (82 mol %) with VBAc (2 mol %) and VBA (16 mol %) units.
(b): 1–VBAc copolymer (3 mol %) with VBA (97 mol %) units; 2–styrene copolymer (48 mol %) with VBAc (7 mol %) and VBA (45 mol %) units; 3–polystyrene; 4–styrene copolymer (16 mol %) with VBAc (3 mol %) and VBA (81 mol %) units.
(c): 1–styrene copolymer (16 mol %) with VBAc (3 mol %) and VBA (81 mol %) units; 2–styrene copolymer (38 mol %) with VBAc (3 mol %) and VBA (59 mol %) units.

Table 4. Contact angles and the hardness of saponified VBA c copolymers' films with styrene

Content of styrene units in the copolymer, mol %	Solvent	Contact angle of wetting, degree	Hardness
100	1,4-dioxane	90	H
82		85	
48		80	
38		77	
16			HB
0			
16	Isopropanol	62	B

Table 5. Fungi growth on film coatings of the styrene copolymers with VBA of various compositions, in scores

Styrene copolymers with VBAc and VBA units, mol %			Fungi growth, scores
Styrene	VBAc	VBA	
100	0	0	3
82	2	16	1
48	7	45	0
38	3	59	
16	3	81	
0	3	97	

of VBA units (16 mol %) into the composition of a macromolecule led to an increase in the copolymer biocidal activity. A further increase in the VBA units' concentration in the copolymer (45 mol % or more) led to complete suppression of the microorganisms' growth.

Thus, the styrene copolymers with VBA units are effective biocides that inhibit the growth of mold fungi.

CONCLUSIONS

It has been demonstrated that copolymerization of VBAc followed by saponification of ester groups in these copolymers yields soluble VBA copolymers in a wide range of compositions. Saponification occurs quantitatively in mild conditions. ^{1}H NMR and IR spectroscopy established the structure of styrene copolymers with VBAc and these copolymers, after saponification of the ester groups of the VBAc units with the formation of the VBA units.

IR spectroscopy of copolymers and the viscometry of the solutions of saponified and unsaponified copolymers mixtures, solutions of mixtures of saponified copolymer with PVA, and viscometry of saponified copolymers in different solvents reveal that the hydroxyl groups in these saponified polymers form inter and intramolecular hydrogen bonds when interacting with each other and carbonyl groups of ester groups of unreacted VBA units.

It is shown that all saponified copolymers form smooth, transparent film coatings on metals and silicate glass. The hardness and edge angle of wetting of these films decreases with increasing concentration in the copolymer of the VBA units and depends on the solvent's polarity from which the films are formed. In terms of mold fungi, these coatings have high biocidal activity.

Authors' contribution

M.V. Gusarov– design and conducting the experiments, discussion of the results;

A.V. Krylov – NMR spectrometry studies, data processing;

E.A. Deshevaya – evaluation of the microbiological properties of compounds according to GOST 9.049-91;

V.A. Tverskoy – development of a research concept, consultation during individual stages of the research, data processing.

The authors declare no conflicts of interest.

REFERENCES

1. Afinogenov G.E., Panarin E.F. *Antimikrobnye polimery* (*Antimicrobial polymers*). St. Peterburg: Gippokrat; 1993. 264 p. (in Russ.). ISBN 5-8232-0116-8

2. Timofeeva L., Kleshcheva N. Antimicrobial polymers: mechanism of action, factors of activity, and applications. *Appl. Microbiol. Biotechnol.* 2011;89(3):475–492. https://doi.org/10.1007/s00253-010-2920-9

3. Tashiro T. Antibacterial and Bacterium Absorbing Macromolecules. *Macromol. Mater. Eng.* 2001;286(2):63–87. https://onlinelibrary.wiley.com/doi/10.1002/1439-2054(20010201)286:2%3C63::AID-MAME63%3E3.0.CO;2-H

4. Kenawy E.-R., Worley S.D., Broughton R. The Chemistry and Applications of Antimicrobial Polymers: A State-of-the-Art Review. *Biomacromolecules*. 2007;8(5):1359–1384. https://doi.org/10.1021/bm061150q

5. Gilbert P., Moore L.E. Cationic Antiseptics: Diversity of Action under a Common Epithet. *J. Appl. Microbiol.* 2005;99(4):703–715. https://doi.org/10.1111/j.1365-2672.2005.02664.x

6. Kaur R., Liu S. Antibacterial surface design-Contact kill. *Prog. Surf. Sci.* 2016;91(3):136–153. https://doi.org/10.1016/j.progsurf.2016.09.001

7. Siedenbiedel F., Tiller J.C. Antimicrobial Polymers in Solution and on Surfaces: Overview and Functional Principles. *Polymers.* 2012;4(1):46–71. https://doi.org/10.3390/polym4010046

8. Tiller J.C. Antimicrobial Surfaces. In: Börner H., Lutz JF. (Eds.). Bioactive Surfaces. *Advances in Polymer Science.* 2011;240:193–217. https://doi.org/10.1007/12_2010_101

9. Chen A., Peng H., Blakey I., Whittaker A.K. Biocidal Polymers: A mechanistic overview. *Polym. Rev.* 2017;57(2):276–310. https://doi.org/10.1080/15583724.2016.1223131

10. Kenawy E.-R., Abdel-Hay F., El-Newehy M., El-Zaher E.H.F.A., Ibrahim E.M.A.-E. Novel biocidal polymers based on branched and linear poly(hydroxystyrene). *Int. J. Polym. Mater.* 2016;65(14):712–719. https://doi.org/10.1080/00914037.2016.1163563

11. McDonnel G., Russell A.D. Antiseptics and Disinfectants: Activity, Action, and Resistance. *Clin. Microbiol. Rev.* 1999;12(1):147–179. https://doi.org/10.1128/CMR.12.1.147

12. Bamford C.H., Lindsay H. Introduction of hydroxymethyl groups into polystyrene and styrene. *Polymer*. 1973;14(7):330–332. https://doi.org/10.1016/0032-3861(73)90128-6

СПИСОК ЛИТЕРАТУРЫ

1. Афиногенов Г.Е., Панарин Е.Ф. *Антимикробные полимеры.* СПб.: Гиппократ; 1993. 264 с. ISBN 5-8232-0116-8

2. Timofeeva L., Kleshcheva N. Antimicrobial polymers: mechanism of action, factors of activity, and applications. *Appl. Microbiol. Biotechnol.* 2011;89(3):475–492. https://doi.org/10.1007/s00253-010-2920-9

3. Tashiro T. Antibacterial and Bacterium Absorbing Macromolecules. *Macromol. Mater. Eng.* 2001;286(2):63–87. https://onlinelibrary.wiley.com/doi/10.1002/1439-2054(20010201)286:2%3C63::AID-MAME63%3E3.0.CO;2-H

4. Kenawy E.-R., Worley S.D., Broughton R. The Chemistry and Applications of Antimicrobial Polymers: A State-of-the-Art Review. *Biomacromolecules*. 2007;8(5):1359–1384. https://doi.org/10.1021/bm061150q

5. Gilbert P., Moore L.E. Cationic Antiseptics: Diversity of Action under a Common Epithet. *J. Appl. Microbiol.* 2005;99(4):703–715. https://doi.org/10.1111/j.1365-2672.2005.02664.x

6. Kaur R., Liu S. Antibacterial surface design-Contact kill. *Prog. Surf. Sci.* 2016;91(3):136–153. https://doi.org/10.1016/j.progsurf.2016.09.001

7. Siedenbiedel F., Tiller J.C. Antimicrobial Polymers in Solution and on Surfaces: Overview and Functional Principles. *Polymers.* 2012;4(1):46–71. https://doi.org/10.3390/polym4010046

8. Tiller J.C. Antimicrobial Surfaces. In: Börner H., Lutz JF. (Eds.). Bioactive Surfaces. *Advances in Polymer Science*. 2011;240:193–217. https://doi.org/10.1007/12_2010_101

9. Chen A., Peng H., Blakey I., Whittaker A.K. Biocidal Polymers: A mechanistic overview. *Polym. Rev.* 2017;57(2):276–310. https://doi.org/10.1080/15583724.2016.1223131

10. Kenawy E.-R., Abdel-Hay F., El-Newehy M., El-Zaher E.H.F.A., Ibrahim E.M.A.-E. Novel biocidal polymers based on branched and linear poly(hydroxystyrene). *Int. J. Polym. Mater.* 2016;65(14):712–719. https://doi.org/10.1080/00914037.2016.1163563

11. McDonnel G., Russell A.D. Antiseptics and Disinfectants: Activity, Action, and Resistance. *Clin. Microbiol. Rev.* 1999;12(1):147–179. https://doi.org/10.1128/CMR.12.1.147

12. Bamford C.H., Lindsay H. Introduction of hydroxymethyl groups into polystyrene and styrene. *Polymer.* 1973;14(7):330–332. https://doi.org/10.1016/0032-3861(73)90128-6

13. Stamberg J., Wichterle O., Doskocilova D. Comment on the paper “Introduction of hydroxymethyl groups into polystyrene and styrene” by Bamford C.H., Lindsay H. *Polymer*. 1973;14:330–332. *Polymer*. 1974;15(5):323–324. https://doi.org/10.1016/0032-3861(74)90131-1

14. Dyakova M.G., Sklyarevskaya N.M., Deshevaya E.A., Kravchenko V.V., Shevlyakova N.V., Novikova N.D., Tverskoy V.A. Chemical modification of 4-vinylbenzylchloride polymers and antimicrobial properties of produced polymers containing hydroxyl groups. *Tonk. Khim. Tekhnol. = Fine Chem. Technol*. 2012;7(2):65–69 (in Russ.).

15. Nishikubo T., Iizawa T., Kobayashi K., Okawara M. Alkylation reaction of poly(chloromethylstyrene) with malononitrile and diethyl methylmalonate using phase transfer catalysts. *Makromol. Chem., Rapid. Commun*. 1981;2(6–7):387–392. https://doi.org/10.1002/marc.1981.030020605

16. Gibson H.W., Baily F.C. Chemical modification of polymers. II. Reaction of poly(vinylbenzyl chloride) and phenols. *J. Polym. Chem.* Ed. 1974;12(9):2141–2143. https://doi.org/10.1002/pol.1974.170120933

17. Beihoffer T.W., Glass J.E. The introduction of hydroxyl functionality into polymers: the synthesis, polymerization and hydrolysis of vinylbenzyl acetate. *J. Polymer Sci. A: Polymer Chem.* 1988;26(2):343–353. https://doi.org/10.1002/pola.1988.080260201

18. Yakovlev A.D. *Khimiya i tekhnologiya lakokrasochnykh pokrytii*: Uchebnik dlya vuzov (Chemistry and technology of paint and varnish coatings: Textbook for universities.) St. Peterburg: KHIMIZDAT; 2008. 448 p. (in Russ.). ISBN 978-5-93808-160-4

19. Mitsumori T., Craig I.M., Martini I.B., Schwartz B.J., Wudl F. Synthesis and Color Tuning Properties of Blue Highly Fluorescent Vinyl Polymers Containing a Pendant Pyrrolopyridazine. *Macromolecules*. 2005;38(11):4698–4704. https://doi.org/10.1021/ma048091y

20. Moskala E.J., Howe S.E., Painter P.C., Coleman M.M. On the Role of Intermolecular Hydrogen Bonding in Miscible Polymer Blends. *Macromolecules*. 1984;17(9):1671–1678. https://doi.org/10.1021/ma00139a006

13. Stamberg J., Wichterle O., Doskocilova D. Comment on the paper “Introduction of hydroxymethyl groups into polystyrene and styrene” by Bamford C.H., Lindsay H. *Polymer.* 1973;14:330–332. *Polymer.* 1974;15(5):323–324. https://doi.org/10.1016/0032-3861(74)90131-1

14. Дьякова М.Г., Скрялевская Н.М., Дешевая Е.А., Кравченко В.В., Щевлякова Н.В., Новикова Н.Д., Тверской В.А. Химическая модификация полимеров 4-винилбензилхлорида и антимикробные свойства образующихся гидроксилсодержащих полимеров. *Тонкие химические технологии.* 2012;7(2):65–69

15. Nishikubo T., Iizawa T., Kobayashi K., Okawara M. Alkylation reaction of poly(chloromethylstyrene) with malononitrile and diethyl methylmalonate using phase transfer catalysts. *Makromol. Chem., Rapid. Commun*. 1981;2(6–7):387–392. https://doi.org/10.1002/marc.1981.030020605

16. Gibson H.W., Baily F.C. Chemical modification of polymers. II. Reaction of poly(vinylbenzyl chloride) and phenols. *J. Polym. Chem. Ed.* 1974;12(9):2141–2143. https://doi.org/10.1002/pol.1974.170120933

17. Beihoffer T.W., Glass J.E. The introduction of hydroxyl functionality into polymers: the synthesis, polymerization and hydrolysis of vinylbenzyl acetate. *J. Polymer Sci. A: Polymer Chem.* 1988;26(2):343–353. https://doi.org/10.1002/pola.1988.080260201

18. Яковлев А.Д. *Химия и технология лакокрасочных покрытий*: Учебник для вузов. СПб.: ХИМИЗДАТ; 2008. 448 с. ISBN 978-5-93808-160-4

19. Mitsumori T., Craig I.M., Martini I.B., Schwartz B.J., Wudl F. Synthesis and Color Tuning Properties of Blue Highly Fluorescent Vinyl Polymers Containing a Pendant Pyrrolopyridazine. *Macromolecules.* 2005;38(11):4698–4704. https://doi.org/10.1021/ma048091y

20. Moskala E.J., Howe S.E., Painter P.C., Coleman M.M. On the Role of Intermolecular Hydrogen Bonding in Miscible Polymer Blends. *Macromolecules.* 1984;17(9):1671–1678. https://doi.org/10.1021/ma00139a006

About the authors:

Maxim V. Gusarov, Postgraduate Student, S.S. Medvedev Department of Chemistry and Technology of Macromolecular Compounds, M.V. Lomonosov Institute of Fine Chemical Technologies, MIREA – Russian Technological University (86, Vernadskogo pr., Moscow, 119571, Russia). E-mail: gusarovmv@mail.ru. https://orcid.org/0000-0002-7334-6227

Alexander V. Krylov, Cand. Sci. (Chem.), Associate Professor, Ya.K. Syrkin Department of Physical Chemistry, M.V. Lomonosov Institute of Fine Chemical Technologies, MIREA – Russian Technological University (86, Vernadskogo pr., Moscow, 119571, Russia). E-mail: allylnmr@yandex.ru. https://orcid.org/0000-0002-2389-9026

Elena A. Deshevaya, Cand. Sci. (Biol.), Leading Scientific Researcher, State Research Center of the Russian Federation, Institute of Biomedical Problems, Russian Academy of Sciences (76a, Khoroshevskoe sh., Moscow, 123007, Russia). E-mail: deshevaya@imbp.ru. Scopus Author ID 6508235645, https://orcid.org/0000-0002-7121-9232

Vladimir A. Tverskoy, Dr. Sci. (Chem.), Professor, S.S. Medvedev Department of Chemistry and Technology of Macromolecular Compounds, M.V. Lomonosov Institute of Fine Chemical Technologies, MIREA – Russian Technological University (86, Vernadskogo pr., Moscow, 119571, Russia). E-mail: tverskoy@mitht.ru. Scopus Author ID 6604012434, https://orcid.org/0000-0003-4348-8854

Об авторах:

Гусаров Максим Витальевич, аспирант кафедры химии и технологии высокомолекулярных соединений им. С.С. Медведева Института тонких химических технологий им. М.В. Ломоносова ФГБОУ ВО «МИРЭА – Российский технологический университет» (119571, Россия, Москва, пр-т Вернадского, д. 86). E-mail: gusarovmv@mail.ru. https://orcid.org/0000-0002-7334-6227

Крылов Александр Владимирович, к.х.н., доцент кафедры физической химии им. Я.К. Сыркина Института тонких химических технологий им. М.В. Ломоносова ФГБОУ ВО «МИРЭА – Российский технологический университет» (119571, Россия, Москва, пр-т Вернадского, д. 86). E-mail: allylnmr@yandex.ru. https://orcid.org/0000-0002-2389-9026

Дешевая Елена Андреевна, к.б.н., ведущий научный сотрудник, Государственный научный центр Российской Федерации Институт медико-биологических проблем Российской академии наук (123007, Россия, Москва, Хорошевское ш., д. 76а). E-mail: deshevaya@imbp.ru. Scopus Author ID 6508235645, https://orcid.org/0000-0002-7121-9232

Тверской Владимир Аркадьевич, д.х.н., профессор кафедры химии и технологии высокомолекулярных соединений им. С.С. Медведева Института тонких химических технологий им. М.В. Ломоносова ФГБОУ ВО «МИРЭА – Российский технологический университет» (119571, Россия, Москва, пр-т Вернадского, д. 86). E-mail: tverskoy@mitht.ru. Scopus Author ID 6604012434, https://orcid.org/0000-0003-4348-8854

The article was submitted: September 30, 2021; approved after reviewing: October 04, 2021; accepted for publication: October 30, 2021.

Translated from Russian into English by N. Isaeva
Edited for English language and spelling by Enago, an editing brand of Crimson Interactive Inc.

CHEMISTRY AND TECHNOLOGY OF MEDICINAL COMPOUNDS AND BIOLOGICALLY ACTIVE SUBSTANCES
ХИМИЯ И ТЕХНОЛОГИЯ ЛЕКАРСТВЕННЫХ ПРЕПАРАТОВ И БИОЛОГИЧЕСКИ АКТИВНЫХ СОЕДИНЕНИЙ

ISSN 2686-7575 (Online)

https://doi.org/10.32362/2410-6593-2021-16-5-414-425

УДК 541.64+57.083.3+535.371+616-097

RESEARCH ARTICLE

Characterization of iron-doped crystalline silicon nanoparticles and their modification with citrate anions for *in vivo* applications

Kirill I. Rozhkov[1,@], Elena Y. Yagudaeva[2], Svetlana V. Sizova[2], Michael A. Lazov[1], Evgeniya V. Smirnova[2], Vitaliy P. Zubov[1,2], Anatoliy A. Ischenko[1]

[1]MIREA – Russian Technological University (M.V. Lomonosov Institute of Fine Chemical Technologies), Moscow, 119571 Russia
[2]Shemyakin and Ovchinnikov Institute of Bioorganic Chemistry, Russian Academy of Sciences, Moscow, 117997 Russia
[@]Corresponding author, e-mail: rokirill58@mail.ru

Abstract

Objectives. *This paper presents data on the development and study of the structural properties of iron-doped crystalline silicon (nc-Si/SiO_x/Fe) nanoparticles obtained using the plasma-chemical method for application in magnetic resonance imaging diagnostics and treatment of oncological diseases. This work aimed to use a variety of analytical methods to study the structural properties of nc-Si/SiO_x/Fe and their colloidal stabilization with citrate anions for in vivo applications.*
Methods. *Silicon nanoparticles obtained via the plasma-chemical synthesis method were characterized by laser spark emission spectroscopy, atomic emission spectroscopy, Fourier-transform infrared spectroscopy, and X-ray photoelectron spectroscopy. The hydrodynamic diameter of the nanoparticles was estimated using dynamic light scattering. The toxicity of the nanoparticles was investigated using a colorimetric MTT test for the cell metabolic activity. Elemental iron with different Fe/Si atomic ratios was added to the feedstock during loading.*
Results. *The particles were shown to have a large silicon core covered by a relatively thin layer of intermediate oxides (interface) and an amorphous oxide shell, which is silicon oxide with different oxidation states SiO_x ($0 \le x \le 2$). The samples had an iron content of 0.8–1.8 at %. Colloidal solutions of the nanoparticles stabilized by citrate anions were obtained and characterized. According to the analysis of the cytotoxicity of the modified nanosilicon particles using monoclonal K562 human erythroleukemia cells, no toxicity was found for cells in culture at particle concentrations of up to 5 μg/mL.*

Conclusions. *Since the obtained modified particles are nontoxic, they can be used in in vivo theranostic applications.*

Keywords: *silicon nanoparticles, iron, magnetic resonance imaging, citrate anions, X-ray photoelectron spectroscopy, Fourier-transform infrared spectroscopy, cytotoxicity*

For citation: Rozhkov K.I., Yagudaeva E.Y., Sizova S.V., Lazov M.A., Smirnova E.V., Zubov V.P., Ischenko A.A. Characterization of iron-doped crystalline silicon nanoparticles and their modification with citrate anions for *in vivo* applications. *Tonk. Khim. Tekhnol. = Fine Chem. Technol.* 2021;16(5):414–425 (Russ., Eng.). https://doi.org/10.32362/2410-6593-2021-16-5-414-425

НАУЧНАЯ СТАТЬЯ

Характеризация наночастиц кристаллического кремния, легированного железом, и их модификация цитрат-анионами для использования *in vivo*

К.И. Рожков[1,@], Е.Ю. Ягудаева[2], С.В. Сизова[2], М.А. Лазов[1], Е.В. Смирнова[2], В.П. Зубов[1,2], А.А. Ищенко[1]

[1]МИРЭА – Российский технологический университет (Институт тонких химических технологий им. М.В. Ломоносова), Москва, 119571 Россия
[2]Институт биоорганической химии им. академиков М.М. Шемякина и Ю.А. Овчинникова Российской академии наук, Москва, 117997 Россия
[@]Автор для переписки, e-mail: rokirill58@mail.ru

Аннотация

Цели. *В работе приводятся данные по разработке и изучению структурных свойств полученных плазмохимическим методом наночастиц кремния nc-Si/SiO_x/Fe, легированных железом. Цель работы – исследование свойств наночастиц кремния, легированных железом, комплексом аналитических методов и их стабилизация цитрат-анионами для применения в диагностике методом магнитно-резонансной томографии и лечении онкологических заболеваний.*

Методы. *Наночастицы кремния, полученные плазмохимическим методом синтеза, были охарактеризованы лазерно-искровым эмиссионным методом, методом атомной эмиссионной спектроскопии, Фурье-ИК-спектроскопией, рентгеновской фотоэлектронной спектроскопией. Гидродинамический диаметр наночастиц оценивали методом динамического светорассеяния. Исследование токсичности наночастиц проводили с помощью колориметрического МТТ теста на метаболическую активность клеток. В исходное сырье при загрузке добавляли элементарное железо с разным атомным соотношением Fe/Si.*

Результаты. *Было показано, что частица имеет кремниевое ядро с аморфной оксидной оболочкой, представляющей собой оксиды кремния с разной степенью окисления SiO_x ($0 \le x \le 2$). Содержание железа в образцах составило от 0.8 до 1.8 ат. %. Были получены и охарактеризованы коллоидные растворы наночастиц, стабилизированные цитрат-анионами. Анализ цитотоксичности модифицированных частиц нанокремния с использованием моноклонизированных клеток эритролейкоза человека K562 показал отсутствие токсичности для клеток в культуре при концентрации частиц до 5 мкг/мл.*

Выводы. *Полученные модифицированные частицы не обладают токсичностью, поэтому их можно рекомендовать для использования в in vivo приложениях для тераностики.*

Ключевые слова: *наночастицы кремния, железо, цитрат-анионы, рентгеновская фотоэлектронная спектроскопия, Фурье-инфракрасная спектроскопия, цитотоксичность*

Для цитирования: Рожков К.И., Ягудаева Е.Ю, Сизова С.В., Лазов М.А., Смирнова Е.В., Зубов В.П., Ищенко А.А. Характеризация наночастиц кристаллического кремния, легированного железом, и их модификация цитрат-анионами для использования *in vivo*. *Тонкие химические технологии*. 2021;16(5):414–425. https://doi.org/10.32362/2410-6593-2021-16-5-414-425

INTRODUCTION

Various nanoparticles, such as paramagnetic complexes of gadolinium(III), iron(III), and manganese(III), are currently used in magnetic resonance imaging (MRI). Despite the high efficiency of contrasting properties and widespread use in medicine, these complexes can cause allergic reactions and nephrogenic systemic fibrosis and accumulate in the brain for a long time [1, 2]. The use of superparamagnetic iron oxide (Fe_2O_3) nanoparticles is unsafe for living organisms because their high magnetic moment causes significant disturbances in the magnetic field in the body [3]. Therefore, the search for new contrast agents is still ongoing.

Many researchers are interested in using nanosized silicon particles and their composites for *in vivo* applications because they do not exhibit toxic properties and are biodegradable and biocompatible [4]. Silicon is one of the most important trace elements involved in the connective tissue repair mechanisms of the body [5]. Silicon nanoparticles in living organisms undergo biodegradation, forming orthosilicic acid, which is then easily removed [6].

The superparamagnetic properties of porous silicon dioxide nanoparticles with embedded magnetic nanoparticles have been demonstrated to be promising for magnetically targeted delivery of therapeutic molecules and have significant clinical application potential [7]. Hollow silicon nanospheres doped with Fe^{3+} ions, of which the surface is modified with silane-polyethylene glycol (silane-PEG-COOH), can be used as a low-cytotoxic and dual-mode ultrasonic and magnetic resonance (US–MR) specific imager in biopharmaceutical applications and clinical diagnosis and treatment [8]. Magnetic particles based on Fe_3O_4 with a surface stabilized by silicon dioxide and citrate ions are promising for the creation of drug delivery vehicles for the treatment of oncological diseases [9]. According to electron paramagnetic resonance (EPR) data, silicon nanoparticle samples obtained by synthesizing crystalline silicon nanoparticles (nc-Si/SiO_x) via the plasma-chemical method contain ~10^{18} particles/g of paramagnetic centers [10]. Intratumoral administration of sols of iron-doped crystalline silicon (nc-Si/SiO_x/Fe) nanoparticles to mice with Lewis lung carcinoma (CLL) reduces tumor cell growth [11]. The authors believe that when nanoparticles dissolve, iron ions are released, resulting in the formation of reactive oxygen species. The MRI method was used to conduct experiments on the observation of nanoparticle accumulation in tumors and tumor growth inhibition. Thus, nc-Si/SiO_x/Fe nanoparticles obtained via the plasma-chemical method of synthesis can be used in MRI diagnostics, targeted drug delivery, and oncological disease therapy as thermal sensitizers for hyperthermia. However, for wider nanoparticle applications, the nanoparticles must be colloid stabilized to provide their delivery to tumors in an pristine form. The presence of iron oxides

in the near-surface layer of the nanoparticles was also believed to facilitate their modification by colloidal stability stabilizers.

Numerous experimental and theoretical studies have shown that reducing the size of the investigated particles to the nanometer range causes a qualitative change in the properties of the object. In this case, structural elements can acquire physical, physicochemical, and chemical properties that differ significantly from the properties of a bulk analog. Conversely, the properties of objects with sizes in the order of several nanometers differ from the properties of individual atoms or molecules that compose these objects. This applies to nanoscale crystals and clusters. Therefore, a set of complementary analysis methods are used to obtain information on the structural and physical properties of nanoparticles [12, 13].

This work aimed to study the properties of iron-containing silicon nanoparticles using a variety of analytical methods, as well as their colloidal stabilization with citrate anions for theranostic applications, e.g., as MRI contrast agents.

MATERIALS AND METHODS

We used iron-containing nanocrystalline silicon (*GNIIKhTEOS*, Russia) obtained using the plasma-chemical method [12], deionized water from a Milli-Q water purification unit with a specific conductivity of 18 μS/cm, trisodium citric acid dihydrate (*Helicon*, Russia), and a pH 7.4 phosphate salt buffer solution (*Helicon*) for the modification.

We used K562 erythroleukemia cells (*BioloT*, Russia), a Rosewell Park Memorial Institute medium (*PanEco*, Russia) containing 10% fetal bovine serum (FBS) (BIOSERA, France), 100 U/mL penicillin, and 100 μg/mL streptomycin (*PanEco*) to assess cytotoxicity. A solution of 3-[4,5-dimethylthiazol-2-yl] 2,5-diphenyltetrazolium bromide (MTT) (*Sigma-Aldrich*, USA) in a phosphate buffer solution with a concentration of 5 mg/mL was used for the MTT test. The viability of the nanoparticle-treated cells was measured on a plate spectrophotometer after the cell lines were grown in a CO_2 incubator.

Plasmochemical synthesis of nc-Si/SiO_x. The plasma-chemical method was used to produce nanosilicon. The synthesis was carried out in a closed-cycle gas system. The system was filled with a highly purified inert gas (Ar, HP, 99.998%) from the line [12]. A plasma evaporator–condenser operating in a low-frequency arc discharge was used as a reactor. A gas flow from an appropriate metering device was used to feed the initial raw material, silicon powder (99.99%), into the reactor. The reactor was fed with elemental iron (from 2.5 to 10 at %), and at a temperature of ~10000°C, the powder evaporated in the reactor.

Elemental composition analysis. Laser spark emission spectroscopy was used to determine the following main impurity elements in silicon nanoparticles obtained without the addition of iron [12]: Fe, Cu, W, Ca, Mg, Al, Ni, Pb, Ti, Zr, Zn, Sn, Cr, P, and Mo (arranged in decreasing order of the intensity of the analytical signal). The analysis was carried out after a tablet was formed from the powder sample. The total impurity element content in the investigated samples did not exceed 0.8%. Elemental analysis was performed independently using atomic emission spectroscopy with an excitation of the spectrum in an alternating current arc. The following main impurity elements were determined in the obtained nanosilicon samples: Mg (0.03%), Al (0.02%), Ca (0.002%), Fe (0.006%), Ni (0.002%), and Cu (0.019%). Thus, the total content of impurity elements W, Pb, Ti, Zr, Zn, Sn, Cr, P, and Mo did not exceed ~0.6%.

Fourier-transform infrared (FTIR) Spectroscopy. We used a Nicolet iS5 infrared Fourier spectrometer (*Thermo Scientific*, USA) with an iD1 attachment and a resolution of 4 cm^{-1} (32 scans each for each sample) in the transmission mode and in the wavenumber range of 4000–400 cm^{-1} to measure the absorption spectra of the nc-Si/SiO_x samples and an aerosil sample (SiO_2 powder) with a particle size of about 15 nm. The samples were pre-compressed into tablets using potassium bromide (KBr) as an optically transparent matrix (0.30 mg of the sample per 100 mg KBr).

Sample analysis by X-ray photoelectron spectroscopy (XPS). The electronic structure and valence states of the obtained nc-Si/SiO_x/Fe samples were analyzed by XPS using an ESCALAB MK2 electronic spectrometer (*VG Scientific*, Great Britain) with an X-ray source MgK_α ($h\nu$ = 1253.6 eV). A nanoparticle powder sample was applied to a conductive vacuum tape, and the total area of the sample was analyzed (about 1 cm^2). Survey spectra had a transmission energy of −50 eV, while individual lines of elements had a transmission energy of 20 eV. The accumulation time per point was 0.3 s per 1 pass. The binding energies for the element spectra ranged from ±10 to15 eV relative to the position of the peak maximum. The measurement steps were 0.1 eV for the spectra of the individual lines of elements and 0.25 eV for the survey spectra. The pressure in the analysis chamber of the spectrometer was up to $5 \cdot 10^{-7}$ Pa.

The charge of the samples was corrected using the standard binding energy (285.0 eV) of the C 1*s* line of carbon contained in the adhesive tape. The valence states of the elements in the samples were determined

from the chemical shift and the shape (width) of the lines. For elemental and chemical analysis of the samples, Si 2*p*, C 1*s*, O 1*s*, and Fe 2*p* analytical lines were used, which were measured separately and in the form of an overview spectrum [14].

Preparation of the nc-Si/SiO_x/Fe colloidal solution. To obtain an aqueous colloidal solution of nc-Si/SiO_x/FeO_x nanoparticles, 20 mg of the particles was suspended in 10 mL of water. The resulting suspension was dispersed for 5 min using an INLAB ultrasonic generator (16–25 kHz frequency, power no less than 630 W). The samples were centrifuged for 2 min at a rotation speed of 5000 rpm, and the supernatant was collected and passed through a filter with a pore diameter of 0.45 μm (CHROMAFIL AO-45/25 MN). The final particle concentration was 0.14 mg/mL, as determined gravimetrically.

Modification of the nc-Si/SiO_x/FeO_x nanoparticles with citrate ions. For modification, 20 mg of nc-Si/SiO_x/Fe nanoparticles was suspended in a solution of citric acid trisodium salt dihydrate (1%, 2%, and 5%) and subsequently dispersed for 5 min in an ultrasonic bath using a QSONICA SONICATORS ultrasonic generator (USA) (frequency 20 kHz, power 125 W). The mixture was stirred in a magnetic stirrer for 24 h at a stirring rate of 600 rpm and centrifuged for 2 min at a rotation rate of 5000 rpm. The supernatant was collected and passed through a filter with a pore diameter of 0.45 μm (CHROMAFIL AO-45/25 MN). Thereafter, the prepared solutions were dialyzed against water for 24 h in a dialysis bag. The final particle concentration was 0.6 mg/mL, as determined gravimetrically.

The particle hydrodynamic diameter was evaluated using a zeta potential and molecular weight 90Plus Particle Size Analyzer (*Brookhaven Instruments Corporation*, USA). The measured particle sizes ranged from 4 nm to 6 μm. The measurements were recorded at a temperature of 25°C and a fixed laser scattering angle of 90° at 661 nm. The dispersion medium was deionized water from a Milli-Q water purification unit with a specific conductivity of 18 μS/cm.

The zeta potential of the obtained particles was evaluated using a zeta potential and molecular weight 90Plus Partical Size Analyzer with an additional device called Zeta-PALS, which has a sensitivity that allows it to detect the zeta potential three orders of magnitude more accurately than traditional light scattering methods.

Analysis of nanosilicon cytotoxicity. A standard colorimetric MTT test, which allows for the quantitative determination of viable cells using a Multiskan Ascent plate reader (*Thermo Fisher Scientific*, USA), was used to investigate the toxicity of silicon nanoparticles. The K562 erythroleukemia cells in a volume of 100 μL were seeded in a 96-well plate. The initial suspension of the nanosilicon particles was diluted in a physiological solution with phosphate-buffered saline in a ratio of 1:100, resulting in a concentration of 730 μg/mL, and thereafter, it was sonicated. Next, a series of 5-fold dilutions was prepared from the first dilution of 1:100. For each point, 5 μL of the obtained diluted suspensions was added to the cells four times. Four wells with cells that had not been treated with any compound (control wells) remained. The plate was placed in a CO_2 incubator. After 48 h, 5 μL of the MTT reagent solution was added to all wells, and the plate was placed in a CO_2 incubator for 3 h. After incubation, 100 μL of lysis buffer was added to all the wells, and the plate was sealed in a bag and left overnight at room temperature to allow cell lysis and dissolution of the formed formazan crystals. The next day, absorbance was measured at 540 nm (formazan) and 690 nm (background) using a plate spectrophotometer. For each well with cells, the optical density (OD) of formazan, which is proportional to the number of cells in the well, was calculated:

$$\text{OD (well with cells)} = (\text{OD540} - \text{OD690}) \times$$
$$\times \text{(well with cells)} - \text{average (OD540} - \text{OD690)} \times$$
$$\times \text{(wells without cells)}.$$

Next, the average of the four repetitions at each point was calculated. The average OD values for the points where compounds were added were divided by the average OD value for the point where no compound was added, which was set as 1, to obtain the proportion of surviving cells relative to the control (untreated) cell.

RESULTS AND DISCUSSION

In this study, we used nc-Si/SiO_x/Fe nanoparticles obtained from silicon powder (sample No. 1) using the plasma-chemical method. According to the laser spark emission spectroscopy and XPS results, the resulting particles contain iron (about 0.2 at %). Arc laser ablation of iron ions from the surface of metal electrodes may have occurred during synthesis. According to the EPR data, nc-Si/SiO_x/Fe contains about ~10^{18} particles/g of paramagnetic centers [10]. To increase magnetic susceptibility, the nanoparticles were enriched with iron during the synthesis. During loading, elemental iron with different Fe/Si atomic ratios (from 2.5 to 10 at %, samples 2–7) was added to the feedstock. Immediately after the synthesis, the dispersion of the powder in different batches of material was controlled by measuring nitrogen adsorption isotherms at 77 K using the Brunauer–Emmett–Teller (BET) method [12]. Samples were obtained with different specific surface

areas ranging from 28 to 57 m^2/g, which correspond to the average particle size D_{BET} ranging from 45 to 92 nm when converted to the diameter of an equivalent sphere (Table 1).

To diagnose and predict the properties of a nanomaterial, detailed information about its structural and morphological properties is required. Therefore, a detailed analysis of the particle structure of the obtained material was conducted before its practical application.

Analysis of the FTIR spectrum of the silicon nanoparticles. FTIR spectroscopy can be used to obtain information on the composition of the shell of silicon nanocrystals, the state of their surface, and the dynamics of their possible degradation.

The FTIR spectrum of the No. 1 nc-Si/SiO_x/Fe sample (Fig. 1a) was compared with that of the aerosil sample (SiO_2 powder) with a particle size of about 15 nm (Fig. 1b). Intense absorption bands were found in the FTIR spectrum of the nanosilicon particle sample obtained via plasma-chemical synthesis, indicating the formation of an oxide shell (461, 799, and 1097 cm^{-1} SiO_2 or SiO_x, $0 \le x \le 2$) [12]. The low-intensity absorption peak corresponding to the vibration of the Fe–O bond (580 cm^{-1}) [11] indicates the presence of iron oxide in the near-surface layer of the nanoparticle.

XPS data analysis. We used previously reported data [15–17] to interpret the results obtained on the possible oxide states of silicon in the investigated samples. According to these data, the binding energy of the Si^0 $2p_{3/2}$ line is 99.8 eV [14, 18, 19], and the chemical shifts of the oxide forms of Six+ relative to Si^0 are 0.9–1.0 eV (Si^{1+}), 1.7–1.85 eV (Si^{2+}), 2.5–2.6 eV (Si^{3+}), and 3.5–3.7 eV (Si^{4+}). According to Crist [16], the peak widths at half maximum for Si 2p and various silicon oxide forms are 1.0 eV (Si^0), 1.8 eV (Si^{1+}), 1.9 eV (Si^{2+}), 2.1 eV (Si^{3+}), and 1.4–1.5 eV (Si^{4+}).

The spectra of the Si 2*p* line were decomposed using the technique proposed in a previous report [20]. The nonlinear background of secondary electrons was subtracted using the Shirley method [21]. For each oxidation state of silicon, a Si 2*p* spin doublet (Si $2p_{3/2}$ and Si $2p_{1/2}$) with a spin-orbit splitting of 0.61 eV and an area ratio of 2:1 was specified. For different oxidation states of silicon, the binding energies and the abovementioned peak widths at half maximum were set [16, 17].

The spectra of the Si 2*p* line were decomposed on the assumption that silicon was present on the surface of the analyzed particles only in the form of elemental silicon and oxygen-containing compounds, except for the formation of silicon carbide and the presence of residual hydride (SinHm) or iron silicide (FeSi, $FeSi_2$), which are indistinguishable from Si^{1+} in terms of chemical shift and Si^0 and are present in small amounts.

The binding energies of Si $2p_{3/2}$, O 1*s*, C 1*s*, and Fe $2p_{3/2}$ were 99.6, 532.8, 285.0, and 706.7 eV, respectively [16, 17]. In the case of sample charging and line broadening, the possible peak widths at half maximum in the decomposition of the spectra for various forms of silicon and carbon were set in the form of intervals, monotonically increasing as the oxidation state of silicon increased. For the iron line, the spectra had a more complex shape due to a large number of valence electrons, but they were set similarly, with a shift relative to the standard position.

Table 1. Characteristics of the nc-Si/SiO_x/Fe samples

Sample	1	2	3	4	5	6	7
Iron content in raw materials, at %	0	2.5	2.5	5.0	5.0	10.0	10.0
Specific surface, m^2/g	57.0	28.0	57.0	31.6	48.1	41.6	48.3
Average particle diameter, D_{BET}, nm	45.2	91.9	45.2	81.5	53.5	61.0	53.3
Si* content, at %	34.1 ± 1.7	20.6 ± 1.0	9.5 ± 0.5	36.5 ± 1.8	35.9 ± 1.8	61.6 ± 3.1	32.1 ± 1.6
Fe* content, at %	0.2	0.5	0.4	0.4	0.5	2.2	0.8
Atomic ratio Fe/Si, %	0.6	2.5	4.0	1.1	1.5	3.5	2.6

*Element content in near-surface nc-Si/SiO_x/Fe layers according to the XPS data (scanning depth up to 5 nm).

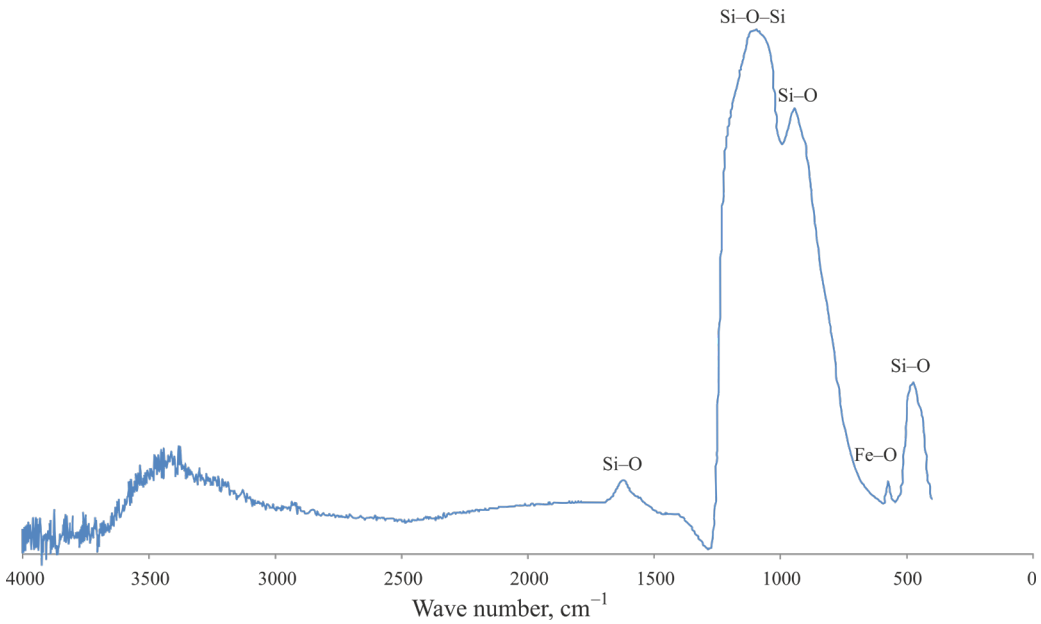

a

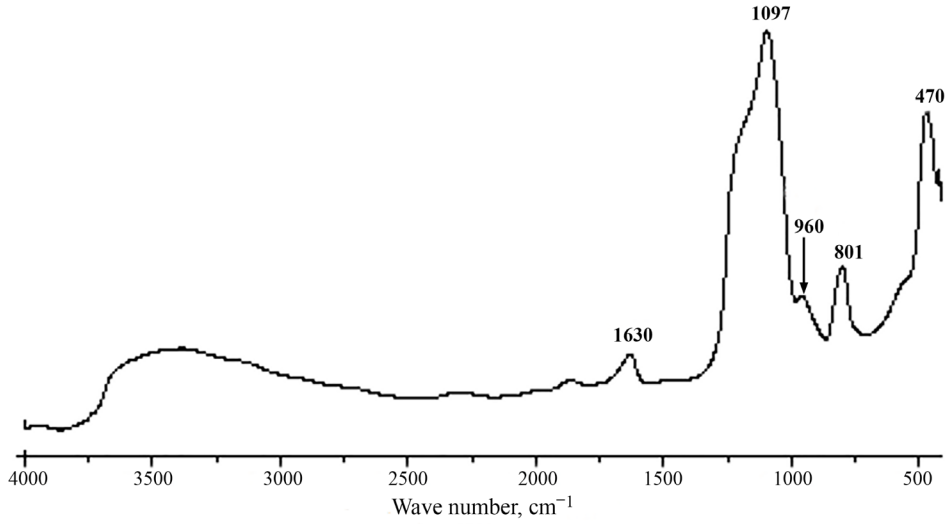

b

Fig. 1. FTIR spectrum of (a) the studied nc-Si/SiO_x/Fe sample (0.3 mass % in KBr) and (b) the aerosil sample (powdered SiO_2 with a particle size of 15 nm).

Table 1 shows a summary of the measurement results. The particle composition was assumed to be average and constant up to the depth of selection of analytical information in the calculations, with components in the order of 5 nm for silicon and silicon dioxide.

The following conclusions can be drawn from the calculated atomic percentages. Sample 6 mainly contains silicon dioxide on the surface. Samples 2, 3, 4, and 7 have a very similar distribution of silicon oxide forms. The significant difference in the silicon content in the different samples can be explained by the peculiarities of sample preparation for XPS and the ability of the nanosilicon surface to adsorb various impurities.

The difference between the diminished iron content and the estimated one based on the initial load can be explained as follows. Since the process of mixing iron with the silicon starting material occurs at elevated temperatures, iron oxide particles melt and become covered with silicon, which oxidizes into silicon dioxide during oxidation, significantly reducing the signal from iron (exponential decay of the photoelectron intensity due to the coating layer).

This could also explain why silicon is predominantly present in the form of dioxide. Thus, samples in which the iron content is proportional to the iron content in the feedstock or slightly exceeds its value (measurement and processing error) have a large specific surface area and small particle size, and therefore, silicon (or its dioxide) does not cover iron oxide particles to the same extent as in samples with a relatively small specific surface.

Based on the obtained data, the particle can be assumed to have a silicon core with an amorphous oxide shell, which is silicon oxide with different oxidation states SiO_x ($0 \le x \le 2$). This is consistent with the data obtained in a previous study [10] based on the analysis of transmission electron images, microscope images, and radiographs. X-ray diffraction studies [11] revealed that the oxidation of the surface of silicon particles resulted in the formation of particles with a "core-shell" structure, which has a silicon nanocrystal as the core and silicon oxides of various oxidation states in the shell. The degree of crystallinity of the sample is ~10% for the amorphous shell and ~42% for the crystalline core [11].

For modification with citrate anions, we used an nc-Si/SiO_x/Fe sample (No. 5) with a diameter of about 48.1 nm and an iron content of about 0.5 at %.

Modification of nc-Si/SiO_x/Fe nanoparticles with citrate anions

Crystalline silicon nanoparticles doped with iron oxide are hydrophilic and form a colloidal solution in aqueous media. However, even freshly prepared nc-Si/SiO_x/Fe colloidal solutions are unstable. Sols are characterized by a wide particle size distribution. The average particle diameter was about 100 nm, and it increased to 200 nm within a week, then reaching 1000 nm (Table 2). The concentration of the sols changes because of the agglomeration and sedimentation of the particles. The large variation in the zeta potential values of nc-Si/SiO_x/Fe (from –20 to +20 mV) also indicates the instability of the colloidal system. An increase in the diameter of silicon nanoparticles results in a change in their physicochemical characteristics [22]. Thus, it is necessary to stabilize silicon nanoparticle sols to use them *in vivo* for theranostics.

To stabilize nc-Si/SiO_x/Fe, the use of citric acid salt was proposed. Citric acid anions have previously been shown to bind to the surface of hematite (Fe_2O_3) through chemisorption [23]. The surface of the nc-Si/SiO_x/Fe particles was shown to be stabilized after being modified with citrate anions. Stable colloidal solutions with a monomodal particle size distribution were formed (Fig. 2). Sols of nc-Si/SiO_x/Fe-citric nanoparticles modified with citrate anions using a 1% concentration of citric acid trisodium salt dihydrate have a monomodal size distribution with an average diameter of about 60 nm that does not change for a long time (up to 1.5 years). Thus, chemosorption of citrate anions electrostatically stabilizes the interaction forces that determine the tendency of silicon nanoparticles particles to agglomerate.

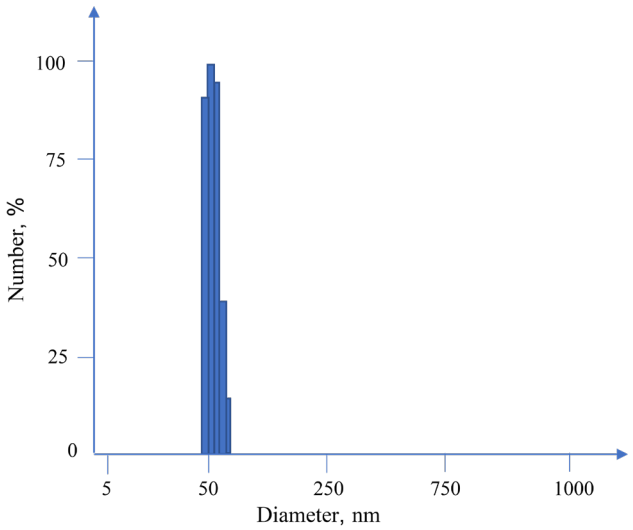

Fig. 2. Molecular weight distribution of modified nc-Si/SiO_x/Fe-citric nanoparticles (1%). The average hydrodynamic diameter was 57 nm.

Table 2. Changes in the particle size and aggregation stability of nc-Si/SiO_x/Fe sols in the original solution and in the solution one week after receiving

Sample	Nanoparticles concentration *C*, mg/mL	D_1, nm	D_2, nm
nc-Si/SiO_x/Fe	0.14	112	255–1000
nc-Si/SiO_x/Fe-citric 1%	0.54	57	64
nc-Si/SiO_x/Fe-citric 2%	0.70	240	263

Nanoparticles can be modified with citrate anions because of the presence of iron oxides in the near-surface layer of the nanoparticles. An attempt to stabilize iron-free nc-Si/SiO_x-citric acid nanoparticles obtained by laser CO_2 pyrolysis of silane [24] resulted in their complete precipitation. Therefore, the presence of iron ions in the investigated samples is indirectly confirmed by the formation of stable nc-Si/SiO_x/Fe-citric colloidal solutions.

Cytotoxicity analysis of citrate-modified nanosilicon

The cytotoxicity of citrate-modified nanoparticles was investigated. We used monoclonal K562 human erythroleukemia cell lines for this purpose.

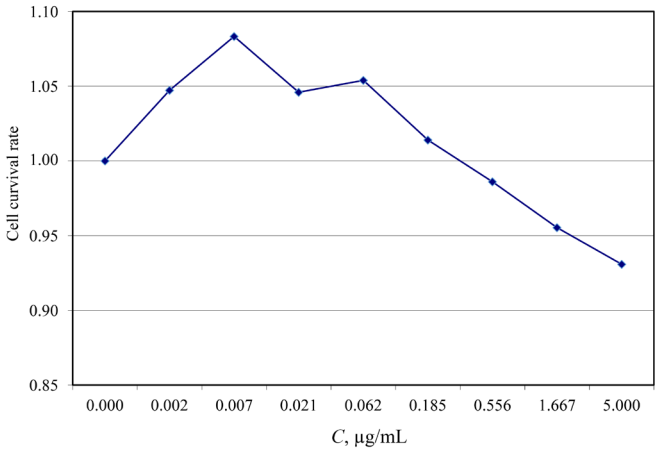

Fig. 3. Dependence of the number of surviving cells on the concentration *C* of added nc-Si/SiO_x/Fe-citric nanoparticles after 48 h of exposure.

Figure 3 shows that nc-Si/SiO_x/Fe-citric nanoparticles do not exhibit cellular toxicity at a concentration of 5 μg/mL. At low concentrations of nc-Si/SiO_x/Fe-citric nanoparticles, a slight increase in cell proliferation is observed.

CONCLUSIONS

Iron-containing hybrid silicon nanoparticles were obtained using the plasma-chemical synthesis method. Complementary analytical methods, including laser spark emission spectroscopy, FTIR spectroscopy, X-ray phase analysis, and XPS, were used to analyze the nanoparticles. Based on the obtained data, the nanocrystalline silicon particle can be concluded to have a silicon core covered with a relatively thin layer of intermediate oxides (interface) and an amorphous oxide shell, which is silicon oxide with different oxidation states SiO_x ($0 \le x \le 2$). The degree of crystallinity of the sample is ~10% for the amorphous shell and ~42% for the crystalline core According to the XPS data, iron oxides and/or silicides were present in the particle shell in amounts ranging from 0.2 to 2.2 at %, depending on the amount of elemental iron in the starting material. The total content of impurity elements W, Pb, Ti, Zr, Zn, Sn, Cr, P, and Mo did not exceed ~0.6%.

A technique for stabilizing the surface of nanosilicon particles with citrate anions has been developed. It was demonstrated that the presence of iron oxides in the near-surface layer of nanoparticles allows them to be modified with citrate anions, resulting in the formation of stable nc-Si/SiO_x/Fe colloidal solutions. Since the obtained modified particles are nontoxic, they can be recommended for use in *in vivo* theranostic applications, such as MRI diagnostics.

Acknowledgments

The authors are grateful to S.N. Malakhov for carrying out research by the method of IR spectroscopy using the equipment of the resource center "Optics" of the National Research Center "Kurchatov Institute."

Authors' contribution

K.I. Rozhkov – selection and analysis of literature, Fourier-transform infrared spectroscopy experiment, data processing, discussion of the results, writing the text of the manuscript;

E.Y. Yagudaeva – modification of nanoparticles with citrate ions, data processing, discussion of the results, writing the text of the manuscript;

S.V. Sizova – data processing, discussion of the results;

M.A. Lazov – X-ray photoelectron spectroscopy experiment, data processing, discussion of the results, writing the text of the manuscript;

E.V. Smirnova – study of the toxicity of nanoparticles using a standard colorimetric MTT test, data processing, discussion of the results, writing the text of the manuscript;

V.P. Zubov – guidance of work on modification of nanoparticles, discussion of the results;

A.A. Ischenko – guidance of work on the synthesis of silicon nanoparticles and characterization of their properties, discussion of the results, writing the text of the manuscript.

The authors declare no conflicts of interest.

REFERENCES

1. Elbeshlawi I., AbdelBaki M.S. Safety of gadolinium administration in children. *Pediatr. Neurol.* 2018;86:27–32. https://doi.org/10.1016/j.pediatrneurol.2018.07.010

2. Franckenberg S., Berger F., Schaerli S., Ampanozi G., Thali M. Fatal anaphylactic reaction to intravenous gadobutrol, a gadolinium-based MRI contrast agent. *Radiol. Case Rep.* 2018;13(1):299–301. https://doi.org/10.1016/j.radcr.2017.09.012

3. Xu C., Sun S. New forms of superparamagnetic nanoparticles for biomedical applications. *Adv. Drug Deliv. Rev*. 2013;65(5):732–743. https://doi.org/10.1016/j.addr.2012.10.008

4. Osminkina L.A., *et al*. Porous silicon nanoparticles as efficient sensitizers for sonodynamic therapy of cancer. *Micropor. Mesopor. Mater.* 2015;210:169–175. https://doi.org/10.1016/j.micromeso.2015.02.037

5. Samira F., Sheikhahmadi A. Effect of nanosilicon dioxide on growth performance, egg quality, liver histopathology and concentration of calcium, phosphorus and silicon in egg, liver and bone in laying quails. *Appl. Nanosci.* 2017;7(1–2):765–772. https://doi.org/10.1007/s13204-017-0620-9

6. Ksenofontova O.I., Vasin A.V., Egorov V.V., *et al.* Porous Silicon and Its Application in Biology and Medicine. *Tech. Phys.* 2014;59(1):66–77. https://doi.org/10.1134/S1063784214010083

7. Wang L., Jang G., Ban D., *et al*. Multifunctional stimuli responsive polymer-gated iron and gold-embedded silica nano golf balls: Nanoshuttles for targeted on-demand theranostics. *Bone Res.* 2017;5(1):17051. https://doi.org/10.1038/boneres.2017.51

8. Li X., Xia S., Zhou W., Zhan W. Targeted Fe-doped silica nanoparticles as a novel ultrasound–magnetic resonance dual-mode imaging contrast agent for HER2-positive breast cancer. *Int. J. Nanomedicine*. 2019;14:2397–2413. https://doi.org/10.2147/IJN.S189252

9. Vaytulevich E.A., Yurmazova T.A., Tuan H.T. Sorbents based on magnetite nanoparticles for biomedical application. *Nanotechnol Russia.* 2019;14(1–2):33–40. https://doi.org/10.1134/S1995078019010129

[Original Russian Text: Vaytulevich E.A., Yurmazova T.A., Tuan H.T. Sorbents based on magnetite nanoparticles for biomedical application. *Rossiiskie nanotekhnologii.* 2019;14(1–2):31–38 (in Russ.). https://doi.org/10.21517/1992-7223-2019-1-2-31-38]

10. Kargina Yu.V., Kharin A.Yu., Zvereva E., *et al.* Silicon Nanoparticles Prepared by Plasma-Assisted Ablative Synthesis: Physical Properties and Potential Biomedical Applications. Phys. Status Solidi A. 2019;216(14):1800897-1–1800897-7. https://doi.org/10.1002/pssa.201800897

11. Kargina Yu.V., Zinovyev S.V., Perepukhov A.M., *et al.* Silicon nanoparticles with iron impurities for multifunctional applications. *Funct. Mater. Lett*. 2020;13(4):2040007-1–2040007-5. https://doi.org/10.1142/S179360472040007X

12. Ishchenko A.A., Fetisov G.V., Aslanov L.A. *Nanokremnii: svoistva, poluchenie, primenenie, metody issledovaniya i kontrolya* (*Nanosilicon: properties, production, application, research and control methods*). Moscow: FIZMATLIT; 2012. 648 p. (in Russ.). ISBN 978-5-9221-1369-4

13. Shtikov S.N. (Ed.). *Problemy analiticheskoi khimii. Nanoob"ekty i nanotekhnologii v khimicheskom analize* (*Analytical chemistry problems. Nanoobjects and nanotechnology in chemical analysis*). V. 20. Moscow: Nauka; 2015. 431 p. (in Russ.). ISBN 978-5-02-039185-7

СПИСОК ЛИТЕРАТУРЫ

1. Elbeshlawi I., AbdelBaki M.S. Safety of gadolinium administration in children. *Pediatr. Neurol.* 2018;86:27–32. https://doi.org/10.1016/j.pediatrneurol.2018.07.010

2. Franckenberg S., Berger F., Schaerli S., Ampanozi G., Thali M. Fatal anaphylactic reaction to intravenous gadobutrol, a gadolinium-based MRI contrast agent. *Radiol. Case Rep.* 2018;13(1):299–301. https://doi.org/10.1016/j.radcr.2017.09.012

3. Xu C., Sun S. New forms of superparamagnetic nanoparticles for biomedical applications. *Adv. Drug Deliv. Rev.* 2013;65(5):732–743. https://doi.org/10.1016/j.addr.2012.10.008

4. Osminkina L.A., *et al*. Porous silicon nanoparticles as efficient sensitizers for sonodynamic therapy of cancer. *Micropor. Mesopor. Mater.* 2015;210:169–175. https://doi.org/10.1016/j.micromeso.2015.02.037

5. Samira F., Sheikhahmadi A. Effect of nanosilicon dioxide on growth performance, egg quality, liver histopathology and concentration of calcium, phosphorus and silicon in egg, liver and bone in laying quails. *Appl. Nanosci.* 2017;7(1–2):765–772. https://doi.org/10.1007/s13204-017-0620-9

6. Ksenofontova O.I., Vasin A.V., Egorov V.V., *et al*. Porous Silicon and Its Application in Biology and Medicine. *Tech. Phys.* 2014;59(1):66–77. https://doi.org/10.1134/S1063784214010083

7. Wang L., Jang G., Ban D., *et al*. Multifunctional stimuli responsive polymer-gated iron and gold-embedded silica nano golf balls: Nanoshuttles for targeted on-demand theranostics. *Bone Res*. 2017;5(1):17051. https://doi.org/10.1038/boneres.2017.51

8. Li X., Xia S., Zhou W., Zhan W. Targeted Fe-doped silica nanoparticles as a novel ultrasound–magnetic resonance dual-mode imaging contrast agent for HER2-positive breast cancer. *Int. J. Nanomedicine*. 2019;14:2397–2413. https://doi.org/10.2147/IJN.S189252

9. Вайтулевич Е.А., Юрмазова Т.А., Чан Т.Х. Сорбенты на основе наночастиц магнетита для применения в биомедицине. *Российские нанотехнологии.* 2019;14(1–2):31–38. https://doi.org/10.21517/1992-7223-2019-1-2-31-38

10. Kargina Yu.V., Kharin A.Yu., Zvereva E., *et al*. Silicon Nanoparticles Prepared by Plasma-Assisted Ablative Synthesis: Physical Properties and Potential Biomedical Applications. *Phys. Status Solidi A.* 2019;216(14):1800897-1–1800897-7. https://doi.org/10.1002/pssa.201800897

11. Kargina Yu.V., Zinovyev S.V., Perepukhov A.M., *et al*. Silicon nanoparticles with iron impurities for multifunctional applications. *Funct. Mater. Lett.* 2020;13(4):2040007-1–2040007-5. https://doi.org/10.1142/S179360472040007X

12. Ищенко А.А., Фетисов Г.В., Асланов Л.А. *Нанокремний: свойства, получение, применение, методы исследования и контроля*. М.: ФИЗМАТЛИТ; 2012. 648 с. ISBN 978-5-9221-1369-4

13. Штыков С.Н. (ред.). *Проблемы аналитической химии.* Т. 20. *Нанообъекты и нанотехнологии в химическом анализе*. М.: Наука; 2015. 431 с. ISBN 978-5-02-039185-7

14. Mosmann T. Rapid colorimetric assay for cellular growth and survival: application to proliferation and cytotoxicity assays. *J. Immunol. Methods.* 1983;65(1–2):55–63. https://doi.org/10.1016/0022-1759(83)90303-4

15. Wagner T., Wang J.Y., Hofmann S. Sputter Depth Profiling in AES and XPS. In book: Briggs D., Grant J.T. (Eds.). *Surface Analysis by Auger and X-ray Photoelectron Spectroscopy*. 2003. P. 619–649.

14. Mosmann T. Rapid colorimetric assay for cellular growth and survival: application to proliferation and cytotoxicity assays. *J. Immunol. Methods.* 1983;65(1–2):55–63. https://doi.org/10.1016/0022-1759(83)90303-4

15. Wagner T., Wang J.Y., Hofmann S. Sputter Depth Profiling in AES and XPS. In book: Briggs D., Grant J.T. (Eds.). *Surface Analysis by Auger and X-ray Photoelectron Spectroscopy*. 2003. P. 619–649.

16. Naumkin A.V., Kraut-Vass A., Gaarenstroom S.W., Powell C.J. NIST X-ray Photoelectron Spectroscopy Database. NIST Standard Reference Database 20, Version 4.1 (Web Version), 2012. http://dx.doi.org/10.18434/T4T88K

17. Crist B.V. Handbook of Monochromatic XPS Spectra: The Elements and Their Native Oxides [Book Review]. *IEEE Electr. Insul. M.* 2003;19(4):73. https://doi.org/10.1109/MEI.2003.1226740

18. Gongalsky M.B., Kargina Yu.V., Osminkina L.A., Perepukhov A.M., Gulyaev M.V., Vasiliev A.N., Pirogov Yu A., Maximychev A.V., Timoshenko V.Yu. Porous silicon nanoparticles as biocompatible contrast agents for magnetic resonance imaging. *Appl. Phys. Lett.* 2015;107(23):233702-1-233702-4. https://doi.org/10.1063/1.4937731

19. Berridge M.V., Herst P.M., Tan A.S. Tetrazolium dyes as tools in cell biology: new insights into their cellular reduction. *Biotechnol. Annu. Rev.* 2005;11:127–152. https://doi.org/10.1016/s1387-2656(05)11004-7

20. Seah M.P., Spencer S.J. Ultrathin SiO_2 on Si (IV). Intensity measurement in XPS and deduced thickness linearity. *Surf. Interface Anal*. 2003;35(6):515–524. https://doi.org/10.1002/sia.1565

21. Vegh J. The Shirley background revised. *J. Electron Spectrosc.* 2006;151(3):159–164. https://doi.org/10.1016/j.elspec.2005.12.002

22. Sharonova N.V., Yagudaeva E.Yu., Sizova S.V., *et al.* Modification of nanocrystalline silicon by polymers for biomedical applications. *Izv. Vyssh. Uchbn. Zaved. Khim. Khim. Tekhnol. = Chem. Chem. Tech.* 2019;62(9):86–96 (in Russ.). https://doi.org/10.6060/ivkkt.20196209.5929

23. Răcucin M., Creangă D.E., Airinei A. Citric-acid-coated magnetite nanoparticles for biological applications. *Eur. Phys. J. E.* 2006;21(2):117–121. https://doi.org/10.1140/epje/i2006-10051-y

24. Dorofeev S.G., Kononov N.N., Ishchenko A.A., *et al.* Optical and structural properties of thin films precipitated from the sol of silicon nanoparticles. *Semiconductors*. 2009;43(11):1420–1427. https://doi.org/10.1134/S1063782609110050

16. Naumkin A.V., Kraut-Vass A., Gaarenstroom S.W., Powell C.J. NIST X-ray Photoelectron Spectroscopy Database. NIST Standard Reference Database 20, Version 4.1 (Web Version), 2012. http://dx.doi.org/10.18434/T4T88K

17. Crist B.V. Handbook of Monochromatic XPS Spectra: The Elements and Their Native Oxides [Book Review]. *IEEE Electr. Insul. M.* 2003;19(4):73. https://doi.org/10.1109/MEI.2003.1226740

18. Gongalsky M.B., Kargina Yu.V., Osminkina L.A., Perepukhov A.M., Gulyaev M.V., Vasiliev A.N., Pirogov Yu A., Maximychev A.V., Timoshenko V.Yu. Porous silicon nanoparticles as biocompatible contrast agents for magnetic resonance imaging. *Appl. Phys. Lett.* 2015;107(23):233702-1-233702-4. https://doi.org/10.1063/1.4937731

19. Berridge M.V., Herst P.M., Tan A.S. Tetrazolium dyes as tools in cell biology: new insights into their cellular reduction. *Biotechnol. Annu. Rev.* 2005;11:127–152. https://doi.org/10.1016/s1387-2656(05)11004-7

20. Seah M.P., Spencer S.J. Ultrathin SiO_2 on Si (IV). Intensity measurement in XPS and deduced thickness linearity. *Surf. Interface Anal*. 2003;35(6):515–524. https://doi.org/10.1002/sia.1565

21. Vegh J. The Shirley background revised. *J. Electron Spectrosc.* 2006;151(3):159–164. https://doi.org/10.1016/j.elspec.2005.12.002

22. Шаронова Н.В., Ягудаева Е.Ю., Сизова С.В. и др. Модификация нанокристаллического кремния полимерами для биомедицинских приложений. *Изв. вузов. Химия и хим. технология.* 2019;62(9):86–96. https://doi.org/10.6060/ivkkt.20196209.5929

23. Răcucin M., Creangă D.E., Airinei A. Citric-acid-coated magnetite nanoparticles for biological applications. *Eur. Phys. J. E.* 2006;21(2):117–121. https://doi.org/10.1140/epje/i2006-10051-y

24. Дорофеев С.Г., Кононов Н.Н., Ищенко А.А. и др. Оптические и структурные свойства тонких пленок, осажденных из золя наночастиц кремния. *Физика и техника полупроводников*. 2009;43(11):1460–1467.

About the authors:

Kirill I. Rozhkov, Postgraduate Student, I.P. Alimarin Department of Analytical Chemistry, M.V. Lomonosov Institute of Fine Chemical Technologies, MIREA – Russian Technological University (86, Vernadskogo pr., Moscow, 119571, Russia). E-mail: rokirill58@mail.ru. https://orcid.org/0000-0003-4120-837X

Elena Y. Yagudaeva, Cand. Sci. (Chem.), Senior Researcher, M.M. Shemyakin & Yu.A. Ovchinnikov Institute of Bioorganic Chemistry, Russian Academy of Sciences (Miklukho-Maklaya ul., 16/10, Moscow, 117997, Russia). E-mail: elena-yagudaeva@yandex.ru. https://orcid.org/0000-0001-9782-0811

Svetlana V. Sizova, Cand. Sci. (Chem.), Researcher, M.M. Shemyakin & Yu.A. Ovchinnikov Institute of Bioorganic Chemistry, Russian Academy of Sciences (Miklukho-Maklaya ul., 16/10, Moscow, 117997, Russia). E-mail: sv.sizova@gmail.com. https://orcid.org/0000-0003-0846-4670

Michael A. Lazov, Assistant, I.P. Alimarin Department of Analytical Chemistry, M.V. Lomonosov Institute of Fine Chemical Technologies, MIREA – Russian Technological University (86, Vernadskogo pr., Moscow 119571, Russia). E-mail: lazovm@gmail.com. https://orcid.org/0000-0001-8578-1683

Evgeniya V. Smirnova, Cand. Sci. (Biol.), Researcher, M.M. Shemyakin & Yu.A. Ovchinnikov Institute of Bioorganic Chemistry, Russian Academy of Sciences (Miklukho-Maklaya ul., 16/10, Moscow, 117997, Russia). E-mail: smirnova.evgeniya@gmail.com. https://orcid.org/0000-0002-9744-952X

Vitaliy P. Zubov, Dr. Sci. (Chem.), Professor, S.S. Medvedev Department of Chemistry and Technology of High-Molecular Compounds, M.V. Lomonosov Institute of Fine Chemical Technologies, MIREA – Russian Technological University (86, Vernadskogo pr., Moscow, 119571, Russia). E-mail: zubov@mirea.ru. Principal Researcher, M.M. Shemyakin & Yu.A. Ovchinnikov Institute of Bioorganic Chemistry, Russian Academy of Sciences (Miklukho-Maklaya ul., 16/10, Moscow, 117997, Russia). E-mail: zubov@ibch.ru. https://orcid.org/0000-0003-3429-0272

Anatoliy A. Ischenko, Dr. Sci. (Chem.), Professor, I.P. Alimarin Department of Analytical Chemistry, M.V. Lomonosov Institute of Fine Chemical Technologies, MIREA – Russian Technological University (86, Vernadskogo pr., Moscow, 119571, Russia). E-mail: aischenko@yasenevo.ru. https://orcid.org/0000-0003-1532-377X

Об авторах:

Рожков Кирилл Игоревич, аспирант кафедры аналитической химии им. И.П. Алимарина Института тонких химических технологий им. М.В. Ломоносова ФГБОУ ВО «МИРЭА – Российский технологический университет» (119571, Россия, Москва, пр-т Вернадского, д. 86). E-mail: rokirill58@mail.ru. https://orcid.org/0000-0003-4120-837X

Ягудаева Елена Юрьевна, к.х.н., старший научный сотрудник Института биоорганической химии им. акад. М.М. Шемякина и Ю.А. Овчинникова Российской академии наук (117997, Россия, Москва, ул. Миклухо-Маклая, д.16/10). E-mail: elena-yagudaeva@yandex.ru. https://orcid.org/0000-0001-9782-0811

Сизова Светлана Викторовна, к.х.н., научный сотрудник Института биоорганической химии им. акад. М.М. Шемякина и Ю.А. Овчинникова Российской академии наук (117997, Россия, Москва, ул. Миклухо-Маклая, д.16/10). E-mail: sv.sizova@gmail.com. https://orcid.org/0000-0003-0846-4670

Лазов Михаил Александрович, ассистент кафедры аналитической химии им. И.П. Алимарина Института тонких химических технологий им. М.В. Ломоносова ФГБОУ ВО «МИРЭА – Российский технологический университет» (119571, Россия, Москва, пр-т Вернадского, д. 86). E-mail: lazovm@gmail.com. https://orcid.org/0000-0001-8578-1683

Смирнова Евгения Владимировна, к.б.н., научный сотрудник Института биоорганической химии им. акад. М.М. Шемякина и Ю.А. Овчинникова Российской академии наук (117997, Россия, Москва, ул. Миклухо-Маклая, д.16/10). E-mail: smirnova.evgeniya@gmail.com. https://orcid.org/0000-0002-9744-952X

Зубов Виталий Павлович, д.х.н., профессор, кафедра химии и технологии высокомолекулярных соединений им. С.С. Медведева Института тонких химических технологий им. М.В. Ломоносова ФГБОУ ВО «МИРЭА – Российский технологический университет» (119571, Россия, Москва, пр-т Вернадского, д. 86). E-mail: zubov@mirea.ru. Главный научный сотрудник Института биоорганической химии им. акад. М.М. Шемякина и Ю.А. Овчинникова Российской академии наук (117997, Россия, Москва, ул. Миклухо-Маклая, д.16/10). E-mail: zubov@ibch.ru. https://orcid.org/0000-0003-3429-0272

Ищенко Анатолий Александрович, д.х.н., профессор, заведующий кафедрой аналитической химии им. И.П. Алимарина Института тонких химических технологий им. М.В. Ломоносова ФГБОУ ВО «МИРЭА – Российский технологический университет» (119571, Россия, Москва, пр-т Вернадского, д. 86). E-mail: aischenko@yasenevo.ru. https://orcid.org/0000-0003-1532-377X

The article was submitted: July 23, 2021; approved after reviewing: September 15, 2021; accepted for publication: October 18, 2021.

Translated from Russian into English by H. Moshkov
Edited for English language and spelling by Enago, an editing brand of Crimson Interactive Inc.

CHEMISTRY AND TECHNOLOGY OF INORGANIC MATERIALS

ХИМИЯ И ТЕХНОЛОГИЯ НЕОРГАНИЧЕСКИХ МАТЕРИАЛОВ

ISSN 2686-7575 (Online)

https://doi.org/10.32362/2410-6593-2021-16-5-426-437

UDC 546.311:546.812:546.161:548.734.036

RESEARCH ARTICLE

Synthesis and X-ray-graphical characteristics of the $MeSn_2F_5$ (Me = Na, K, Rb, Cs) fluoride-ion conductors

Ruslan M. Zakalyukin[1,2,@], Ekaterina A. Levkevich[1,2], Anastasia V. Nikolaeva[3]

[1]MIREA – Russian Technological University, Moscow, 119571 Russia
[2] Federal Scientific Research Center "Crystallography and Photonics," Russian Academy of Sciences, Moscow, 119333 Russia
[3]Lomonosov Moscow State University, Moscow, 119991 Russia
[@]Corresponding author, e-mail: rmzakalyukin@mitht.ru

Abstract

Objectives. *Pentafluorodistannates of alkali metals are promising materials for use as electrolytes in fluoride-ion batteries due to their electrophysical properties, such as high fluoride-ion conductivity. This work aims to synthesize crystals of alkali metals $MeSn_2F_5$ (Me = Na, K, Rb, Cs), carry out X-ray diffraction studies on them, and investigate the possibility of obtaining lithium fluorostannates.*

Methods. *Supersaturated aqueous solutions were employed to synthesize the crystals. The X-ray diffraction (XRD) analysis was carried out.*

Results. *Oversaturated solutions yield microcrystalline powders of sodium, potassium, rubidium, and cesium pentafluorodistannates. The presence of a single-phase was confirmed by XRD analysis of the powders corresponding to the $MeSn_2F_5$ (Me = Na, K, Rb, Cs) composition. XRD data analysis and literature indicated that $MeSn_2F_5$ (Me = K, Rb, Cs) have a fluorite-like structure, with the cations forming three-layer closest packing. The $RbSn_2F_5$ compound was discovered to be isostructural to KSn_2F_5. Based on this discovery, $RbSn_2F_5$ was reindexed to a hexagonal unit cell with parameters a = 7.40(3) Å, c = 10.12(6) Å (KSn_2F_5 P3, a = 7.29(3) Å, c = 9.86(2) Å). The $CsSn_2F_5$ compound was reindexed to a monoclinic unit cell (a = 10.03(4) Å, b = 5.92(7) Å, c = 11.96(9) Å, β = 107.4(5)°). A crystallochemical analysis of the pentafluorodistannates was carried out, and common structural motifs were discovered. The motifs are similar to lead tetrafluorostannate $PbSnF_4$, the best fluoride-ion conductor. The effect of the pentafluorodistannates structures on the ionic conductivity is considered. The $LiF–SnF_2$ system contains no compounds; the compositions were obtained by melting the original fluorides.*

Conclusions. *$MeSn_2F_5$ (Me = Na, K, Rb, Cs) were synthesized and investigated by XRD analysis. The structural characteristics of the $RbSn_2F_5$ and $CsSn_2F_5$ compounds have been redefined. The crystallochemical structure is analyzed in relation to the electrophysical properties of the alkali metal pentafluorodistannates. Pentafluorodistannates $MeSn_2F_5$ (Me = K, Rb, Cs) have a fluorite-like structural motif with cubic parameters a = 5.694 Å (KSn_2F_5), a = 5.846 Å ($RbSn_2F_5$), a = 6.100 Å ($CsSn_2F_5$), with the cations forming three-layer closest packing. The cationic layers alternate like Me–Sn–Sn–Me (Me = K, Rb, Cs). For KSn_2F_5 and $RbSn_2F_5$, they are normal to the three-fold axis and normal to the four-fold axis in the case of $CsSn_2F_5$.*

Keywords: *fluorostannates, X-ray diffraction analysis, fluoride-ion conductivity, tin fluoride, fluorides, crystal chemistry, layered structures*

For citation: Zakalyukin R.M., Levkevich E.A., Nikolaeva A.V. Synthesis and X-ray-graphical characteristics of the $MeSn_2F_5$ (Me = Na, K, Rb, Cs) fluoride-ion conductors. *Tonk. Khim. Tekhnol. = Fine Chem. Technol*. 2021;16(5):426–437 (Russ., Eng.). https://doi.org/10.32362/2410-6593-2021-16-5-426-437

НАУЧНАЯ СТАТЬЯ

Синтез и рентгенографические характеристики фтор-ионных проводников $MeSn_2F_5$ (Me = Na, K, Rb, Cs)

Р.М. Закалюкин[1,2,@], Е.А. Левкевич[1,2], А.В. Николаева[3]

[1]МИРЭА – Российский технологический университет, Москва, 119571 Россия
[2]ФНИЦ «Кристаллография и фотоника», Российская академия наук, Москва, 119333 Россия
[3]Московский государственный университет им. М.В. Ломоносова, Москва, 119991 Россия
[@]Автор для переписки, e-mail: rmzakalyukin@mitht.ru

Аннотация

Цель. *Пентафтордистаннаты щелочных элементов являются перспективными материалами для практического применения в качестве электролитов во фторионных аккумуляторах за счет своих электрофизических характеристик, а именно высокой фторионной проводимости. Цель работы заключается в синтезе из раствора и рентгенографическом изучении кристаллов пентафтордистаннатов щелочных металлов $MeSn_2F_5$ (Me = Na, K, Rb, Cs) и исследовании возможности получения фторстаннатов лития.*

Методы. *Синтезировали кристаллы из пересыщенных водных растворов. Исследование проводили методом рентгенофазового анализа (РФА).*

Результаты. *Получены мелкокристаллические порошки пентафтордистаннатов натрия, калия, рубидия и цезия. Исследование методом РФА синтезированных порошков показало их однофазность и соответствие составу $MeSn_2F_5$ (Me = Na, K, Rb, Cs). Анализ данных рентгеновской дифрактометрии и литературных данных показал, что соединения $MeSn_2F_5$ (Me = K, Rb, Cs) являются флюоритоподобными – катионы образуют трехслойную плотнейшую упаковку. Было выявлено, что $RbSn_2F_5$ изоструктурен KSn_2F_5, на основании чего выполнено переиндицирование на гексагональную ячейку: a = 7.40(3) Å, c = 10.12(6) Å (KSn_2F_5 P3, a = 7.29(3) Å, c = 9.86(2) Å). Соединение $CsSn_2F_5$ переиндицировано на моноклинную ячейку (a = 10.03(4) Å, b = 5.92(7) Å, c = 11.96(9) Å; β = 107.4(5)°). Проведен кристаллохимический анализ указанных пентафтордистаннатов, выявлены общие структурные мотивы, подобные лучшему фторионному проводнику – тетрафторстаннату свинца $PbSnF_4$, и рассмотрено влияние строения пентафтордистаннатов на ионную проводимость. В системе $LiF–SnF_2$ соединений не обнаружено, взаимодействие исследовали сплавлением исходных фторидов.*

Выводы. *Синтезированы и охарактеризованы методом РФА пентафтордистаннаты $MeSn_2F_5$ (Me = Na, K, Rb, Cs). Для соединений $RbSn_2F_5$ и $CsSn_2F_5$ переопределены структурные характеристики. Проанализировано кристаллохимическое строение в приложении к электрофизическим свойствам пентафтордистаннатов щелочных металлов. Пентафтордистаннаты $MeSn_2F_5$ (Me = K, Rb, Cs) имеют флюоритоподобный структурный мотив с приведенным параметром ячейки куба a = 5.694 Å (KSn_2F_5), a = 5.846 Å ($RbSn_2F_5$), a = 6.100 ($CsSn_2F_5$) Å, при этом катионы образуют трехслойную плотнейшую упаковку. Слои катионов чередуются в последовательности Me–Sn–Sn–Me (Me = K, Rb, Cs) в случае KSn_2F_5 и $RbSn_2F_5$ перпендикулярно оси третьего порядка, а в случае $CsSn_2F_5$ – оси четвертого порядка.*

Ключевые слова: *фторстаннаты, рентгенофазовый анализ, фторионная проводимость, фторид олова, фториды, кристаллохимия, слоистые структуры*

Для цитирования: Закалюкин Р.М., Левкевич Е.А., Николаева А.В. Синтез и рентгенографические характеристики фтор-ионных проводников $MeSn_2F_5$ (Me = Na, K, Rb, Cs). *Тонкие химические технологии.* 2021;16(5):426–437. https://doi.org/10.32362/2410-6593-2021-16-5-426-437

The need for compact and rechargeable current sources has given rise to various types of lithium batteries development. Although the characteristics of lithium batteries have not yet reached their practical limits, it is clear that new classes of electrochemical devices are required. Sodium batteries are currently being actively developed. The use of other alkali metals is being considered, and the development of batteries based on metallic magnesium, titanium, or aluminum is drawing attention [1]. Batteries operate based on an electrochemical reaction involving the transfer of a cation in an electrochemical cell. Because cations are smaller than anions by nature, they have greater mobility and penetrating ability as charge carriers. Also, the electrolyte in an electrochemical cell must be solid (superionic), which significantly improves such cells' operational characteristics. Fluorine is likely to be the only anion that can be used in solid-state electrochemical cells, as it outperforms its closest competitors: oxygen and chlorine. Fluoride ionic conductors have several advantages over other solid-state anionic conductors: relatively high conductivity, solid electrolytes stability at room temperature, and a reasonably large theoretically possible potential difference of a charged cell. Fluorine has the highest electron affinity, second only to chlorine, suggesting the possibility of obtaining high potentials comparable to lithium batteries on electrochemical cells with a mobile fluorine anion. Fluoride ionic electrochemical cells allow using fluorides of less active metals as an anode and cathode, which is safer than lithium batteries, from which lithium metal or its highly active compounds are obtained, and the electrochemical cell can be depressurized and ignited. These advantages lead us to believe that fluoride ionic batteries will find practical applications and fill a niche in electronic devices that is both safe and compact.

The creation of fluoride ionic batteries requires the study of several practical issues, for example, the choice of electrochemical pairs for electrode materials. Tin(II) fluoride is one of the possible materials of the cathode; it exhibits a high fluoride ionic conductivity and a low electrochemical potential formation. Although using pure tin fluoride is promising, it imposes some restrictions. The first is the possibility of recrystallization into a monolithic material, resulting in a significant decrease in the phase boundary area, consequently decreasing

the current characteristics of the electrochemical elements (current density decreases). Second, dendrites (crystals of metallic tin) may form, leading to the breakdown of the electrochemical cell. In this case, using fluorostannates is more advantageous because the released metal fluorides prevent the growth of tin particles with the ability to accumulate sorbed fluoride ions on themselves during the reduction of tin fluoride. Alkali metal fluorostannates are promising. The presence of trifluorostannates and pentafluorodistannates of sodium, potassium, cesium, and rubidium is demonstrated. Pentafluorodistannates are superior to trifluorostannates in terms of electrophysical characteristics, as they have a higher fluoride ionic conductivity, whereas the conductivity of trifluorostannates does not exceed the order of 10^{-9} S/cm [2].

The melting of tin fluoride with potassium, rubidium, and cesium fluorides leads to smoothing its phase transition from monoclinic to tetragonal modification with a concomitant increase in conductivity. At the same time, doping with rubidium ions (5% RbF, $6.31 \cdot 10^{-2}$ Cm/cm at 453 K) has the most significant influence, while doping with sodium ions with the formation of the $NaSn_2F_5$ phase ($2.62 \cdot 10^{-4}$ Cm/cm at 453 K) has the least. At 438 K, the conductivity of cesium pentafluorodistannate $CsSn_2F_5$ reaches $3.54 \cdot 10^{-3}$ Cm/cm, while that of potassium pentafluorodistannate KSn_2F_5 reaches $2.02 \cdot 10^{-2}$ Cm/cm at 463 K [3]. In the case of the phase formation of rubidium pentafluorodistannate $RbSn_2F_5$, its conductivity reaches $1.25 \cdot 10^{-1}$ Cm/cm at 473 K [4].

Works based on the structural studies of these compounds, for the most part, date back to the 1960s–1980s and contain ambiguous and even contradictory data on the structures. The structure of sodium pentafluorodistannate was determined by single-crystal X-ray diffraction (XRD) analysis in 1964. The compound crystallizes in tetragonal syngony with parameters a = 6.37 Å, c = 13.71 Å, V = 556 Å^3 according to [5] and the authors [6] decided the structure in the same year and specified that $NaSn_2F_5$ has the space group $P4_2/nbc$ and parameters a = 9.02 Å, c = 13.685 Å.

Donaldson [5] gives the first data on the structure of potassium pentafluorodistannate, stating that fluorostannate corresponds to an orthorhombic system with parameters a = 12.54 Å, b = 9.80 Å, c = 7.71 Å, V = 948 Å^3. The structure of KSn_2F_5 was refined in [7, 8], and the authors captured the phase transition as follows: at room temperature, the hexagonal unit cell $P3$, a = 7.291 Å, c = 9.861 Å, and V = 454 Å^3, at 443 K, $P3m1$, a = 4.268 Å, c = 9.911 Å, and V = 156.3 Å^3. The results of the single-crystal XRD analysis in a later work [9] confirmed the identity of the crystals KSn_2F_5 to be a hexagonal crystal system $P3$, a = 7.266 Å, c = 9.796 Å, V = 447.89 Å^3 (at 200 K), $P3$, a = 7.302 Å, c = 9.872 Å, V = 455.85 Å^3 (at 350 K).

Cesium pentafluorodistannate $CsSn_2F_5$ crystallizes in the orthorhombic crystal system (a = 19.20 Å, b = 12.44 Å, c = 8.54 Å, V = 2040 Å^3). Rubidium pentafluorodistannate $RbSn_2F_5$ crystallizes in the orthorhombic crystal system (a = 12.48 Å, b = 9.92 Å, c = 7.35 Å. V = 910 Å^3) according to powder X-ray diffraction [10]. The structures of these fluorostannates' high-temperature phases were later determined using neutron powder diffraction [11]. At 538 K, $CsSn_2F_5$ has a space group $I4/mmm$ with parameters a = 4.2606 Å, c = 19.739 Å, V = 358.31 Å^3, and at 473 K, $RbSn_2F_5$ has the hexagonal crystal system: $P3$, a = 4.3581 Å, c = 10.1704 Å, V = 167.29 Å^3.

Our work aims to synthesize from a aqueous solution and carry out an X-ray study of crystals of alkali metal pentafluorodistannates, namely: sodium, potassium, cesium, and rubidium, and study the possibility of obtaining lithium fluorostannates.

EXPERIMENTAL

The synthesis was performed using tin(II) fluoride SnF_2 (*Sigma-Aldrich*, USA), cesium fluoride CsF (pure), sodium fluoride NaF (pure), lithium fluoride LiF (chemically pure), potassium carbonate K_2CO_3 (pure), rubidium carbonate Rb_2CO_3 (pure) and hydrofluoric acid HF (chemically pure). At 80°C, cesium fluoride was pre-dried. Potassium and rubidium fluorides were obtained by dissolving metal carbonates in hydrofluoric acid.

The method of crystallization from an aqueous solution was employed to synthesize the compounds $NaSn_2F_5$, KSn_2F_5, $CsSn_2F_5$, $RbSn_2F_5$. The calculated fluoride weighted amount based on molar ratios was placed in plastic tubes and dissolved in distilled water. The test tubes were heated to 70°C in an ultrasonic bath to obtain a concentrated solution and achieve supersaturation during cooling. An ice bath was utilized to increase the crystallization product yield as the solution was gradually cooled, resulting in abundant fluorostannates crystallization.

Some solutions were acidified with hydrofluoric acid to prevent the hydrolysis of tin(II) fluoride and tin oxide SnO precipitation.

Tin(II) fluoride and lithium fluoride were melted (in the stoichiometric ratios of 1:2, 2:1) in a glassy carbon crucible in a nitrogen atmosphere heated to 300°C and held at the specified temperature for 20 min to search for compounds in the LiF–SnF_2 system.

The size and morphology control of the obtained crystals were implemented using an optical microscope POLAM S-111 (*LOMO*, Russia) with

crossed polarizers. Sodium pentafluorodistannate $NaSn_2F_5$ formed needle-like crystals, KSn_2F_5 and $CsSn_2F_5$—bulk crystals, $RbSn_2F_5$—hexagonal-shaped platy crystals.

The obtained mixed fluorides crystals were ground in a jasper mortar and examined by XRD analysis on a Shimadzu XRD 6000 diffractometer (*Shimadzu*, Japan). Powder diffraction patterns were taken in the range of angles 2θ from 10° to 60° with a step of 0.02°, 1 s exposure time per point and CuKα radiation.

The peak positions were determined using the Profit program [12], and indexing by the least-squares technique was performed using the Powder program[1]. The difference between the experimental and calculated indexing parameters ΔQ expressed as $Q = 10^4/d^2$, where d is the interplanar distance (Å), determines the indexing quality. $\Delta Q < 5$ indicates high imaging and indexing quality.

RESULTS AND DISCUSSION

The samples obtained by melting SnF_2 and LiF in the molar ratio 1:2 and 2:1 did not form co-phases. According to the card 04-0857 of powder database PCPDFWIN, all the samples were two-phase and showed a predominantly monoclinic modification of tin(II) fluoride and smaller amounts compared to the amount of lithium fluoride (peaks at angles 2θ ~ 38.696°, 44.996°). The calculated cell parameters ($C2/c$, a = 13.35 Å, b = 4.908 Å, c = 13.78 Å, β = 109.1°, V = 853.97 Å^3) correspond to the card 15-0744 SnF_2. The immutability of the SnF_2 parameters implies that lithium fluoride does not form solid solutions with tin difluoride.

Alkali metals (Na, K, Rb, Cs) form pentafluorodistannates and trifluorostannates with tin(II) fluoride. The pentafluorodistannates of interest to us are those synthesized and crystallized from the aqueous solutions. Figure 1 shows the powder diffraction patterns of the $NaSn_2F_5$, KSn_2F_5, $RbSn_2F_5$, $CsSn_2F_5$ compounds.

The sodium and potassium pentafluorodistannates diffraction patterns indexing showed good convergence with the powder database cards (Table 1).

The sodium salt diffraction pattern differs significantly from the similar diffraction patterns of potassium, rubidium, and cesium salts (Fig. 1). The diffraction patterns of KSn_2F_5 and $RbSn_2F_5$ are almost identical. All of this indicates that these compounds have a similar structural motif, and potassium and rubidium pentafluorodistannates are isostructural. Based on these assumptions, reindexing was

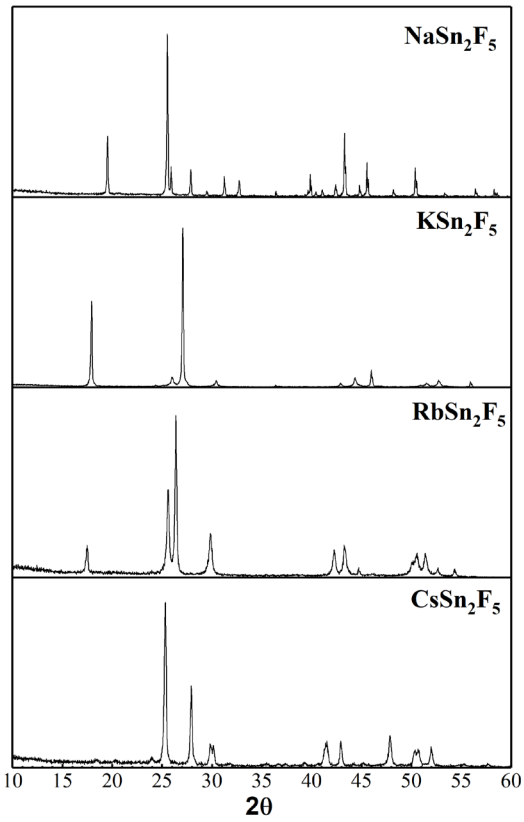

Fig. 1. Powder diffraction patterns of $NaSn_2F_5$, KSn_2F_5, $RbSn_2F_5$, $CsSn_2F_5$.

performed on a powder diffraction pattern of $RbSn_2F_5$ on a hexagonal cell similar to KSn_2F_5 (Table 2). The obtained primitive unit cell parameters for rubidium pentafluorodistannate are a = 7.40(3) Å, c = 10.12(6) Å. Compared to the cell proposed in [10] with a volume twice as large, this indexing is characterized by higher quality.

A distorted fluorite-like cell with the given parameter a = 5.694 Å, formed by tin and potassium cations, can be distinguished in the structure of potassium pentafluorodistannate (hexagonal syngony, according to [7]). Figure 2 depicts the unit cell of KSn_2F_5. For convenience, only the cations are left in the model. As shown, the tin cations at the hexagonal cell's base are arranged according to the law of the three-layer closest packing, while the cations above and below it are located above and below its voids. Both layers are represented by the closest packing, having different positions above the voids and indicating the formation of a three-layer closest packing (ABCABC). Layers A and B are represented by Sn cations in the three-layer packaging sequence, while K cations represent layer C. Such layer sequence is perpendicular to the crystallographic axis c of the hexagonal structure, corresponding to the fluorite-like cube's large diagonal, and equal to the parameter

[1] Faculty of Chemistry, M.V. Lomonosov Moscow State University, Moscow.

Table 1. Results of $NaSn_2F_5$, KSn_2F_5 powder diffraction patterns indexing

Compound	Cell parameters from the results of the indexing	Cell parameters from the literature data
$NaSn_2F_5$	$P4_2/nbc$, a = 9.035(2) Å, c = 13.715(5) Å, V = 1119.6(4) Å^3	$P4_2/nbc$, a = 9.020(3) Å, c = 13.686(3) Å, V = 1113.50 Å^3 (Card PCPDFWIN 21-1233)
KSn_2F_5	$P3$, a = 7.293(6) Å, c = 9.862(2) Å, V = 454.2(7) Å^3	$P3$, a = 7.291(1) Å, c = 9.862(1) Å, V = 453.97 Å^3 (Card PCPDFWIN 76-1977)

Table 2. $RbSn_2F_5$ powder diffraction pattern indexing

No.	2θ	d, Å	Q_{exp}	I/I_o	$h\ k\ l$	Q_{calc}	ΔQ
1	17.50	5.0668	389.5	16	0 0 2	390.1	−0.6
2	25.64	3.4730	829.1	87	1 1 1	827.3	1.8
3	26.38	3.3772	876.8	100	0 0 3	877.7	−0.9
4	27.86	3.2019	975.4	1	2 0 0	973.1	2.3
5	29.88	2.9902	1118.4	53	1 1 2	1119.9	−1.5
6	42.28	2.1371	2189.5	24	3 0 0	2189.4	0.1
7	43.32	2.0887	2292.2	43	1 1 4	2290.2	2.0
8	44.74	2.0252	2438.2	6	0 0 5	2438.1	0.1
9	50.06	1.8221	3012.0	18	2 2 1	3016.8	−4.8
10	50.52	1.8068	3063.3	29	3 0 3	3067.2	−3.9
11	51.44	1.7765	3168.6	31	1 1 5	3168.0	0.6
12	52.70	1.7367	3315.5	9	2 2 2	3309.3	6.2
13	54.36	1.6878	3510.4	5	0 0 6	3510.9	−0.5

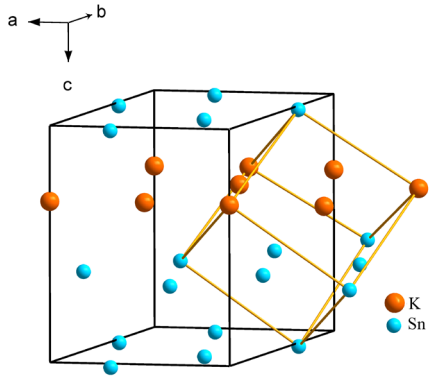

Fig. 2. Transformation of the unit cell of KSn_2F_5: fluorine atoms are removed from the model; hexagonal cell accords to [7] (the coordinate system is for this lattice); orange cubic cell is fluorite-like cell.

c = 9.862 Å of the KSn_2F_5 cell. Fluorine atoms do not fill all tetrahedral voids; instead, the majority of them are statistically located. There are no fluorine anions in the interlayer space of Sn cations.

A similar motif is observed in the $RbSn_2F_5$ structure (Fig. 3). From [11], rubidium cations are located at the hexagonal cell's base according to the law of the closest packing. According to the same law, tin cations are located above and below the voids of this layer, and their positions do not coincide with the rubidium cations, indicating the formation of a three-layer closest packing of cations with alternating Sn–Sn–Rb layers. The parameter c for the orthorhombic cell proposed in [10] is equal to the hexagonal cell's parameter c = 10.126 Å. Rubidium cations are also located at the orthorhombic cell's

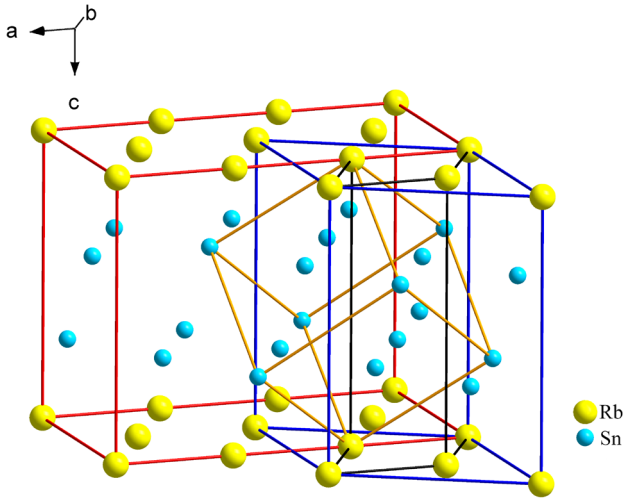

Fig. 3. Transformation of the unit cell of $RbSn_2F_5$: fluorine atoms are removed from the model; black hexagonal cell accords to [11] (the coordinate system is for this lattice); red orthorhombic cell accords to [10]; the orange cubic cell is fluorite-like cell; the blue hexagonal cell is obtained by the indexing results.

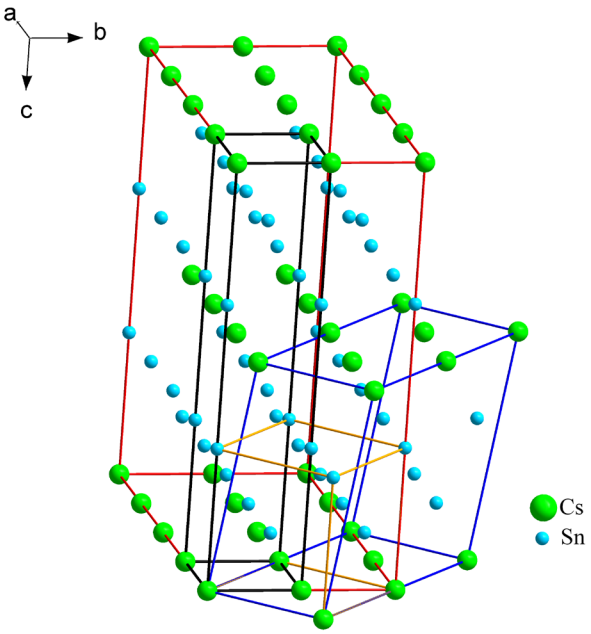

Fig. 4. Transformation of the unit cell of $CsSn_2F_5$: fluorine atoms are removed from the model; black tetragonal cell according to [11] (the coordinate system is for this lattice); red orthorhombic cell according to [10]; the orange cubic cell is fluorite-like cell; the blue monoclinic cell is obtained by the indexing results.

base, having an area six times larger than the cell area [11]. The hexagonal cell's base obtained by reindexing due to the isostructure of potassium and rubidium pentafluorodistannates is similarly represented by rubidium cations; however, its area is three times larger than the cell area [11]. The three-layer closest packing of cations, the fluorite motif with the given parameter a = 5.846 Å, is preserved in all cases. The parameter of the fluorite-like cell increased by 2.6% compared to potassium pentafluorodistannate, indicating the isostructure of these compounds.

The structure of $CsSn_2F_5$ shows a fluorite structural motif, similar to that of potassium and rubidium pentafluorodistannates (Fig. 4). Due to the larger ionic radius of cesium than potassium and rubidium, the reduced cubic cell is larger than in the first two cases, and its parameter is a = 6.100 Å. The $CsSn_2F_5$ powder diffraction pattern was reindexed to a monoclinic primitive unit cell with parameters a = 10.03(4) Å, b = 5.92(7) Å, c = 11.96(9) Å, β = 107.4(5)°, V = 679.0(1) Å^3 (Table 3).

The Miller indices were redefined based on a crystal-chemical analysis of the literature data [5–11]. A densely packed layer of cesium atoms lies at the monoclinic cell's base, with tin atoms forming dense layers above and below it in the voids. As Fig. 4 shows, the rectangular face of a monoclinic cell with dimensions b = 5.927 Å and c = 11.969 Å corresponds to two faces of a fluorite cube with cesium atoms at the base, and the parameter a = 10.034 Å connects the two nearest layers of cesium atoms. Compared to potassium pentafluorodistannate, the fluorite cube's parameter a = 6.100 Å increased by 7.1%, explaining the difference between the cationic motif and the two previous structures. Unlike KSn_2F_5 and $RbSn_2F_5$, the Sn–Sn–Cs layers are now located perpendicular to one of the fourth-fold axes (the fluorite cell), rather than the fluorite motif's third-fold axis, causing cations to be collected in the dense layers, rather than the densest layers. The planes of cesium cations limit the orthorhombic cell presented in [10], forming its bases. The side of cell b's base is the diagonal of the fluorite cube's face, and the side a is the doubled diagonal. The height of cell c corresponds to the tripled side of the cube. The base area is four times that of the base area of a fluorite-like cell, and the volume is 12 times larger. The authors of [11] presented a much more simplified tetragonal cell. According to [10], its height coincides with the parameter c of the orthorhombic cell. The base area is half that of the fluorite-like cell's face, implying that the cell parameter "a" differs from the cubic cell parameter by a factor $\sqrt{2}$.

Let us consider the influence of the structure of pentafluorodistannates on their fluoride-ion conductivity. Fluorostannates have a significant ionic conductivity and compete with fluoride-ion conductors containing rare earth elements (REE). High-conducting fluorides have fluorite or tisonite

Table 3. $CsSn_2F_5$ powder diffraction pattern indexing

No.	2θ	*d*, Å	Q_{exp}	I/I_o	*h k l*	Q_{calc}	Δ*Q*
1	18.530	4.7844	436.86	1	2 0 0	436.53	0.33
2	20.343	4.3620	525.57	2	1 1 1	525.36	0.20
3	23.936	3.7147	724.69	2	2 1 0	721.20	3.49
4	25.310	3.5161	808.87	100	1 1 2	810.33	−1.46
5	27.908	3.1944	979.99	48	3 0 0	982.20	−2.21
6	29.823	2.9935	1115.94	14	−1 0 4	1116.87	−0.93
7	30.143	2.9624	1139.50	12	0 2 0	1138.66	0.83
8	31.869	2.8058	1270.24	2	−1 2 1	1269.63	0.61
9	35.630	2.5178	1577.46	4	2 2 0	1575.19	2.26
10	36.637	2.4509	1664.75	3	1 2 2	1664.32	0.42
11	39.258	2.2930	1901.92	3	3 1 2	1902.86	−0.94
12	40.644	2.2180	2032.72	1	−3 2 1	2032.96	−0.25
13	41.339	2.1823	2099.77	17	1 2 3	2102.69	−2.92
14	41.557	2.1714	2120.90	14	3 2 0	2120.86	0.04
15	42.917	2.1056	2255.53	17	−1 2 4	2255.53	0
16	44.256	2.0450	2391.19	2	2 1 4	2387.32	3.86
17	45.159	2.0062	2484.57	3	−5 0 2	2486.47	−1.90
18	47.471	1.9137	2730.56	1	5 0 0	2728.33	2.23
19	47.843	1.8997	2770.96	25	−5 1 2	2771.14	−0.18
20	50.281	1.8132	3041.65	16	0 1 6	3045.86	−4.21
21	50.671	1.8001	3086.08	15	1 3 2	3087.65	−1.57
22	51.985	1.7577	3236.76	14	−4 2 4	3234.14	2.62
23	55.314	1.6595	3631.16	4	−6 0 3	3631.51	−0.35
24	57.631	1.5982	3915.05	3	−6 1 3	3916.18	−1.12

structure. Usually pure fluorites and tisonites have low conductivity. Their conductivity is increased by introducing heterovalent cation substitution. REE is introduced into the fluorites, resulting in the additional interstitial fluorine ion into the fluorite cell. Alkaline earth fluoride dopant elements are introduced into the composition of tisonites, causing fluorine vacancies to form in the structure. All of this allows the increase of the initial compounds' fluoride ionic conductivity.

Despite all attempts to increase the fluoride ionic conductivity of tisonites and fluorites, the compound lead tetrafluorostannate $PbSnF_4$ is the best fluoride-ion conductor at room temperature [13]. Although this compound is stoichiometric, it has a rich polymorphism. Attempts to increase its conductivity by introducing impurities have been ineffective. Only by doping lead tetrafluorostannate with lithium fluoride this was possible [4]. Increasing

the conductivity of $PbSnF_4$ is a promising task. It is possible to understand this compound's fluoride ionic conductivity mechanism by considering the structure of the compounds with fragments, such as $PbSnF_4$. Studying lead tetrafluorostannate directly [14] is very difficult due to its polymorphism and inhibition of phase transitions. A three-layer closest packing of cations represents all polymorphic modifications of the $PbSnF_4$ compound. The cations forming the packing are collected in dense layers that alternate with Sn–Sn–Pb–Pb pairs; there are no fluorine anions in the gaps between the layers of tin atoms. A similar layered structure is observed on the pentafluorodistannates of alkali metals. They are stoichiometric compounds with high mobility fluorine ions. Analysis of their structure and ionic conductivity parameters will allow us to understand better the ionic conductivity mechanism of the $PbSnF_4$ compound and possibly identify ways to increase it.

Let us consider the pentafluorodistannates of alkali metals successively. In fluorostannates, the fluorine atoms that coordinate tin(II) are located in one hemisphere. Lithium fluorostannates are not formed because the tin atoms coordinate alkali metals with their fluorine. Sterically, a lithium atom with its small size will not be able to coordinate such large structural fragments.

The sodium pentafluorodistannate structure consists of chains of tin cations located along the fourth-fold axis' direction. Tin cations form tetrahedra, which are connected along their edges. The fluorine anions in the tin atom's coordination sphere have angles between them that are slightly less than a right one and are turned outward from the tin tetrahedra's axis. In this case, the fluorine atoms coordinate the sodium atoms located in the channels between the chains. Compared to other alkali metal fluorostannates, all the fluorine atoms are strongly bound to the tin atoms, which explains the worst fluoride-ion conductivity.

The cations are arranged according to the law of the closest three-layer cubic packing (not ideal) for the potassium, rubidium, and cesium compounds. In the case of potassium and rubidium (Figs. 2 and 3), the densest layers alternate as A_{Sn}, B_{Sn}, C_{Me} (Me = K, Rb). There are no fluorine atoms in the space between the tin layers. The fluorine atom is quite firmly fixed, and the bond with the tin atom is located perpendicular to the plane of the tin atoms. The remaining fluorine atoms form almost a plane near the atomic layer of tin. The fluorine anions in these layers are statistically located under or near the tetrahedral voids. These fluorine atoms carry out charge transfer. The conductivity in the crystal volume is anisotropic and two-dimensional. By increasing the distances in the layers of the tin atoms, which creates broader and deeper valleys on the atomic surface of tin atoms for the movement of fluorine ions, rubidium pentafluorodistannate has a higher fluoride-ion conductivity (Table 4) compared to potassium pentafluorodistannate.

This structure changes during the transition to cesium pentafluorodistannate (Fig. 4); cations also form a three-layer closest packing, and tin and cesium planes form closely packed layers perpendicular to the fourth-fold axis [11]. There are no fluorine atoms in the space between the tin cations, and a firmly fixed fluorine atom is perpendicular to the plane of the tin atoms by its Sn–F bond. Because the cesium atoms are located above the tin packaging's voids, the mobile fluorine atoms form a plane parallel to the tin cation layer's surface and are located in the gaps between the nearest neighbors, preventing the fluorine atoms' free movement along the tin layer's atomic surface. This explains the sharp drop in the cesium salt's fluoride-ion conductivity by three orders of magnitude and increased activation energy (Table 4).

Table 4. Comparison of the electrophysical and crystallochemical characteristics of fluorostannates

Compound	Conductivity at the room temperature, S/cm [2]	Activation energy, eV [2]	Interlayer distance between the Sn cation layers, Å	Distance between the Sn cations inside the layer, Å
$NaSn_2F_5$	$8\cdot10^{-9}$	0.57	–	–
KSn_2F_5	$5\cdot10^{-6}$	0.55	3.444	4.200
$RbSn_2F_5$	$2\cdot10^{-5}$	0.68	3.491	4.358
$CsSn_2F_5$	$4\cdot10^{-8}$	0.76	3.227	4.260
$PbSnF_4$	$(1–10)\cdot10^{-3}$	0.11–0.42	3.042	4.224

CONCLUSIONS

This study investigates the possibility of obtaining lithium fluorostannates in the $LiF–SnF_2$ system by fusing lithium fluoride and tin(II) fluoride in molar ratios of 1:2 and 2:1. There were no compounds and solid solutions found in the XRD data. This is due to the lithium atom's inability to coordinate large structural fragments characteristic of alkali metal pentafluorodistannates.

Crystals of alkali metal pentafluorodistannates (sodium, potassium, rubidium, and cesium) were synthesized from aqueous solutions, and their X-ray phase study was conducted. The results of indexing the XRD data confirmed the single-phase nature of the obtained samples and good correspondence to the composition of $MeSn_2F_5$ (Me = Na, K, Rb, Cs). The cells parameters for $NaSn_2F_5$ ($P4_2/nbc$, a = 9.035(2) Å, c = 13.715(5) Å, V = 1119.6(4) Å^3), and KSn_2F_5 ($P3$, a = 7.293(6) Å, c = 9.862(2) Å, V = 454.2(7) Å^3) calculated by a least-square technique has shown good agreement with the literature data and cards of PCPDFWIN powder database. It was revealed during a crystal-chemical analysis of pentafluorodistannates that the compounds $MeSn_2F_5$ (Me = K, Rb, Cs) with high fluoride-ion conductivity have a layered structure corresponding to the three-layer packing type of fluorite, in which a pair of tin layers alternate with the layers of cations of alkali metal Sn–Sn–Me (Me = K, Rb, Cs) pentafluorodistannate. The reduced fluorite-like cells parameters naturally increase down the group: 5.694 Å (KSn_2F_5), 5.846 Å ($RbSn_2F_5$), 6.100 Å ($CsSn_2F_5$). For potassium and rubidium pentafluorodistannates, the Sn–Sn–Me (Me = K, Rb) layers are the densest, and the conductivity increases from KSn_2F_5 to $RbSn_2F_5$. Rubidium pentafluorodistannate $RbSn_2F_5$ is isostructural with KSn_2F_5, and the compound was reindexed to a hexagonal cell with parameters a = 7.40(3) Å and c = 10.12(6) Å. In the $CsSn_2F_5$ compound, the Sn–Sn–Cs layers are dense but not the densest and oriented along one of the axes of the fourth-fold of the fluorite motif. The fluoride-ion conductivity is significantly reduced due to the cationic packaging's global rearrangement. Cesium pentafluorodistannate $CsSn_2F_5$ was reindexed from orthorhombic (according to literature data) to a monoclinic system with cell parameters a = 10.03(4) Å, b = 5.92(7) Å, c = 11.96(9) Å, β = 107.4(5)°. Surprisingly, $CsSn_2F_5$ is the closest to $PbSnF_4$ in terms of the structure and packing of the layers. This suggests that their conductivity mechanisms are distinct. Perhaps, suppose a $PbSnF_4$ compound or a similar $BaSnF_4$ compound with the same type of cation layer packing as KSn_2F_5 and $RbSn_2F_5$ can be obtained. In that case, a higher value of fluoride ionic conductivity can be achieved. It is still not completely clear how to accomplish this.

Acknowledgments

This study was supported by the Ministry of Science and Higher Education within the State assignment of Federal Scientific Research Center "Crystallography and Photonics," Russian Academy of Sciences, and was performed using the equipment of the Shared Science and Training Center for Collective Use of MIREA – Russian Technological University.

Authors' contribution

R.M. Zakalyukin – conducting synthesis, X-ray diffraction analysis, and crystallochemical analysis, writing the text of the article, powder diffraction patterns indexing;

E.A. Levkevich – conducting synthesis, working with the literature, writing and editing the text of the article, powder diffraction patterns indexing;

A.V. Nikolaeva – conducting synthesis, working with the literature, powder diffraction patterns indexing.

The authors declare no conflicts of interest.

REFERENCES

1. Gschwind F., Rodriguez-Garcia G., Sandbeck D.J.S., Gross A., Weil M., Fichtner M., Hörmann N. Fluoride ion batteries: Theoretical performance, safety, toxicity, and a combinatorial screening of new electrodes. *J. Fluor. Chem.* 2016;182:76–90. https://doi.org/10.1016/j.jfluchem.2015.12.002

2. Sorokin N.I. SnF_2-Based Solid Electrolytes. *Inorg. Mater.* 2004;40(9):989–997. https://doi.org/10.1023/B:INMA.0000041335.17098.d1

3. Podgorbunsky A.B., Sinebryukhov S.L., Gnedenkov S.V., Goncharuk V.K., Kavun V.Ya. Usoltseva T.I. Effect of fluorides of the first group elements on the ionic conductivity of SnF_2-MF system. *Vestnik DVO RAS*. 2010;5(153):12–17 (in Russ.).

СПИСОК ЛИТЕРАТУРЫ

1. Gschwind F., Rodriguez-Garcia G., Sandbeck D.J.S., Gross A., Weil M., Fichtner M., Hörmann N. Fluoride ion batteries: Theoretical performance, safety, toxicity, and a combinatorial screening of new electrodes. *J. Fluor. Chem.* 2016;182:76–90. https://doi.org/10.1016/j.jfluchem.2015.12.002

2. Sorokin N.I. SnF_2-Based Solid Electrolytes. *Inorg. Mater.* 2004;40(9):989–997. https://doi.org/10.1023/B:INMA.0000041335.17098.d1

3. Подгорбунский А.Б., Синебрюхов С.Л., Гнеденков С.В., Гончарук В.К., Кавун В.Я., Усольцева Т.И. Влияние фторидов элементов первой группы на ионную проводимость системы SnF_2-MF. *Вестник ДВО РАН.* 2010;5(153):12–17.

4. Podgorbunsky A.B., Sinebryukhov S.L., Gnedenkov S.V. Comparison of superionic phases for some fluorine conducting materials. *Physics Procedia.* 2012;23:94–97. https://doi.org/10.1016/j.phpro.2012.01.024

5. Donaldson J.D., O'Donoghue J.D. Complex tin(II) fluorides. *J. Chem. Soc.* 1964;44:271–275. https://doi.org/10.1039/JR9640000271

6. McDonald R., Larson A., Cromer D.T. The crystal structure of sodium pentafluorodistannate(II), $NaSn_2F_5$. *Acta Cryst.* 1964;17(9):1104–1108. https://doi.org/10.1107/S0365110X64002894

7. Vilminot S., Bachmann R., Schulz H. Structure and conductivity in KSn_2F_5. *Solid State Ionics*. 1983;9–10(1):559–562. https://doi.org/10.1016/0167-2738(83)90295-3

8. Vilminot S., Schulz H. Evidence for a new structural modification in KSn_2F_5. *Acta Cryst. Section B: Structural Science.* 1988;44(33):233–236. https://doi.org/10.1107/S0108768188001260

9. Yamada K., Ahmad M.M., Ohki H., Okuda T., Ehrenberg H., Fuess H. Structural phase transition of the two-dimensional fluoride ion conductor KSn_2F_5 studied by X-ray diffraction. *Solid State Ionics.* 2004;167(3–4):301–307. https://doi.org/10.1016/j.ssi.2003.09.004

10. Donaldson J.D., O'Donoghue J.D., Oteng R. Formation of Complex Tin(II) Species in Molten Tin(II) Fluoride. *J. Chem. Soc.* (*Resumed*). 1965:3876–3879. http://dx.doi.org/10.1039/JR9650003854

11. Berastegui P., Hull S., Eriksson S.G. A high temperature superionic phase of $CsSn_2F_5$. *J. Solid State Chem.* 2010;183(2):373–378. https://doi.org/10.1016/j.jssc.2009.11.020

12. Zhurov V.V., Ivanov S.A. Profit Computer Program for Processing Powder Diffraction Data on an IBM PC Computer with a Graphic User Interface. *Cryst. Rep*. 1997;42:202–206.

13. Zakalyukin R.M., Levkevich E.A., Kumskov A.S., Orekhov A.S. Superionic conductor $PbSnF_4$ in the inner channel of SWNT. AIP Conference Proceedings. 2018;1957(1):030001. https://doi.org/10.1063/1.5034325

14. Fedorov P.P., Goncharuk V.K., Maslennikova I.G., Telin I.A., Glazunova T.Yu. Diagram of the PbF_2–SnF_2 system. *Russ. J. Inorg. Chem.* 2016;61(2):239–242. https://doi.org/10.1134/S0036023616020078

4. Podgorbunsky A.B., Sinebryukhov S.L., Gnedenkov S.V. Comparison of superionic phases for some fluorine conducting materials. *Physics Procedia*. 2012;23:94–97. https://doi.org/10.1016/j.phpro.2012.01.024

5. Donaldson J.D., O'Donoghue J.D. Complex tin(II) fluorides. *J. Chem. Soc*. 1964;44:271–275. https://doi.org/10.1039/JR9640000271

6. McDonald R., Larson A., Cromer D.T. The crystal structure of sodium pentafluorodistannate (II), $NaSn_2F_5$. *Acta Cryst.* 1964;17(9):1104–1108. https://doi.org/10.1107/S0365110X64002894

7. Vilminot S., Bachmann R., Schulz H. Structure and conductivity in KSn_2F_5. *Solid State Ionics*. 1983;9–10(1):559–562. https://doi.org/10.1016/0167-2738(83)90295-3

8. Vilminot S., Schulz H. Evidence for a new structural modification in KSn_2F_5. *Acta Cryst. Section B: Structural Science.* 1988;44(33):233–236. https://doi.org/10.1107/S0108768188001260

9. Yamada K., Ahmad M.M., Ohki H., Okuda T., Ehrenberg H., Fuess H. Structural phase transition of the two-dimensional fluoride ion conductor KSn_2F_5 studied by X-ray diffraction. *Solid State Ionics*. 2004;167(3–4):301–307. https://doi.org/10.1016/j.ssi.2003.09.004

10. Donaldson J.D., O'Donoghue J.D., Oteng R. Formation of Complex Tin(II) Species in Molten Tin(II) Fluoride. *J. Chem. Soc.* (*Resumed*). 1965:3876–3879. http://dx.doi.org/10.1039/JR9650003854

11. Berastegui P., Hull S., Eriksson S.G. A high temperature superionic phase of $CsSn_2F_5$. *J. Solid State Chem.* 2010;183(2):373–378. https://doi.org/10.1016/j.jssc.2009.11.020

12. Zhurov V.V., Ivanov S.A. Profit Computer Program for Processing Powder Diffraction Data on an IBM PC Computer with a Graphic User Interface. *Cryst. Rep*. 1997;42:202–206.

13. Zakalyukin R.M., Levkevich E.A., Kumskov A.S., Orekhov A.S. Superionic conductor $PbSnF_4$ in the inner channel of SWNT. AIP Conference Proceedings. 2018;1957(1):030001. https://doi.org/10.1063/1.5034325

14. Fedorov P.P., Goncharuk V.K., Maslennikova I.G., Telin I.A., Glazunova T.Yu. Diagram of the PbF_2–SnF_2 system. *Russ. J. Inorg. Chem.* 2016;61(2):239–242. https://doi.org/10.1134/S0036023616020078

About the authors:

Ruslan M. Zakalyukin, Cand. Sci. (Chem.), Senior Lecturer, Department of Electrotechnical Systems, Institute of Radio Engineering and Telecommunication Systems, MIREA – Russian Technological University (86, Vernadskogo pr., Moscow, 119571, Russia); Senior Researcher, Federal Scientific Research Center "Crystallography and Photonics," Russian Academy of Sciences (59, Leninskii pr., Moscow, 119333, Russia). E-mail: rmzakalyukin@mitht.ru. Scopus Author ID 6602502445, ResearcherID O-3799-2014, https://orcid.org/0000-0002-4398-4893

Ekaterina A. Levkevich, Teaching Assistant, Department of Electrotechnical Systems, Institute of Radio Engineering and Telecommunication Systems, MIREA – Russian Technological University (86, Vernadskogo pr., Moscow, 119571, Russia); Postgraduate Student, Federal Scientific Research Center "Crystallography and Photonics," Russian Academy of Sciences (59, Leninskii pr., Moscow, 119333, Russia). E-mail: levkevich@mitht.ru. Scopus Author ID 57207661566, ResearcherID Z-1981-2018, https://orcid.org/0000-0003-2668-1783

Anastasia V. Nikolaeva, Student, Faculty of Chemistry, Lomonosov Moscow State University (1, Leninskie gory, Moscow, 119991, Russia) E-mail: nnik3003@bk.ru. https://orcid.org/0000-0001-9564-7736

Об авторах:

Закалюкин Руслан Михайлович, к.х.н., доцент кафедры электротехнических систем Института телекоммуникационных и радиотехнических систем ФГБОУ ВО «МИРЭА – Российский технологический университет» (119571, Россия, Москва, пр-т Вернадского, д. 86); старший научный сотрудник Федерального научно-исследовательского центра «Кристаллография и фотоника» Российской академии наук (119333, Россия, Москва, Ленинский пр-т, 59). E-mail: rmzakalyukin@mitht.ru. Scopus Author ID 6602502445, ResearcherID O-3799-2014, https://orcid.org/0000-0002-4398-4893

Левкевич Екатерина Александровна, ассистент кафедры электротехнических систем Института телекоммуникационных и радиотехнических систем ФГБОУ ВО «МИРЭА – Российский технологический университет» (119571, Россия, Москва, пр-т Вернадского, д. 86); аспирант Федерального научно-исследовательского центра «Кристаллография и фотоника» Российской академии наук (119333, Россия, Москва, Ленинский пр-т, 59). E-mail: levkevich@mitht.ru. Scopus Author ID 57207661566, ResearcherID Z-1981-2018, https://orcid.org/0000-0003-2668-1783

Николаева Анастасия Владимировна, студентка Химического факультета МГУ им. М.В. Ломоносова (119991, Россия, Москва, Ленинские горы, д.1, с.3). E-mail: nnik3003@bk.ru. https://orcid.org/0000-0001-9564-7736

The article was submitted: June 03, 2021; approved after reviewing: June 25, 2021; accepted for publication: October 04, 2021.

Translated from Russian into English by N. Isaeva
Edited for English language and spelling by Enago, an editing brand of Crimson Interactive Inc.

CHEMISTRY AND TECHNOLOGY OF INORGANIC MATERIALS

ХИМИЯ И ТЕХНОЛОГИЯ НЕОРГАНИЧЕСКИХ МАТЕРИАЛОВ

ISSN 2686-7575 (Online)

https://doi.org/10.32362/2410-6593-2021-16-5-438-447

UDC 541.1+669.21/.23+669.849

RESEARCH ARTICLE

Application of pulse current for dissolution of heat-resistant GS32-VI alloy

Oxana V. Chernyshova[1,@], Turar B. Yelemessov[2], Dmitry V. Drobot[1]

[1]MIREA – Russian Technological University (M.V. Lomonosov Institute of Fine Chemical Technologies), Moscow, 119571 Russia
[2]Institute of High Technologies, Almaty, 050012 Republic of Kazakhstan
Correspondence author, e-mail: oxcher@mitht.ru

Abstract

Objectives. *To identify the regularities of electrochemical processing of the heat-resistant GS32-VI alloy in a sulfuric acid electrolyte with a concentration of 100 g/dm^3 under the action of a pulsed current in a pulsed mode.*

Methods. *Using the electrochemical technological complex EHK-1012 (developed by IP Tetran) and a non-compensatory method of measuring potential, polarization and depolarization curves with a change in pulse duration and a pause between them were recorded. The current pulses had an amplitude ranging from 0 to 3.5 A (when recording the polarization and depolarization curves), pulse durations ranging from 200 to 1200 ms, and a pause (delay) between pulses ranging from 50 to 500 ms. There were no reverse current pulses.*

Results. *The parameters of the current program that provide the maximum values of the alloy dissolution rate and current output were determined: with a current pulse amplitude of 2 A, a current pulse duration of 500 ms, and a pause duration between pulses of 250 ms, the maximum dissolution rate of the alloy is 0.048 g/h·cm^2, while the current output for nickel is 61.6% with an anode area of 10 cm^2. The basic technological scheme for processing the heat-resistant GS32-VI alloy, which includes anodic alloy dissolution in a pulsed mode, is proposed.*

Conclusions. *Electrochemical dissolution of GS32-VI alloy under pulsed current action results in an optimal dissolution rate ratio of the alloy components, ensuring the production of a cathode precipitate with a total nickel and cobalt content of 97.5%.*

Keywords: *pulse current, sulfuric acid, GS32-VI alloy, polarization and depolarization curves, amplitude of pulse current, duration of pulse current, pause between pulse current*

For citation: Chernyshova O.V., Yelemessov T.B., Drobot D.V. Application of pulse current for dissolution of heat-resistant GS32-VI alloy. *Tonk. Khim. Tekhnol. = Fine Chem. Technol.* 2021;16(5):438–447 (Russ., Eng.). https://doi.org/10.32362/2410-6593-2021-16-5-438-447

НАУЧНАЯ СТАТЬЯ

Применение импульсного тока для растворения жаропрочного сплава ЖС32-ВИ

О.В. Чернышова[1,@], Т.Б. Елемесов[2], Д.В. Дробот[1]

[1]МИРЭА – Российский технологический университет (Институт тонких химических технологий им. М.В. Ломоносова), Москва, 119571 Россия
[2]Институт высоких технологий, Алматы, 050012 Республика Казахстан
[@]Автор для переписки, e-mail: oxcher@mitht.ru

Аннотация

Цели. *Выявить закономерности электрохимической переработки жаропрочного сплава ЖС32-ВИ, проводимой в импульсном режиме в сернокислом электролите с концентрацией 100 г/дм^3 под действием импульсного тока.*

Методы. *Снятие поляризационных и деполяризационных кривых с изменением длительности импульса и паузы между ними проводили с помощью электрохимического технологического комплекса ЭХК-1012 (разработан ООО ИП «Тетран»), использующего некомпенсационный способ измерения потенциала. Амплитуда импульсов тока находилась в диапазоне значений от 0 до 3.5 А (при снятии поляризационных и деполяризационных кривых), длительности импульсов изменялись от 200 до 1200 мс, пауза (задержка) между импульсами – от 50 до 500 мс, импульсы реверсивного тока отсутствовали.*

Результаты. *Определены параметры токовой программы, обеспечивающие максимальные значения скорости растворения сплава и выхода по току. При амплитуде импульса тока 2 А, длительности импульса тока 500 мс и продолжительности паузы между импульсами 250 мс максимальная скорость растворения сплава 0.048 г/ч·см^2, при этом выход по току для никеля равен 61.6% при площади анода 10 см^2. Предложена принципиальная технологическая схема переработки жаропрочного сплава ЖС32-ВИ, включающая анодное растворение сплава в импульсном режиме.*

Выводы. *Электрохимическое растворение сплава ЖС32-ВИ под действием импульсного тока способствует оптимальному соотношению скоростей растворения составляющих сплава, что обеспечивает получение катодного осадка с суммарным содержанием никеля и кобальта 97.5%.*

Ключевые слова: *импульсный ток, серная кислота, сплав ЖС32-ВИ, поляризационная и деполяризационная кривые, амплитуда импульса тока, длительность импульса тока, пауза между импульсами тока*

Для цитирования: Чернышова О.В., Елемесов Т.Б., Дробот Д.В. Применение импульсного тока для растворения жаропрочного сплава ЖС32-ВИ. *Тонкие химические технологии.* 2021;16(5):438–447. https://doi.org/10.32362/2410-6593-2021-16-5-438-447

INTRODUCTION

The high cost of nickel heat-resistant alloy components (rhenium, tantalum, cobalt, etc.) that have reached the end of their service life necessitates their return to industrial production. Processes based on electrochemical methods, which allow for the regeneration of rare refractory metal wastes with high technological and economic indicators, are the most effective and promising paths in metal waste processing technology [1–15]. The literature describes various solutions to the problem under discussion. Thus, processing methods based on opening processed raw materials with acid solutions are well known. The use of sulfuric, hydrochloric, and nitric acids followed by the electrochemical release of the target products at a fixed current density [1–5] is the most common. Another approach that involves the anodic dissolution of the processed metal-containing raw material and subsequent separation of commercial products from the electrolyte solution is described in [6–17].

The dissolution and transfer rate of products into solution during the anodic dissolution of metals or alloys is significantly influenced by the current program. It is worth noting that anodic dissolution processes, in which the magnitude and direction of the current used are variable, are common in the processing of various types of secondary raw materials. Such modes, in contrast to electrochemical processes with a constant current value, are called unsteady electrolysis modes or unsteady electrolysis. In papers [6–11, 13], the dissolution process is carried out using alternating currents of various kinds. The implementation of the anodic dissolution process under these conditions prevents passivation phenomena and increases the anodic dissolution rate.

Unsteady electrolysis in pulse mode has been effectively used in the production of coatings and the electrochemical treatment of materials [17–27]. However, despite the superior characteristics of electrochemical processes, its use in the processing of secondary raw materials is limited.

This work aims at revealing the regularities of the electrochemical processing of the heat-resistant GS32-VI alloy in a sulfuric acid electrolyte in the pulse mode.

EXPERIMENTAL

Electrochemical dissolution of the alloy composition (wt %) Re–4.0; Co–9.3; W–8.6; Y–0.005; La–0.005; Al–6.0; Cr–5.0; Ta–4.0; Nb–1.6; Mo–1.1; C–0.16; B–0.15; Ce–0.025, Ni–60. The polarization and depolarization curves were obtained using electrochemical technological complex EHK-1012 (developed by *IP Tetran*), which uses non-compensation method of potential measurement [28]. The reference electrode was a silver chloride electrode.

Current diagram for polarization and depolarization curves: current pulse amplitude varied from 0 to 3.5 A, pulse duration varied from 200 to 1200 ms, pause pulse (delay) varied from 50 to 500 ms, and no reverse current pulses were used (Fig. 1).

The electrochemical cell consisted of a 300 mL fluoroplastic reservoir, a fragment of a blade from the heat-resistant GS32-VI alloy with an area S = 10 cm^2 (anode), and a titanium (VT1-0) plate with an area S = 9.5 cm^2 (cathode).

Electrode weight loss was determined on analytical scales ANDGR-300 with an accuracy class of +/−0.0001 g. The process was conducted at a temperature of 20–25°C. Elemental analysis was performed using an ICP mass spectrometer for isotopic and elemental analysis ELAN DRC-e (*PerkinElmer*, Canada).

RESULTS AND DISCUSSION

Based on literature data and previously conducted studies, the feasibility of using acidic electrolytes based on sulfuric and nitric acids for processing of nickel-based refractory alloys was revealed [1, 4, 5, 9, 10, 13, 14]. We selected sulfuric acid at a concentration of 100 g/dm^3, which provides a high dissolution rate, to obtain a cathodic nickel-containing product. Lower acid concentrations result in a lower alloy dissolution rate (less than 0.030 g/h·cm^2), while sulfuric acid concentrations of 250 g/dm^3 and higher enhance the probability of increased anode sludge.

The main advantage of pulsed electrolysis is the ability to make abrupt changes in the electrode potential, which significantly affects the charge transfer stage, adsorption and crystallization, the overall kinetics of the process, and determines the course of each electrochemical reaction.

When using pulse current, the significant parameters are pulse duration and amplitude, pause between pulses, and presence of reversing pulse. To analyze the effect of these parameters on the process of electrochemical dissolution of the heat-resistant GS32-VI alloy, anodic polarization curves with changes in the pulse duration and the pause between them were taken. Depolarization curves were taken after the current pulse to show the dynamics of the electrode potential.

Pulsed current, unlike direct current, allows for effective control of electrode processes. The

steep leading edge of the pulses allows for a faster increase in electrode potential from the minimum to the maximum value (Fig. 1). As a result, electrolyte depletion near the electrode is accelerated, current lines are redistributed, and fine crystalline precipitates are formed on the cathode, resulting in the production of smaller anode sludge particles in the case of soluble anodes with heterophase composition. This is presumably true in anodic dissolution since GS32-VI is a multicomponent, heterophase alloy. The main elements of its phase composition are dispersed (<0.5 μm) 1-phase particles γ, which are based on the ordered intermetallic compound Ni_3Al (superstructure Ll2) and a complexly alloyed nickel γ-solid solution, as well as carbide and boride phases of various types [29]. Simultaneously, the steep decline of direct pulses causes an increase in the potential swing, which affects the precipitation structure as well as some electrolysis process parameters.

Figures 2 and 3 show polarization and depolarization curves obtained in pulsed galvanodynamic mode, respectively.

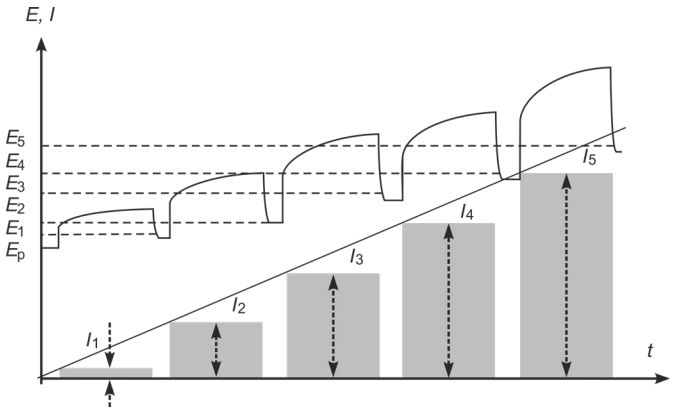

Fig. 1. Current diagram for polarization and depolarization curves.

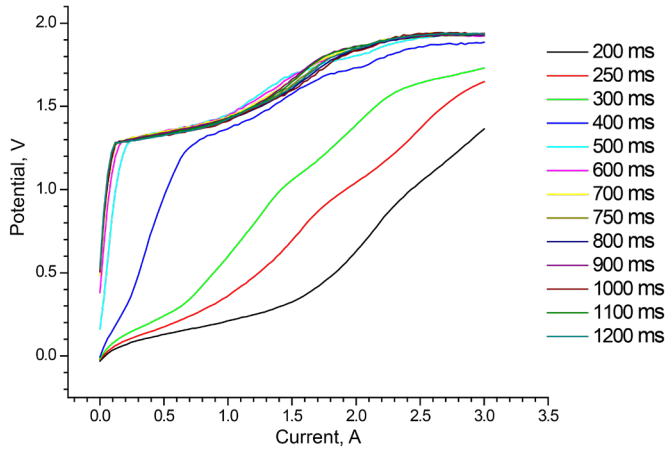

Fig. 2. Polarization curves of GS32-VI alloy dissolution in a sulfuric acid electrolyte with a concentration of 100 g/dm^3 at different pulse durations and a pause of 250 ms.

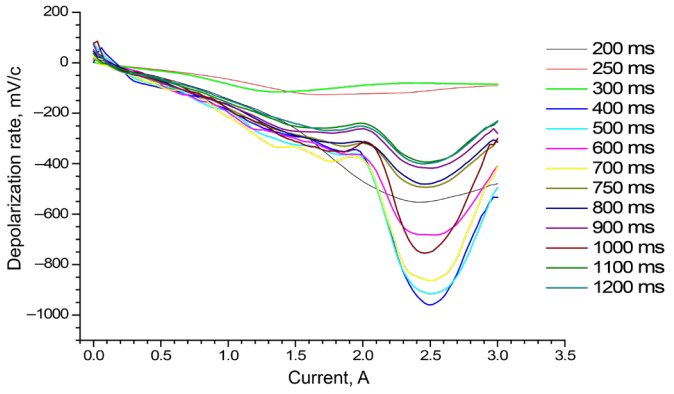

Fig. 3. Depolarization curves of GS32-VI alloy dissolution in a sulfuric acid electrolyte with a concentration of 100 g/dm^3 at different pulse durations and a pause of 250 ms.

Figure 2 illustrates that with a polarization time of 200–300 ms, the shape of the polarization curve has a smoothed form from the obtained dependences of the shape of polarization curves on the pulse duration. When the current pulse duration is increased up to 500 ms, a horizontal area corresponding to the maximum dissolution rate of the alloy appears on the polarization curve. Further increase in pulse duration (up to 1200 ms) has no noticeable effect on the shape of polarization curves.

The described dependences on the influence of current pulse duration on the shape of polarization curves are confirmed by the obtained depolarization curve dependences. At current pulse durations of 400–500 ms, the depolarization curves clearly show areas corresponding to different electrochemical processes (Fig. 3).

The polarization and depolarization curves of GS-32VI alloy dissolution in sulfuric acid electrolyte with a concentration of 100 g/dm^3, a pulse duration of 500 ms, and a delay of 250 ms are shown in Fig. 4 to highlight the areas corresponding to the course of various electrochemical processes.

I area: E = 0.18–1.78 V—the dissolution of the complex-alloyed nickel γ-solid solution phase occurs;

II area: E = 1.78–1.91 V—dissolution γ of 1-phase based on the ordered intermetallic compound Ni_3Al;

III area: $E \geq 1.91$ V—release of oxygen through the formation of intermediate unstable oxides.

Using similar dependencies, the effect of the pause duration between pulses on the shape of polarization and depolarization curves was determined (Fig. 5, 6). The pause in pulsed electrolysis had a significant effect on the metal deposition process and the quality of the resulting cathode precipitation. As a result of migration, the concentration of ions in the near-electrode space equalizes completely or partially depending on the pause duration. Passivation of the electrode surface is also possible, which involves the oxidation or adsorption of impurities in the electrolyte solution on the active parts of the electrode surface.

During GS-32VI alloy dissolution in a sulfuric acid electrolyte with a concentration of 100 g/dm^3 using pulsed current, a high alloy dissolution rate

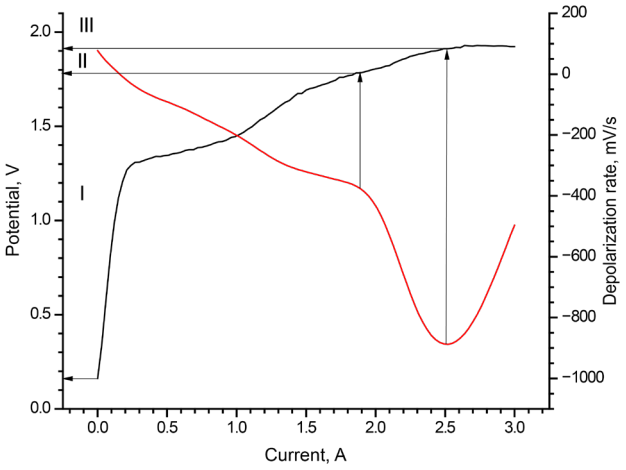

Fig. 4. Polarization and depolarization curves of GS32-VI alloy dissolution in the sulfuric acid electrolyte at a concentration of 100 g/dm^3, 500 ms pulse duration, and a delay of 250 ms.

was attained at a pulse duration of 500–700 ms and a pause pulse delay of 250 ms. The dissolution rate ratio of nickel, cobalt, and rhenium provides a cathode deposit with a nickel and cobalt content of at least 90%

The maximum current pulse amplitude during anodic alloy dissolution is limited to 2.5 A (at anode area S = 10 cm^2); exceeding this value results in an undesirable process–oxygen evolution, which reduces current yield. The optimal value of the current pulse amplitude is determined based on the maximum alloy dissolution rate combined with a high current yield of nickel current yield, which is the base of GS32-VI alloy.

Table 1 shows experimental data results on the effect of current pulse amplitude on the anodic dissolution rate of GS32-VI alloy in sulfuric acid electrolyte with a concentration of 100 g/dm^3. For

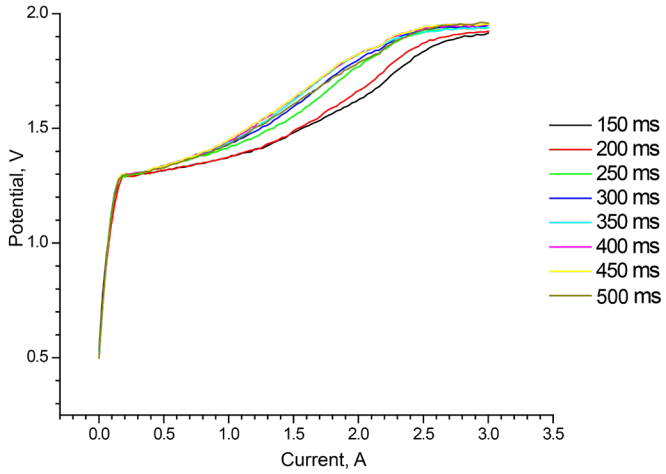

Fig. 5. Polarization curves of GS32-VI alloy dissolution in a sulfuric acid electrolyte with a concentration of 100 g/dm^3, a pulse duration of 500 ms, and different pause times.

each experiment, a new anode, which was a heat-resistant GS32-VI alloy blade fragment with an area S = 10 cm^2.

The dissolution rate of the alloy v was calculated using the mass loss of the dissolved alloy according to the formula:

$$v = (m_1 - m_2)/S \cdot t^{-1},$$

where m_1 is the initial mass of the dissolved sample, m_2 is the mass of the sample after electrochemical dissolution, S is the working area of the electrode, and t is the processing time.

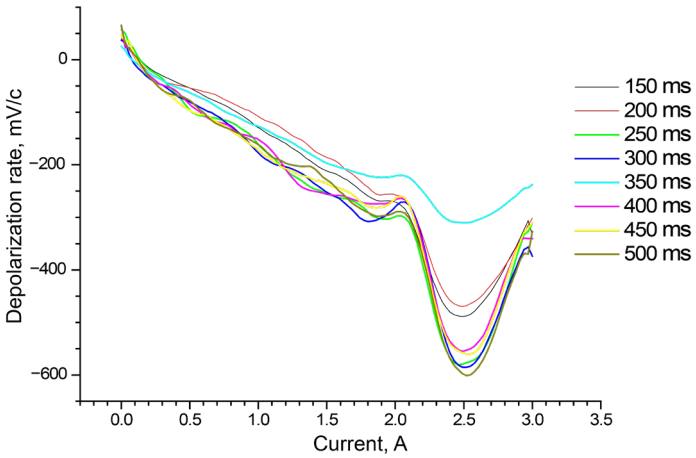

Fig. 6. Depolarization curves of GS32-VI alloy dissolution in a sulfuric acid electrolyte with a concentration of 100 g/dm^3, a pulse duration of 500 ms, and different pause times.

Based on the data obtained, the following technological parameters for reprocessing the GS32-VI alloy by the electrochemical method were selected: current pulse amplitude—2 A (at the anode area S = 10 cm^2), current pulse duration—500 ms, and the pause between pulses—250 ms.

In the pulsed galvanostatic mode, a total of 97.56 g of heat-resistant GS32-VI alloy was processed in a sulfuric acid electrolyte with a concentration of 100 g/dm^3. Afterward, 55.08 g of cathode deposit and 27.32 g of anode sludge were received; their chemical composition is summarized in Table 2.

Thus, refractory metals, such as niobium, tantalum, molybdenum, and tungsten are concentrated in the anode sludge, whereas cobalt and rhenium, as well as the majority of aluminum, chromium, and nickel, pass into the electrolyte in small amounts. It is worth noting that electrochemical processing with pulsed current allows for rhenium concentration in the anode sludge, with a content of 77% of the initial amount obtained for processing. The anode sludge is easily separated from the electrolyte solution by filtration (unlike the anode sludge obtained by direct current in galvanostatic mode, other things being equal): 90% of anode sludge particles are between 146 to 510 μm in size. The resulting anode sludge can be processed using well-known methods [30], such as ammonia leaching with rhenium, tungsten, and molybdenum transfer into a solution, followed by the

Table 1. Influence of current program parameters on the anodic dissolution rate of GS32-VI alloy

Parameter	Value	Nickel concentration, C(Ni), g/dm^3	Dissolution rate of the alloy, g/h·cm^2	Current yield of nickel, η(Ni), %
Current pulse duration—500 ms, pause time between pulses—250 ms				
Amplitude of current pulse, A	0.5	9.75	0.027	60.5
	1.0	9.33	0.038	60.1
	1.5	10.20	0.042	62.5
	2.0	14.05	0.048	61.8
	2.5	15.12	0.054	57.2
Amplitude of current pulse—2.0 A, pause time between pulses—250 ms				
Current pulse duration, ms	200	9.90	0.020	61.,8
	500	10.44	0.038	63.8
	700	11.03	0.038	59.4
	900	12.34	0.044	53.2
	1200	14.75	0.048	49.9
Current pulse amplitude—2.0 A, current pulse duration—500 ms				
Pause time between pulses, ms	150	9.75	0.028	59.5
	250	9.33	0.036	61,1
	350	10.20	0.026	60.5
	450	14.05	0.020	56.8
	500	15.12	0.015	52.2

Table 2. Chemical composition of cathode deposit and anode sludge obtained during the anodic dissolution of GS32-VI alloy

Elements	Cathode deposit		Anode sludge	
	g	%	g	%
Ni	46.58	84.57	6.96	25.49
Co	7.20	13.07	0.54	1.98
Cr	1.03	1.87	1.43	5.23
Re	0.22	0.39	3.01	11.02
Al	0.05	0.10	0.49	1.79
Nb	–	–	1.59	5.82
Mo	–	–	1.05	3.84
Ta	–	–	3.88	14,20
W	–	–	8.37	30.63

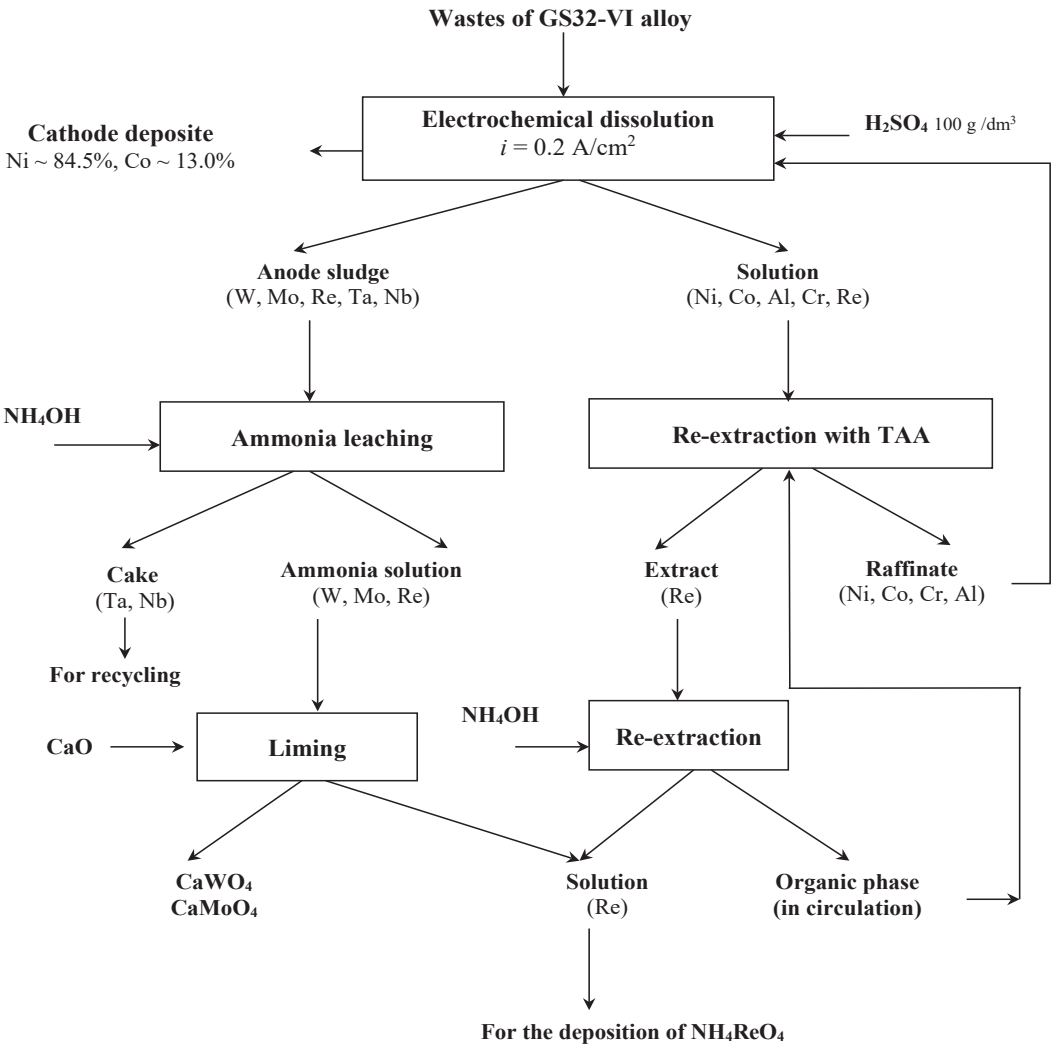

Fig. 7. The basic technological processing scheme for the heat-resistant GS32-VI alloy.
Figure 7. Schematic technological scheme of processing of heat-resistant alloy *HR32-VI*

deposition of artificial scheelite and the formation of a rhenium-containing solution, from which another commercial product is obtained—ammonium perrhenate (or potassium).

The total content of nickel and cobalt in the cathode deposit is 97.5%.

The basic technological scheme for the complex processing of the heat-resistant GS32-VI alloy is proposed based on the research (Fig. 7).

CONCLUSIONS

1. The effect of pulse current parameters (amplitude, pulse duration, and pause between pulses) on the electrochemical dissolution rate of GC32-VI alloy was shown. It was found that the current pulse amplitude was 2 A (with an anode area of S = 10 cm^2), the current pulse duration was 500 ms, the pause between pulses was 250 ms, the maximum dissolution rate of the alloy was 0.048 g/h·cm^2; the current output for nickel was 61.6% with the current program.

2. During the electrochemical dissolution of GC32-VI alloy by pulsed current, the optimal dissolution rate ratio of the alloy components was achieved, ensuring the production of a cathode precipitate with a total nickel and cobalt content of 97.5%.

3. The basic technological scheme for processing GS32-VI alloy was proposed.

Authors' contribution

All authors equally contributed to the research work.

The authors declare no conflicts of interest.

REFERENCES

1. Lutz L.J., Parker S.A., Stephenson J.B. Recycling of Contaminated Superalloy Scrap via Electrochemical Processing. *TMS Annual. Meeting*. 1993: 1211–1220.

2. Prasad V.S., Rao S.A., Prakash U., *et al*. Recycling of Superalloy Scrap through Electro Slag Remelting. *ISIJ International.* 1996;36(12):1459–1464. https://doi.org/10.2355/isijinternational.36.1459

3. Rao S.R. (Ed.). Resource Recovery and Recycling from Metallurgical Wastes. V. 7. Elsevier Science; 2006. 580 p. https://doi.org/10.1016/s0713-2743(06)x8083-2

4. Sibley S.F. (Ed.). *Flow studies for recycling metal commodities in the United States*. Reston, Virginia: US Geological Survey; 2004. V. 1196. https://doi.org/10.3133/cir1196

5. Worrell E., Reuter M.A. *Handbook of Recycling: State of the art for Practitioners, Analysts, and Scientists.* Elsevier; 2014. 600 p.

6. Palant A.A., Bryukvin V.A., Levin A.M., Levchuk O.M. Combined electrochemical processing of the wastes of nickel superalloys containing rhenium, tungsten, tantalum, niobium and other precious metals. *Russ. Metall.* 2014;2014(1):20–22. https://doi.org/10.1134/S0036029514010108

[Original Russian Text: Palant A.A., Bryukvin V.A., Levin A.M., Levchuk O.M. Combined electrochemical processing of the wastes of nickel superalloys containing rhenium, tungsten, tantalum, niobium and other precious metals. *Metally.* 2014;(1):25–27 (in Russ.).]

7. Palant AA, Bryukvin VA, Levchuk OM, Palant AV, Levin AM. *Method of electrochemical treatment of heatproof nickel alloy metal wastes that contain rhenium*: Pat. 2401312 RF. Publ. 10.10.2010.

8. Stoller V., Olbrich A., Meese-Marktscheffel J., *et al. Process for electrochemical decomposition of superalloys*: Pat. 10155791 DE. Publ. 17.07.2003.

СПИСОК ЛИТЕРАТУРЫ

1. Lutz L.J., Parker S.A., Stephenson J.B. Recycling of Contaminated Superalloy Scrap via Electrochemical Processing. *TMS Annual. Meeting*. 1993:1211–1220.

2. Prasad V.S., Rao S.A., Prakash U., *et al*. Recycling of Superalloy Scrap through Electro Slag Remelting. *ISIJ International.* 1996;36(12):1459–1464. https://doi.org/10.2355/isijinternational.36.1459

3. Rao S.R. (Ed.). *Resource Recovery and Recycling from Metallurgical Wastes*. V. 7. Elsevier Science; 2006. 580 p. https://doi.org/10.1016/s0713-2743(06)x8083-2

4. Sibley S.F. (Ed.). *Flow studies for recycling metal commodities in the United States*. Reston, Virginia: US Geological Survey; 2004. V. 1196. https://doi.org/10.3133/cir1196

5. Worrell E., Reuter M.A. *Handbook of Recycling: State of the art for Practitioners, Analysts, and Scientists*. Elsevier; 2014. 600 p.

6. Палант А.А, Брюквин В.А., Левин А.М., Левчук О.М. Комплексная электрохимическая технология переработки отходов жаропрочных никелевых сплавов, содержащих рений, вольфрам, тантал, ниобий и другие ценные металлы. *Металлы.* 2014;(1):25–27.

7. Палант А.А., Брюквин В.А., Левчук О.М., Палант А.В., Левин А.М. *Способ электрохимической переработки металлических отходов жаропрочных никелевых сплавов, содержащих рений*: Пат. 2401312 РФ. Заявка № 2009113255/02; заявл. 09.04.2009; опубл. 10.10.2010. Бюл. 28.

8. Stoller V., Olbrich A., Meese-Marktscheffel J., *et al*. *Process for electrochemical decomposition of superalloys*: Pat. 10155791 DE. Publ. 17.07.2003.

9. Krynitz U., Olbrich A., Kummer W., Schloh M. *Method for the decomposition and recovery of metallic constituents from superalloys*: Pat. 5776329 USA. Publ. 07.07.1998.

9. Krynitz U., Olbrich A., Kummer W., Schloh M. *Method for the decomposition and recovery of metallic constituents from superalloys*: Pat. 5776329 USA. Publ. 07.07.1998.

10. Stoller V., Olbrich A., Meese-Marktscheffel J., *et al. Electrochemical dissolution process for disintegrating superalloy scraps*: Pat. 1312686 EP. Publ. 16.01.2008.

11. Srivastava R., Kim M., Lee J., *et al*. Resource recycling of superalloys and hydrometallurgical challenges. *J. Mate. Sci.* 2014;49(14):4671–4686. https://doi.org/10.1007/s10853-014-8219-y

12. Shipachev V.A. Some Processing Techniques for Rhenium Isolation and Purification from Refractory Alloys. *Khimiya v interesakh ustoichivogo razvitiya = Chemistry for Sustainable Development.* 2012;20(3):323–326.

13. Palant A.A., Bryukvin V.A., Levchuk O.M., *et al.* Complex electrochemical processing of metallic rhenium-containing wastes of heat-temperature nickel alloy in sulphate electrolytes. *Electrometallurgiya = Electrometallurgy.* 2010;(7):29–33 (in Russ.).

14. Petrova A.M., Kasikov A.G., Gromov P.B., Kalinnikov V.T. Rhenium recovery from nickel-based complex heat-resistant alloys. *Tsvetnye metally = Non-Ferrous Metals.* 2011;(11):39–43 (in Russ.).

15. Chernyshova O.V., Drobot D.V., Chernyshov V.I., Makhon'ko M.V. *Method of nickel recovery at electrochemical processing of heat-resistant nickel alloys*: Pat. 2542182 RF. Publ. 20.02.2015 (in Russ.).

16. Agapova L. Ya., Abisheva Z. S., Kilibaeva S. K., Yakhiyaeva Zh. E. Electrochemical processing of technogenic wastes of rhenium-containing heat-resistant nickel alloys in sulfuric acid solutions. *Tsvetnye Metally*. 2017;(10):69–74 (in Russ.). https://doi.org/10.17580/tsm.2017.10.08

17. Agapova L.Y., Kilibayeva S.K., Abisheva Z.S., Sharipova A.S. Complex electrochemical processing of technogenic wastes of rhenium-containing heat-resistant nickel alloys. *Non-ferrous metals.* 2020;(1):24–30. https://doi.org/10.17580/nfm.2020.01.04

18. Frolova I.I., Solov'eva N.D., Rybalkina I.P., Popova N.E. Use of non-stationary modes in electrodeposition of nickel coatings. *Perspektivnye materialy.* 2015;(7):58–63 (in Russ.).

18. Vypirailo S.Yu., Kireeva S.N., Kireev S.Yu. Electrochemical deposition of tin coatings using pulsed electrolysis. *Vestnik Penz. Gos. Un-ta = Vestnik of Penza State University.* 2015;3(11):128–132 (in Russ.).

20. Mikhedova E.V., Chernik A.A., Zharskii I.M., Yaskel'chik V.V. Electrochemical deposition of yellow brass under pulse electrolysis conditions. *Proceeding of the National Academy of Sciences of Belarus. Chemical Series.* 2014;(3):48–52 (in Russ.).

21. Spanou S., Pavlatou E.A. Pulse electrodeposition of Ni/nano-TiO_2 composites: effect of pulse frequency on deposits properties. J. Appl. Electrochem. 2010;40(7):1325–1336. https://doi.org/10.1007/s10800-010-0080-3

22. Seza A., Jafarian H.R., Hasheminiasari M., Aliofkhazraei M. Effect of duty cycle on corrosion resistance and mechanical properties of tertiary Al_2O_3/Y_2O_3/Graphene pulsed electrodeposited Ni-based nano-composite. *Procedia Mater. Sci.* 2015;11:576–582. https://doi.org/10.1016/j.mspro.2015.11.077

23. Atourki L., Bouabid K., Ihalane E., L. Alahyane L., *et al.* Pulse electrodeposition of ZnO for thin absorber solar cells. *Energy Procedia*. 2014;50:376–382. https://doi.org/10.1016/j.egypro.2014.06.045

24. Xu Z., Jia L., Zhu D., Qu N., *et al*. Electrochemical machining of burn-resistant Ti_40 alloy. *Chinese Journal of Aeronautics* (*CJA*). 2015;28(4):1263–1272. https://doi.org/10.1016/j.cja.2015.05.007

10. Stoller V., Olbrich A., Meese-Marktscheffel J., *et al*. *Electrochemical dissolution process for disintegrating superalloy scraps*: Pat. 1312686 EP. Publ. 16.01.2008.

11. Srivastava R., Kim M., Lee J., *et al*. Resource recycling of superalloys and hydrometallurgical challenges. *J. Mate. Sci.* 2014;49(14):4671–4686. https://doi.org/10.1007/s10853-014-8219-y

12. Шипачев В.А. Некоторые технологические приемы выделения и очистки рения из жаропрочных сплавов. *Химия в интересах устойчивого развития.* 2012;20(3):365–368.

13. Палант А.А., Брюквин В.А., Левчук О.М. и др. Комплексная электрохимическая переработка металлических отходов ренийсодержащего жаропрочного никелевого сплава в сернокислых электролитах. *Электрометаллургия*. 2010;(7):29–33.

14. Петрова А.М, Касиков А.Г., Громов П.Б., Калинников В.Т. Извлечение рения из отходов сложнолегированных жаропрочных сплавов на основе никеля. *Цветные металлы*. 2011;(11):39–43.

15. Чернышова О.В., Дробот Д.В., Чернышов В.И., Махонько М.В. *Способ извлечения никеля при электрохимической переработке жаропрочных никелевых сплавов*: Пат. 2542182 РФ. Заявка № 201345573/02; заявл. 11.10.2013; опубл. 20.02.2015. Бюл. № 5.

16. Агапова Л.Я., Абишева З.С., Килибаева С.К., Яхияева Ж.Е. Электрохимическая переработка техногенных отходов ренийсодержащих жаропрочных никелевых сплавов в сернокислых растворах. *Цветные металлы*. 2017;(10):69–74. https://doi.org/10.17580/tsm.2017.10.08

17. Agapova L.Y., Kilibayeva S.K., Abisheva Z.S., Sharipova A.S. Complex electrochemical processing of technogenic wastes of rhenium-containing heat-resistant nickel alloys. *Non-ferrous metals*. 2020;(1):24–30. https://doi.org/10.17580/nfm.2020.01.04

18. Фролова И.И., Соловьева Н.Д., Рыбалкина И.П., Попова Н.Е. Использование нестационарных режимов при электроосаждении никелевых покрытий. *Перспективные материалы*. 2015;(7):58–63.

19. Выпирайло С.Ю., Киреева С.Н., Киреев С.Ю. Электрохимическое осаждение покрытий оловом с использованием импульсного электролиза. *Вестник Пензенского государственного университета*. 2015;3(11):128–132.

20. Михедова Е.В., Черник А.А., Жарский И.М., Яскельчик В.В. Электрохимическое осаждение желтой латуни в условиях импульсного электролиза. *Известия Национальной академии наук Беларуси. Серия химических наук.* 2014;(3):48–52.

21. Spanou S., Pavlatou E.A. Pulse electrodeposition of Ni/nano-TiO_2 composites: effect of pulse frequency on deposits properties. *J. Appl. Electrochem*. 2010;40(7):1325–1336. https://doi.org/10.1007/s10800-010-0080-3

22. Seza A., Jafarian H.R., Hasheminiasari M., Aliofkhazraei M. Effect of duty cycle on corrosion resistance and mechanical properties of tertiary Al_2O_3/Y_2O_3/Graphene pulsed electrodeposited Ni-based nano-composite. *Procedia Mater. Sci*. 2015;11:576–582. https://doi.org/10.1016/j.mspro.2015.11.077

23. Atourki L., Bouabid K., Ihalane E., L. Alahyane L., *et al*. Pulse electrodeposition of ZnO for thin absorber solar cells. *Energy Procedia*. 2014;50:376–382. https://doi.org/10.1016/j.egypro.2014.06.045

24. Xu Z., Jia L., Zhu D., Qu N., *et al*. Electrochemical machining of burn-resistant Ti_40 alloy. *Chinese Journal of Aeronautics* (*CJA*). 2015;28(4):1263–1272. https://doi.org/10.1016/j.cja.2015.05.007

25. Vazquez-Arenas J., Treeratanaphitak T., Pritzker M. Formation of Co–Ni alloy coatings under direct current, pulse current and pulse-reverse plating conditions. *ELECTROCHIM. ACTA.* 2012;62:63–72. https://doi.org/10.1016/j.electacta.2011.11.085

26. Xia F., Xu H., Liu C., Wang J., *et al*. Microstructures of Ni–AlN composite coatings prepared by pulse electrodeposition technology. *Appl. Surf. Sci*. 2013;271:7–11. https://doi.org/10.1016/j.apsusc.2012.12.064

27. Chen Y.l., Chen P., Lin H., Li X. Effect of Selected Process Parameters on Efficiency Enhancement of Electrochemical Etching and Polishing of Tungsten under Forced Convection. *Int. J. Electrochem. Sci.* 2020;15(11):10955–10970. http://doi.org/10.20964/2020.11.72

28. Gaidarenko O.V., Chernyshov V.I., Chernyshov Yu.I. *Method for measuring potential of live main electrode of electrochemical*: Pat. 2106620 RF. Publ. 10.03.1998 (in Russ.).

29. Kablov E.N. Physicochemical and technological features of production of high-temperature rhenium containing alloys. *Moscow University Bulletin*. 2005;60(3):16–28.

30. Palant A.A., Troshkina I.D., Chekmarev A.M. *Metallurgiya reniya* (*Metallurgy of rhenium*). Moscow: Nauka; 2007. 298 p. (in Russ.). ISBN 5-02-034116-9

25. Vazquez-Arenas J., Treeratanaphitak T., Pritzker M. Formation of Co–Ni alloy coatings under direct current, pulse current and pulse-reverse plating conditions. *ELECTROCHIM. ACTA.* 2012;62:63–72. https://doi.org/10.1016/j.electacta.2011.11.085

26. Xia F., Xu H., Liu C., Wang J., *et al*. Microstructures of Ni–AlN composite coatings prepared by pulse electrodeposition technology. *Appl. Surf. Sci.* 2013;271:7–11. https://doi.org/10.1016/j.apsusc.2012.12.064

27. Chen Y.l., Chen P., Lin H., Li X. Effect of Selected Process Parameters on Efficiency Enhancement of Electrochemical Etching and Polishing of Tungsten under Forced Convection. *Int. J. Electrochem. Sci.* 2020;15(11):10955–10970. http://doi.org/10.20964/2020.11.72

28. Гайдаренко О.В., Чернышов В.И., Чернышов Ю.И. *Способ измерения потенциала рабочего электрода электрохимической ячейки под током*: Пат. № 2106620 РФ. Заявка № 9610873225Ж заявл. 26.04.1996; опубл. 10.03.1998. 1998.

29. Каблов Е.Н. Физико-химические и технологические особенности создания жаропрочных сплавов, содержащих рений. *Вестник Московского университета. Серия 2. Химия.* 2005;46(3):155–167.

30. Палант А.А., Трошкина И.Д., Чекмарев А.М. *Металлургия рения*. М.: Наука; 2007. 298 с. ISBN 5-02-034116-9

About the authors:

Oxana V. Chernyshova, Cand. Sci. (Eng.), Associate Professor, K.A. Bolshakov Department of Chemistry and Technology of Rare Elements, M.V. Lomonosov Institute of Fine Chemical Technologies, MIREA – Russian Technological University (86, Vernadskogo pr., Moscow, 119571, Russia). E-mail: oxcher@mitht.ru. Scopus Author ID 8961258100, https://orcid.org/0000-0003-0543-7474

Turar B. Yelemessov, Junior Researcher, Laboratory of New Equipment and Materials. Institute of High Technologies (168, Bogenbai Batyr st., Almaty, 050012, Republic of Kazakhstan). E-mail: baseke@mail.ru

Dmitry V. Drobot, Dr. Sci. (Chem.), Professor, K.A. Bolshakov Department of Chemistry and Technology of Rare Elements, M.V. Lomonosov Institute of Fine Chemical Technologies, MIREA – Russian Technological University (86, Vernadskogo pr., Moscow, 119571, Russia). E-mail: dvdrobot@mail.ru. Scopus Author ID 35580931100, Researcher ID AAR-3711-2019, https://orcid.org/0000-0003-1702-9435

Об авторах:

Чернышова Оксана Витальевна, к.т.н., доцент, доцент кафедры химии и технологии редких элементов им. К.А. Большакова Института тонких химических технологий им. М.В. Ломоносова ФГБОУ ВО «МИРЭА – Российский технологический университет» (119571, Россия, Москва, пр-т Вернадского, 86). E-mail: oxcher@mitht.ru. Scopus Author ID 8961258100, https://orcid.org/0000-0003-0543-7474

Елемесов Турар Берикович, младший научный сотрудник лаборатории нового оборудования и материалов Института высоких технологий (050012, Республика Казахстан, г. Алматы, ул. Богенбай батыра, д. 168). E-mail: baseke@mail.ru

Дробот Дмитрий Васильевич, д.х.н., профессор, профессор кафедры химии и технологии редких элементов им. К.А. Большакова Института тонких химических технологий им. М.В. Ломоносова ФГБОУ ВО «МИРЭА – Российский технологический университет» (119571, Россия, Москва, пр-т Вернадского, 86). E-mail: dvdrobot@mail.ru. Scopus Author ID 35580931100, Researcher ID AAR-3711-2019, https://orcid.org/0000-0003-1702-9435

The article was submitted: September 20, 2021; approved after reviewing: October 01, 2021; accepted for publication: October 18, 2021.

Translated from Russian into English by N. Isaeva
Edited for English language and spelling by Enago, an editing brand of Crimson Interactive Inc.

ERRATUM

ИСПРАВЛЕНИЯ

ISSN 2686-7575 (Online)

https://doi.org/10.32362/2410-6593-2021-16-5-448-449

Erratum to the article “Energy intensity of hydrocarbons in liquid and solid states”

Gennady J. Kabo, Lubov A. Kabo, Larisa S. Karpushenkava, Andrey V. Blokhin

Tonkie khimicheskie tekhnologii = Fine Chemical Technologies. 2021;16(4):273–286 (Russ., Eng.).

Page 276, in **Table 1** instead of

Table 1. Increments of the enthalpies of combustion of C and H atoms in C_nH_m hydrocarbons

$-\Delta_c H^{gross}$ (C), kJ·mol^{-1}	$-\Delta_c H^{gross}$ (H), kJ·mol^{-1}	$-\Delta_c H^{net}$ (C), kJ·mol^{-1}	$-\Delta_c H^{net}$ (H), kJ·mol^{-1}
435.687	110.675	435.687	88.675
$-\Delta_c H^{gross}$ (C), MJ·mol^{-1}	$-\Delta_c H^{gross}$ (H), MJ·mol^{-1}	$-\Delta_c H^{net}$ (C), MJ·mol^{-1}	$-\Delta_c H^{net}$ (H), MJ·mol^{-1}
36.275	109.83	36.275	87.977

should read:

Table 1. Increments of the enthalpies of combustion of C and H atoms in C_nH_m hydrocarbons

$-\Delta_c H^{gross}$ (C), kJ·mol^{-1}	$-\Delta_c H^{gross}$ (H), kJ·mol^{-1}	$-\Delta_c H^{net}$ (C), kJ·mol^{-1}	$-\Delta_c H^{net}$ (H), kJ·mol^{-1}
435.687	110.675	435.687	88.675
$-\Delta_c H^{gross}$ (C), MJ·kg^{-1}	$-\Delta_c H^{gross}$ (H), MJ·kg^{-1}	$-\Delta_c H^{net}$ (C), MJ·kg^{-1}	$-\Delta_c H^{net}$ (H), MJ·kg^{-1}
36.275	109.83	36.275	87.977

The original article can be found under https://doi.org/10.32362/2410-6593-2021-16-4-273-286

Исправление к статье «Энергоемкость углеводородов в жидком и твердом состояниях»

Г.Я. Кабо, Л.А. Кабо, Л.С. Карпушенкова, А.В. Блохин

Тонкие химические технологии = Fine Chemical Technologies. 2021;16(4):273–286

На странице 276 в разделе **Таблица 1** вместо

Таблица 1. Инкременты энтальпий сгорания атомов C и H для углеводородов C_nH_m
Table 1. Increments of the enthalpies of combustion of C and H atoms in C_nH_m hydrocarbons

$-\Delta_cH^B$ (C), кДж·моль$^{-1}$ $-\Delta_cH^{gross}$ (C), kJ·mol^{-1}	$-\Delta_cH^B$ (H), кДж·моль$^{-1}$ $-\Delta_cH^{gross}$ (H), kJ·mol^{-1}	$-\Delta_cH^H$ (C), кДж·моль$^{-1}$ $-\Delta_cH^{net}$ (C), kJ·mol^{-1}	$-\Delta_cH^H$ (H), кДж·моль$^{-1}$ $-\Delta_cH^{net}$ (H), kJ·mol^{-1}
435.687	110.675	435.687	88.675
$-\Delta_cH^B$ (C), МДж·моль$^{-1}$ $-\Delta_cH^{gross}$ (C), MJ·mol^{-1}	$-\Delta_cH^B$ (H), МДж·моль$^{-1}$ $-\Delta_cH^{gross}$ (H), MJ·mol^{-1}	$-\Delta_cH^H$ (C), МДж·моль$^{-1}$ $-\Delta_cH^{net}$ (C), MJ·mol^{-1}	$-\Delta_cH^H$ (H), МДж·моль$^{-1}$ $-\Delta_cH^{net}$ (H), MJ·mol^{-1}
36.275	109.83	36.275	87.977

следует читать:

Таблица 1. Инкременты энтальпий сгорания атомов C и H для углеводородов C_nH_m
Table 1. Increments of the enthalpies of combustion of C and H atoms in C_nH_m hydrocarbons

$-\Delta_cH^B$ (C), кДж·моль$^{-1}$ $-\Delta_cH^{gross}$ (C), kJ·mol^{-1}	$-\Delta_cH^B$ (H), кДж·моль$^{-1}$ $-\Delta_cH^{gross}$ (H), kJ·mol^{-1}	$-\Delta_cH^H$ (C), кДж·моль$^{-1}$ $-\Delta_cH^{net}$ (C), kJ·mol^{-1}	$-\Delta_cH^H$ (H), кДж·моль$^{-1}$ $-\Delta_cH^{net}$ (H), kJ·mol^{-1}
435.687	110.675	435.687	88.675
$-\Delta_cH^B$ (C), МДж·кг$^{-1}$ $-\Delta_cH^{gross}$ (C), MJ·kg^{-1}	$-\Delta_cH^B$ (H), МДж·кг$^{-1}$ $-\Delta_cH^{gross}$ (H), MJ·kg^{-1}	$-\Delta_cH^H$ (C), МДж·кг$^{-1}$ $-\Delta_cH^{net}$ (C), MJ·kg^{-1}	$-\Delta_cH^H$ (H), МДж·кг$^{-1}$ $-\Delta_cH^{net}$ (H), MJ·kg^{-1}
36.275	109.83	36.275	87.977

Оригинальная статья может быть найдена https://doi.org/10.32362/2410-6593-2021-16-4-273-286

MIREA – Russian Technological University
78, Vernadskogo pr., Moscow, 119454, Russian Federation.
Publication date *October 31, 2021.*
Not for sale

МИРЭА – Российский технологический университет
119454, РФ, Москва, пр-т Вернадского, д. 78.
Дата опубликования *31.10.2021.*
Не для продажи

www.finechem-mirea.ru